ANALYSIS OF SECOND HARMONIC GENERATION AT A FREE BOUNDARY FOR OBLIQUE INCIDENCE

A Thesis
Presented to
The Academic Faculty

by

Frank A. Bender

In Partial Fulfillment
of the Requirements for the Degree
Master of Science in Engineering Science and Mechanics in the
School of Civil and Environmental Engineering

Georgia Institute of Technology
December 2010

ANALYSIS OF SECOND HARMONIC GENERATION AT A FREE BOUNDARY FOR OBLIQUE INCIDENCE

Approved by:

Dr. Laurence J. Jacobs, Advisor
School of Civil and Environmental Engineering
Georgia Institute of Technology

Dr. Jin-Yeon Kim
School of Civil and Environmental Engineering
Georgia Institute of Technology

Dr. Jianmin Qu
Department of Civil and Environmental Engineering
Northwestern University

Date Approved: August 26, 2010

ACKNOWLEDGMENTS

My year at the Georgia Institute of Technology and this thesis would not have been possible without the help and support of many people. First, I would like to thank my advisor Dr. Laurence Jacobs for his support during my time at the Georgia Institute of Technology. His dedication to academics and his students in particular helped to make my stay a fruitful experience. I am very grateful to my committee member Dr. Jin-Yeon Kim. His guidance and enthusiasm are greatly appreciated. The many meetings we had did not only help me with my research, but also gave me a better understanding of scientific work in general. I would also like to thank my committee member Dr. Jianmin Qu at Northwestern University for reviewing this work.

Special thanks go to all my fellow research assistants in Dr. Jacobs' laboratory. Our conversations in the lab were always helpful for my research, and the lunch and coffee breaks have become an integral part of my daily life at Georgia Tech.

In Germany, I would like to thank Prof. Dr. Lothar Gaul and Dipl.-Ing. Helge Sprenger from the Institute of Applied and Experimental Mechanics at the University of Stuttgart. At all times, I felt the benefits from this extremely well organized program. Also, Katja Striegel from the Office of International Affairs of the University of Stuttgart helped me with my intentions to study in the United States. The financial support of the German Academic Exchange Service (DAAD) and the Foundation of German Business (SdW) throughout my studies is highly appreciated.

I would also like to thank my friends here in Atlanta for making my stay an unforgettable experience, and my friends in Germany for keeping in touch.

Finally, I want to express my gratitude towards my family. They have always been there for me and supported me at any time in my life.

TABLE OF CONTENTS

LIST OF TABLES

LIST OF FIGURES

LIST OF SYMBOLS

A, B, C, D, E	constants used in solution process
$\mathcal{A}, \mathcal{B}, \mathcal{C}$	3rd order elastic constants (TOECs)
a_i	generalized coordinates in reference configuration
$\boldsymbol{b}$	body force per unit mass
β^{bulk}	bulk parameter
$\beta^{surf}, \gamma^{surf}$	surface parameters
c_0	wave speed, either c_P or c_S
c_P	longitudinal wave speed
c_S	shear wave speed
$\boldsymbol{d}$	displacement unit vector
δ_{ij}	Kronecker delta
$\boldsymbol{E}$	Lagrangian strain tensor
$\boldsymbol{\epsilon}$	strain tensor
$\boldsymbol{F}$	deformation gradient
F	scalar potential
f	frequency
Γ_{PP}, Γ_{PS}	linear reflection coefficients for an incident P-wave
Γ_{SP}, Γ_{SS}	linear reflection coefficients for an incident SV-wave
$\boldsymbol{H}$	vector potential
$\boldsymbol{I}$	second order identity tensor
j	imaginary unit
$\boldsymbol{k}$	wave vector
$\boldsymbol{k}_P$	wavevector corresponding to a P-wave
$\boldsymbol{k}_S$	wavevector corresponding to an SV-wave
$\boldsymbol{k}_R$	wavevector corresponding to an arbitrary reflected wave

k_P	wavenumber corresponding to a P-wave
k_S	wavenumber corresponding to an SV-wave
k_R	wavenumber corresponding to an arbitrary reflected wave
L	thickness of specimen
l	half thickness of a thin plate
λ, μ	second-order elastic constants, Lamé constants
$\boldsymbol{n}$	normal unit vector
∇	Nabla
$\boldsymbol{P}$	first Piola-Kirchhoff stress tensor
$\boldsymbol{P}^L$	Linear part of $\boldsymbol{P}$
$\boldsymbol{P}^{NL}$	Nonlinear part of $\boldsymbol{P}$
Ψ, Φ	angles for second harmonic waves generated by cross-interaction
ρ	density
$\boldsymbol{S}$	second Piola-Kirchhoff stress tensor
S	surface area
$\boldsymbol{\sigma}$	Cauchy stress tensor
$\boldsymbol{t}$	traction per unit mass
t	time
θ_P	angle corresponding to a P-wave
θ_S	angle corresponding to an SV-wave
θ_R	angle corresponding to an arbitrary reflected wave
θ_{cr}	critical angle
$\boldsymbol{u}$	displacement vector
$\boldsymbol{u}^{(1)}$	primary wave field
$\boldsymbol{u}^{(2)}$	secondary wave field
U	wave amplitude
U_{P_i}	amplitude of linear incident P-wave

U_{S_i}	amplitude of linear incident SV-wave
U_{P_r}	amplitude of linear reflected P-wave
U_{S_r}	amplitude of linear reflected SV-wave
V	body volume
$\boldsymbol{v}$	velocity field
ω	angular frequency
$\boldsymbol{x}$	position vector
x, y, z	Cartesian coordinates in the reference configuration
x', z'	Cartesian coordinates for rotated coordiante system

SUMMARY

This thesis investigates the generation of second harmonic bulk waves in the presence of a free boundary. Second harmonic waves have proven to be useful in the field of nondestructive evaluation to detect fatigue in a material at an early stage. Since most experimental setups include a free surface, the influence of such a boundary is of significant practical interest. As a result, the objective of this research is to develop a quantitative understanding of the complete process of second harmonic generation at a free boundary.

This research shows that the interaction of primary waves (with each other) in the nonlinear framework leads to the generation of second harmonic bulk waves. We distinguish between self-interaction of a single primary wave and the cross-interaction of two different primary waves. The proposed approach uses the perturbation method to solve the nonlinear equations of motion, and shows two fundamentally different solutions. In the case of resonance, the secondary waves grow with propagation distance. This is the most important practical case, since the growing amplitudes of these waves should be easier to experimentally measure. In the second, non-resonant case, the amplitudes of the secondary waves are constant.

The complete process of second harmonic generation is analyzed for an incident P- and an incident SV-wave, with the primary and secondary fields given. Finally, the degenerate case of normal incidence is presented. Normal and oblique incidence are compared with regard to their feasibility in experimental setups. The specific behavior of second harmonic waves propagating in aluminum is numerically determined. These results enable a variety of physical insights and conclusions to be drawn from the analytical and numerical investigations.

CHAPTER I

INTRODUCTION

In the last century, the theory and the applications in the field on nondestructive evaluation (NDE) have developed to a high level of expertise. The basic objective of NDE is the detection of defects in the material by sending a wave into the solid and then analyzing the response of the system. This means that the condition of the specimen can be determined without destroying it, which is of course in many cases preferred to destructive evaluation techniques. In its early stage, NDE was mostly concerned with the detection of cracks in specimens, and experiments were based on the principles of linear wave propagation. The linear equations involved have been well understood for a long time, and as a consequence, linear theory and experiments in NDE have developed rapidly and are well established by now.

However, the linear framework has certain limitations. Above all, the linear experiments are only capable of detecting defects that already have become significant. But at this stage, the probability of a fatal failure of the structure is high, and insight from nondestructive experiments might come too late. Therefore, it is desirable to measure parameters that are more sensitive, in order to detect changes in the microstructure of the material before a macroscopic crack appears. Such parameters can be obtained by taking the nonlinearities of the material into account. The effects caused by the material nonlinearities in the system are very small compared to the linear effects, but they can help us to monitor the health of specimens in much more detail.

Unfortunately, the consideration of material nonlinearities results in a much more complicated analysis. When dealing with nonlinear waves, there are effects that have

to be understood, both in theory and in experiments. One of these effects is the generation of higher harmonic waves. In the linear setup, if one launches a wave of circular frequency ω into the medium, only waves with the frequency of the excitation frequency ω travel through the medium. In the nonlinear setup, there will appear waves of frequencies that are multiples of the excitation frequency, i.e. there appear waves with circular frequencies ω, 2ω, 3ω and so on. In weakly nonlinear materials such as metals, the amplitudes of these higher harmonics are small compared to the amplitudes of the fundamental waves. In fact, only the waves of frequency 2ω, which are known as second harmonics, can be exploited in measurements. The amplitudes of the higher harmonics are too small to be used for a reliable analysis.

The generation and measurement of second harmonic waves is a typical objective for modern nonlinear ultrasonic NDE experiments, since these waves show a high sensitivity to changes in the microstructure of the material. Therefore, it is necessary to understand the nonlinear wave phenomena that govern the propagation of the higher harmonic waves. While the linear problem is well understood, the mathematics involved in the nonlinear framework are much more complicated. For instance, there are only few cases in which an analytical solution to the nonlinear equations of motion is available, which means that one can only seek an approximation of the solution.

The behavior of second harmonic waves after reflection at a free boundary is of particular interest to the NDE community. The case of a free boundary appears naturally in many real-world applications, and the involved equations become simpler than in the case of other, more general boundary conditions. Another reason for the large attention drawn to reflection phenomena is caused by the fact that the second harmonics are not only generated when a wave travels through the bulk of a material, but they are also influenced by the boundary at which they are reflected. Hence, the question arises, if reflection at a free boundary can be used to increase the amplitude of the second harmonics.

In this thesis, we will analyze how the reflection at a free boundary affects the generation of second harmonic waves. Therefore, the most important results of linear wave propagation will be given in Chapter 2. This will be followed by an outline of nonlinear wave propagation in Chapter 3. In Chapter 4, we consider two specific cases, namely the incidence of a longitudinal wave and the incidence of a vertically polarized shear (SV) wave, and derive the complete solution of the primary and secondary wave field. In order to illustrate the results, a numerical simulation will be performed and it will be shown how the second harmonic amplitudes develop for the different situations. In Chapter 5, this work will be completed by presenting our conclusions and giving an outlook on possible future impacts on NDE applications.

1.1 Literature Review

Many works have been published on linear wave propagation. For the basics of continuum mechanics, we refer to the book by Malvern [18]. We will use the definition of the stress tensor as introduced in this book. As a reference on linear wave propagation in general, the books by Graff [12] and Achenbach [1] can be recommended. Auld [2] gives a detailed explanation of linear reflection processes at different boundaries, including an illustration of Snell's law and the complete derivation of the Fresnel equations.

There is less literature available on nonlinear wave propagation. The book by Landau and Lifshitz [17] contains a short chapter on nonlinear waves. Green [13] gives an introduction into the generation of higher harmonics, which is based on the work by Gol'dberg [11].

For the interaction of linear waves and the resulting generation of higher harmonics in the bulk, the publications by Jones and Kobett [15], and Thompson and Tiersten [23] can be recommended.

DeLima [9] and Mueller [19] give results on the generation of second harmonic

Lamb waves in a thin plate. They both apply the perturbation method and a modal expansion technique to obtain an approximate solution to the problem. Deng [10] analyzed the problem of second harmonic Lamb wave propagation in a framework similar to the one used in this thesis. This work will be explained in more detail later on.

The process of reflection of nonlinear waves at different boundaries has been investigated by various researchers. Braun [4] analyzes the reflection of a P-wave under normal incidence. Shu and Ginsberg [22] have used the method of characteristics to solve the problem of oblique incidence of a P-wave at a free boundary. Zhou and Shui [26] have used the perturbation method to derive a complete solution of the secondary field. In this work, we mostly follow their framework.

There is a growing number of publications on experiments using second harmonic waves. For instance, Kim et al. [16] have applied nonlinear ultrasonics to characterize fatigue damage in a nickel-base superalloy. Pruell et al. [20] have used nonlinear guided waves to evaluate plasticity-induced damage in an aluminum alloy.

1.2 Objective

The objective of this thesis is to summarize the results on nonlinear wave propagation, give physical insight into the process of second harmonic generation under the presence of a free boundary and, finally, analyze how the second harmonic amplitudes behave before and after reflection. To know how the amplitudes change with propagation distance is important in order to choose the most efficient measurement setup in an experiment.

1.3 Motivation

In order to illustrate the objective of this thesis, we give a simple example. Consider the liquefied natural gas (LNG) storage tank shown in Fig.1.3. Such tanks are frequently used to store liquefied gases at very low temperatures. They usually

consist of double containers, where the inner container contains the LNG and the outer container is filled with insulation materials. These tanks can be found on land, but also on LNG carrier ships. Assume one wants to evaluate the state of fatigue of such a tank. For practical reasons, only the outer surface of the tanks is accessible. This motivates the measurement setups given in Fig.1.2. In both setups presented, a transducer is used to send a wave into the material, the wave is then reflected at the free boundary on the other side and finally measured when it arrives again at the accessible surface. However, there is a crucial difference in the two techniques. Fig.2(a) presents the case of oblique incidence, where the incident wave is reflected under an angle and therefore returns to a different position, where it is measured by Transducer 2. Hence, the reflected wave has not only traveled normal to the surface, but it also propagated in the vertical direction. Fig.2(b) shows a similar setup. Now, the wave is normally launched into the medium. As a consequence, the wave is normally reflected and returns to the location where it has been initiated. The same transducer that has launched the incident wave can be used to measure the reflected wave. In this thesis, it will be seen that the two setups show fundamental differences when it comes to measuring second harmonic waves. In contrast to the simplicity of these experimental setups, the generation of second harmonic waves in the bulk under the presence of a free boundary must be analyzed carefully in order to evaluate the response of the given system. This application shall motivate the analysis performed in the remainder of this thesis.

Figure 1.1: A Liquefied Natural Gas Tank.

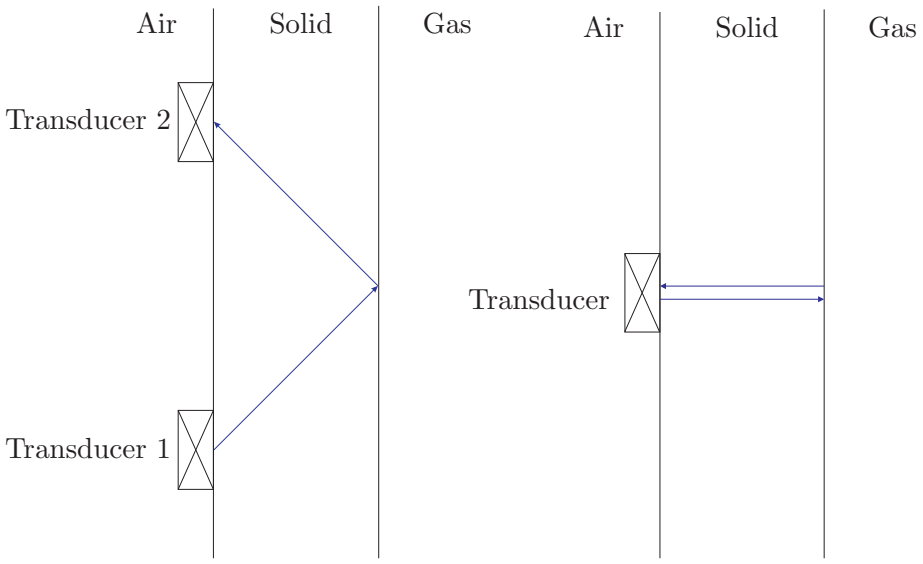

(a) Oblique Incidence. (b) Normal Incidence.

Figure 1.2: Measurement Setup for Nondestructive Testing.

CHAPTER II

LINEAR WAVE PROPAGATION

2.1 Linear Equations of Motion

In order to derive the equation of motion for an elastic solid, we state the balance of linear momentum for a three-dimensional free body of volume V, surface area S and density ρ as

$$\frac{d}{dt}\int_V \rho\,\boldsymbol{v}\,dV = \int_S \boldsymbol{t}\,dS + \int_V \rho\,\boldsymbol{b}\,dV. \tag{2.1}$$

$\boldsymbol{v}$ is the body's velocity field, $\boldsymbol{t}$ is the traction per unit mass and $\boldsymbol{b}$ represents the body force per unit mass. Introducing indicial notation and setting $\boldsymbol{v} = \dot{\boldsymbol{u}}$ with $\boldsymbol{u}$ being the displacement, Eq. (2.1) can be restated as

$$\frac{d}{dt}\int_V \rho\,\dot{u}_i\,dV = \int_S t_i\,dS + \int_V \rho\,b_i\,dV. \tag{2.2}$$

The traction t_i can be expressed in terms of the components of the Cauchy-Stress-Tensor $\boldsymbol{\sigma}$ and the components of the outward normal unit vector $\boldsymbol{n}$ by applying Cauchy's formula

$$t_i = \sigma_{ji}\,n_j. \tag{2.3}$$

With the divergence theorem,

$$\int_S \sigma_{ji}\,n_j\,dS = \int_V \sigma_{ji,j}\,dV \tag{2.4}$$

the surface integral in Eqs. (2.1) and (2.2) can be transformed into a volume integral. Additionally rearranging terms to the right side results in

$$\int_V \left[\rho\,\ddot{u} - \sigma_{ji,j} - \rho\,b_i\right]\,dV = 0. \tag{2.5}$$

Since Eq. (2.5) has to hold true for an arbitrary volume V, one can conclude

$$\rho\,\ddot{u} - \sigma_{ji,j} - \rho\,b_i = 0 \tag{2.6}$$

or in vector notation

$$\rho\,\ddot{\boldsymbol{u}} - \nabla\cdot\boldsymbol{\sigma} - \rho\,\boldsymbol{b} = 0. \tag{2.7}$$

Equations (2.6) and (2.7) are the equations of motion for an elastic solid, also known as *Cauchy's Equations of Motion*. In the absence of body forces, $\boldsymbol{b} = 0$, the equations of motion take the even more compact form

$$\rho\,\ddot{u} = \sigma_{ji,j} \tag{2.8}$$

or

$$\rho\,\ddot{\boldsymbol{u}} = \nabla\cdot\boldsymbol{\sigma}. \tag{2.9}$$

Applying the principle of angular momentum shows that the Cauchy stress tensor must be symmetric,

$$\sigma_{ij} = \sigma_{ji}. \tag{2.10}$$

For a more detailed derivation of the equations of motion, we refer to the books by Achenbach [1] and Malvern [18].

2.2 Compatibility Equations

The compatibility equations give a relationship between the strain $\boldsymbol{\epsilon}$ and the displacement $\boldsymbol{u}$. If only small deformations are considered, higher order terms can be neglected and one can use the small strain tensor ϵ given by

$$\boldsymbol{\epsilon} = \frac{1}{2}(\boldsymbol{u}\nabla + \nabla\boldsymbol{u}) \tag{2.11}$$

or

$$\epsilon_{ij} = \frac{1}{2}(u_{i,j} + u_{j,i}). \tag{2.12}$$

2.3 Constitutive Equations

For the linear case, the relationship between stress $\boldsymbol{\sigma}$ and strain $\boldsymbol{\epsilon}$ is given by

$$\sigma_{ij} = \lambda\, \epsilon_{kk}\, \delta_{ij} + 2\mu\, \epsilon_{ij} \tag{2.13}$$

where λ and μ are the second-order elastic constants, also known as *Lamé* constants, and δ_{ij} is the *Kronecker* delta. Using the compatibility equations from the previous section, one arrives at

$$\sigma_{ij} = \lambda\, u_{kk}\, \delta_{ij}\ + \mu(u_{i,j} + u_{j,i}). \tag{2.14}$$

2.4 Plane Waves

Applying the constitutive equations and the compatibility equations to the equations of motion derived in 2.1 and neglecting body forces leads to the expression

$$\rho\ddot{u}_i - (\lambda + \mu)u_{k,ki} - \mu u_{i,kk} = 0 \tag{2.15}$$

or

$$\rho\ddot{\boldsymbol{u}} - (\lambda + 2\mu)\, \nabla(\nabla \cdot \boldsymbol{u}) - \mu\nabla^2\boldsymbol{u} = 0 \tag{2.16}$$

Using the identity

$$\nabla^2\boldsymbol{u} = \nabla(\nabla \cdot \boldsymbol{u}) - \nabla \times (\nabla \times \boldsymbol{u}) \tag{2.17}$$

yields

$$\rho\ddot{\boldsymbol{u}} - (\lambda + 2\mu)\nabla(\nabla \cdot \boldsymbol{u}) + \mu\nabla \times (\nabla \times \boldsymbol{u}) = 0. \tag{2.18}$$

In this thesis, plane harmonic waves propagating in an isotropic medium are considered. Assume our medium to be of infinite dimensions in the x and y direction. No generality is lost if one lets the wave normal $\boldsymbol{n}$ lie in the x,z-plane. This plane will from now on be referred to as the *vertical plane*, whereas the x,y-plane is called the *horizontal plane*.

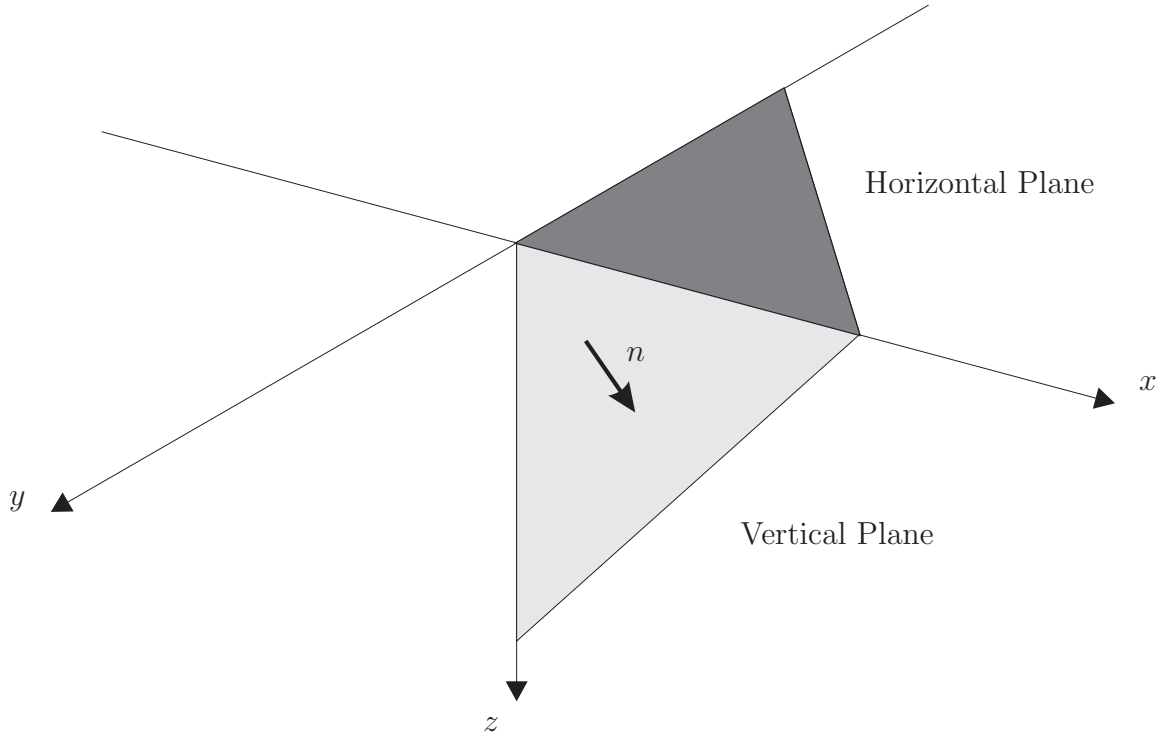

Figure 2.1: Vertical and Horizontal Planes in an Infinite Halfspace.

This setup is illustrated in Fig.2.1. Now assume a plane wave $\boldsymbol{u}$ with components

$$u_1 = u_1(x, z, t), \quad u_2 = 0, \quad u_3 = u_3(x, z, t). \tag{2.19}$$

Note that this wave only has displacements in the vertical plane. In this thesis, we will restrict ourselves to this case of in-plane motion. Furthermore, notice that the displacements are independent of the y-coordinate, $\frac{\partial}{\partial y} = 0$. Therefore, from now on only the $x-$ and $z-$ coordinate will be considered and thus, the problem reduces to two dimensions.

There are two fundamental waves that have to be considered as a solution to the equation of motion: Longitudinal or primary (P-) waves and transverse or shear (S-) waves. Since we only consider in-plane motion, the shear waves can be specified as shear waves in the vertical plane, also known as SV-waves.

2.4.1 Time-harmonic Plane Waves

A plane harmonic displacement wave propagating with phase velocity c_0 in a direction defined by the propagation vector $\boldsymbol{k}$ is in general represented by

$$\boldsymbol{u} = U\boldsymbol{d}\,\cos(\omega t - \boldsymbol{k}\boldsymbol{x}) \tag{2.20}$$

$$= U\boldsymbol{d}\cdot\frac{1}{2}\left[e^{j(\omega t-\boldsymbol{k}\boldsymbol{x})} + c.c.\right], \tag{2.21}$$

where $j = \sqrt{-1}$ is the imaginary unit, U is the wave's amplitude, $\boldsymbol{d}$ is the unit displacement vector. $\omega = c_0 k$ is the circular frequency and k is the wave number being defined by $k = \|\boldsymbol{k}\|$. The additional term *c.c.* refers to the complex conjugate of the exponential term. This term together with the factor $\frac{1}{2}$ makes the expression equal to the expression using *cosine*. The vector x is called the position vector and is given by

$$\boldsymbol{x} = \begin{bmatrix} x_1 \\ x_2 \\ x_3 \end{bmatrix} = \begin{bmatrix} x \\ y \\ z \end{bmatrix} \tag{2.22}$$

We also point out that some of our references, e.g. the book by Achenbach [1], use a different notation, namely

$$\boldsymbol{u} = U\boldsymbol{d}\,e^{j(\omega t-\boldsymbol{k}\boldsymbol{x})}. \tag{2.23}$$

This representation must be accompanied by the statement that only the real part of this term represents the physical wave. Taking the real part leads to Eq.(2.20). The wave representations Eqs. (2.21) and (2.23) can be used equivalently, as long as one keeps in mind that taking the real part $\Re$ is a linear operator and therefore must be applied to primary waves. It cannot be applied to higher harmonics, which are generated by a nonlinear operation (i.e. multiplication). In the remainder of this thesis, we a representation of form (2.23) will be used. Whenever this representation needs special attention, it will be mentioned.

2.4.2 P-Waves

A P-wave has its displacement in the same direction as the direction of propagation, therefore it can be expressed as

$$\boldsymbol{u}_P = U_P \begin{bmatrix} \sin\theta_P \\ 0 \\ \cos\theta_P \end{bmatrix} e^{j(\omega t - k_P x \sin\theta_P - k_P z \cos\theta_P)} \tag{2.24}$$

where U_P is the amplitude of the wave, θ_P defines the direction of propagation and displacement as illustrated in Fig. 2(a), ω is the circular frequency and k_P is the wavenumber corresponding to the wave vector

$$\boldsymbol{k}_P = k_P \begin{bmatrix} \sin\theta_P \\ 0 \\ \cos\theta_P \end{bmatrix}. \tag{2.25}$$

For the wavenumber, we have $k_P = \frac{\omega}{c_P}$, where c_P is the longitudinal wave speed. In an isotropic solid, the longitudinal wave speed is given by

$$c_P = \sqrt{\frac{\lambda + 2\mu}{\rho}}. \tag{2.26}$$

It can easily be shown that the P-wave is *irrotational*, i.e. the curl of this vector field vanishes, $\nabla \times \boldsymbol{u} = 0$. This results in the simpler equation of motion for a P-wave

$$\ddot{u}_i - c_P^2 u_{i,kk} = 0. \tag{2.27}$$

2.4.3 SV-Waves

An SV-wave has its displacement in the direction perpendicular to the direction of propagation and can be expressed as

$$\boldsymbol{u}_S = U_S \begin{bmatrix} \cos\theta_S \\ 0 \\ -\sin\theta_S \end{bmatrix} e^{j(\omega t - k_S \sin\theta_S x - k_S \cos\theta_S z)} \tag{2.28}$$

where U_S, θ_S and ω have similar meaning as in the case of a P-wave. Note that the wave vector is now given by

$$\boldsymbol{k}_S = k_S \begin{bmatrix} \sin\theta_S \\ 0 \\ \cos\theta_S \end{bmatrix}. \tag{2.29}$$

with the wavenumber $k_S = \frac{\omega}{c_S}$ with c_S being the shear wave speed given by

$$c_S = \sqrt{\frac{\mu}{\rho}}. \tag{2.30}$$

Fig.2(b) illustrates the SV-wave. It can be shown that this wave is *solenoidal*, i.e. the divergence of this vector field becomes zero, $\nabla \cdot \boldsymbol{u} = 0$. A simpler equation of motion for an SV-wave is given by

$$\ddot{u}_i - c_S^2 u_{i,kk} = 0. \tag{2.31}$$

For the remainder of this thesis, waves will be illustrated by an arrow representing the wave vector and a bold arrow representing the displacement. Whether the corresponding wave is of P- or SV-type will also be indicated by its indices: $\boldsymbol{u}_{P_i}$ represents an incident P-wave, whereas $\boldsymbol{u}_{S_r}$ represents a reflected SV-wave.

2.5 Linear Reflection at a Free Boundary

In this work, reflection of plane waves at a free boundary will play an important role. Therefore, the basic laws of linear reflection are outlined briefly. Namely, these are *Snell's law*, which gives a relationship of wavenumbers and propagation angles for incident and reflected waves, and the *Fresnel formulae*, which can be used to derive the amplitudes of the reflected waves if the amplitude of the incident wave is known.

2.5.1 Snell's Law

Incident and reflected waves have to satisfy *Snell's law* given by

$$k_P \sin(\theta_P) = k_R \sin(\theta_R) \tag{2.32}$$

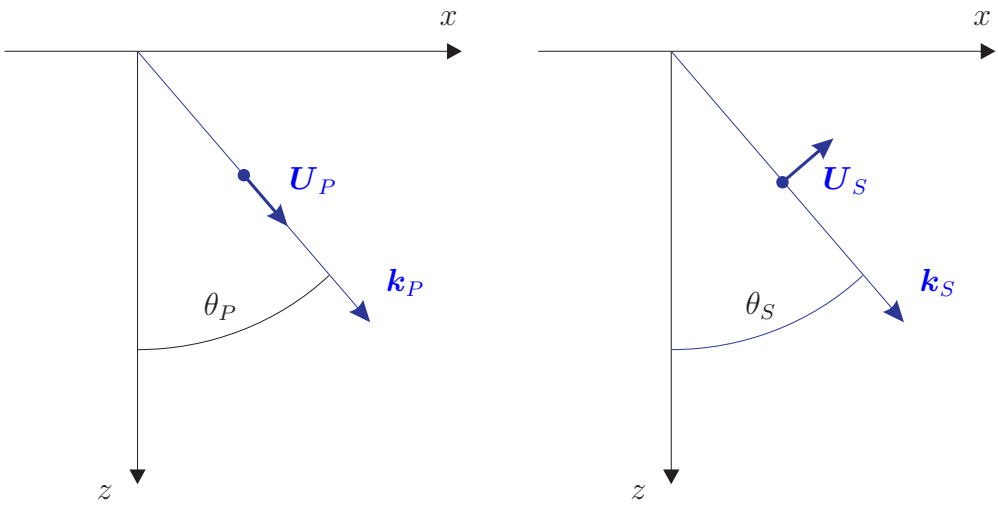

(a) Longitudinal or P-Wave. (b) Shear Vertical or SV-Wave.

Figure 2.2: Illustration of Plane Waves.

with k_R being the wavenumber of the reflected wave and θ_R being the angle of reflection. Also see Fig. 2.3 and the book by Auld [2].

2.5.2 Fresnel Formulae

For a detailed derivation of the Fresnel equations which also includes the case of a rigid boundary, the interested reader is referred to the books by Auld [2] and Graff [12]. In the following, only the results that are important for this work are summarized.

2.5.2.1 Reflection of an Incident P-Wave

Consider the incidence of a P-wave

$$\boldsymbol{u}_{P_i} = U_{P_i} \begin{bmatrix} \sin\theta_P \\ 0 \\ \cos\theta_P \end{bmatrix} e^{j(\omega t - k_P x \sin\theta_P + k_P z \cos\theta_P)} \tag{2.33}$$

propagating in an infinite half-space. Let us assume a free boundary, which means that the tractions have to vanish at $z = 0$,

$$\sigma_{31}|_{z=0} = 0 \tag{2.34}$$

$$\sigma_{33}|_{z=0} = 0. \tag{2.35}$$

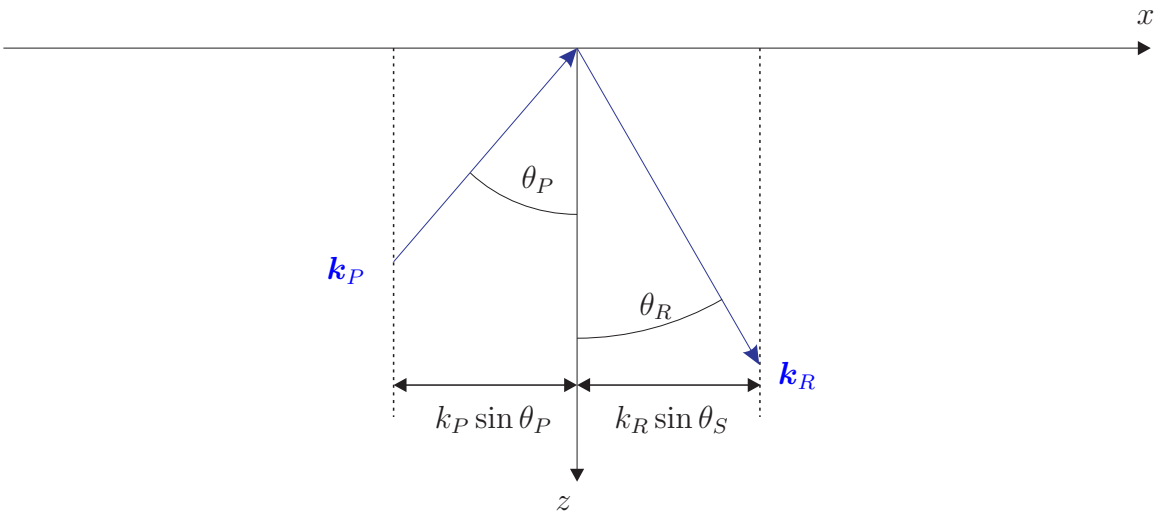

Figure 2.3: Illustration of Snell's Law.

Now assume the incident P-wave is reflected as a single P-wave

$$\boldsymbol{u}_{P_r} = U_{P_r} \begin{bmatrix} \sin\theta_P \\ 0 \\ \cos\theta_P \end{bmatrix} e^{j(\omega t - k_P x \sin\theta_P - k_P z \cos\theta_P)} \tag{2.36}$$

If one derives the expressions for the stresses at the boundary given by Eqs. (2.34) and (2.35), it can be seen that these equations cannot be satisfied if there is only a reflected P-wave. Hence, there also must be a reflected SV-wave

$$\boldsymbol{u}_{S_r} = U_{S_r} \begin{bmatrix} \cos\theta_S \\ 0 \\ -\sin\theta_S \end{bmatrix} e^{j(\omega t - k_S x \sin\theta_S - k_S z \cos\theta_S)}. \tag{2.37}$$

This reflection of an incident P-wave as a P-wave and an SV-wave is known as *mode conversion*. The obtained linear wave field is illustrated in Fig. 2.4.

The amplitudes U_{P_r} and U_{S_r} of the reflected waves can be derived using the boundary conditions. This leads to the *Fresnel* formulae,

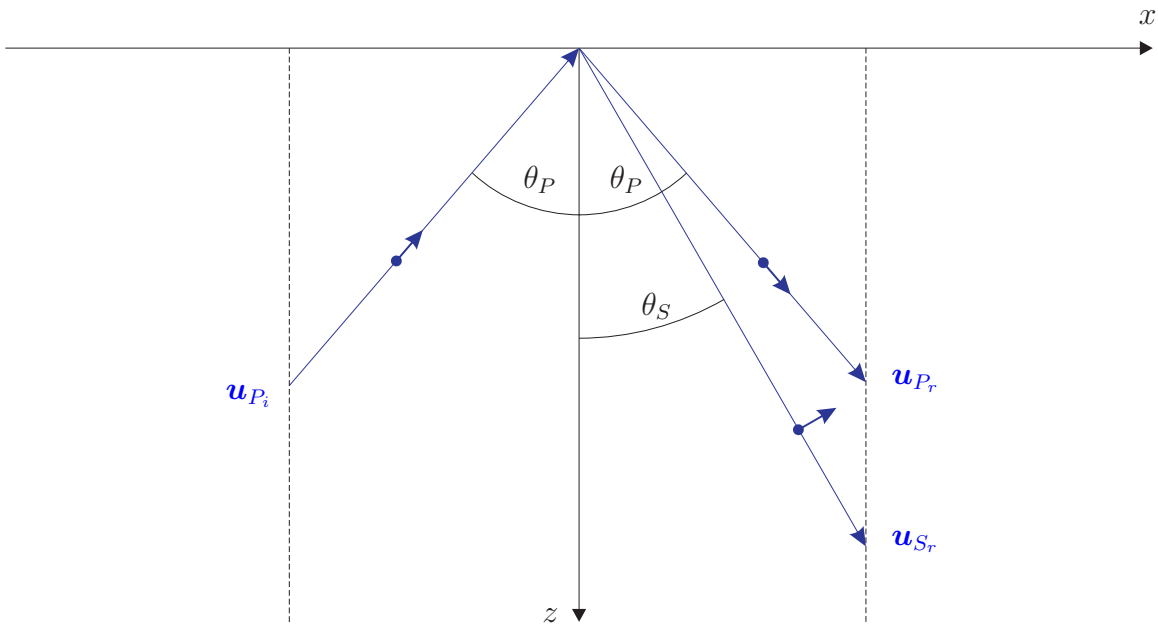

Figure 2.4: Mode Conversion of an Incident P-Wave.

$$U_{P_r} = \frac{\sin(2\theta_P)\sin(2\theta_S) - \frac{\lambda+2\mu}{\mu}\cos^2(2\theta_S)}{\sin(2\theta_P)\sin(2\theta_S) + \frac{\lambda+2\mu}{\mu}\cos^2(2\theta_S)}\, U_{P_i} \tag{2.38}$$

$$U_{S_r} = \frac{2\sqrt{\frac{\lambda+2\mu}{\mu}}\sin(2\theta_P)\cos(2\theta_S)}{\sin(2\theta_P)\sin(2\theta_S) + \frac{\lambda+2\mu}{\mu}\cos^2(2\theta_S)}\, U_{P_i}. \tag{2.39}$$

Note that the amplitudes of the reflected waves depend on the elastic constants, the angles θ_P and θ_S, as well as the incident wave's amplitude U_{P_i}, but not on the circular frequency ω. In Fig. 2.5, the reflection coefficents

$$\Gamma_{PP} = \left|\frac{U_{P_r}}{U_{P_i}}\right|, \qquad \Gamma_{PS} = \left|\frac{U_{S_r}}{U_{P_i}}\right| \tag{2.40}$$

are shown for aluminum as a function of the incident angle θ_P.

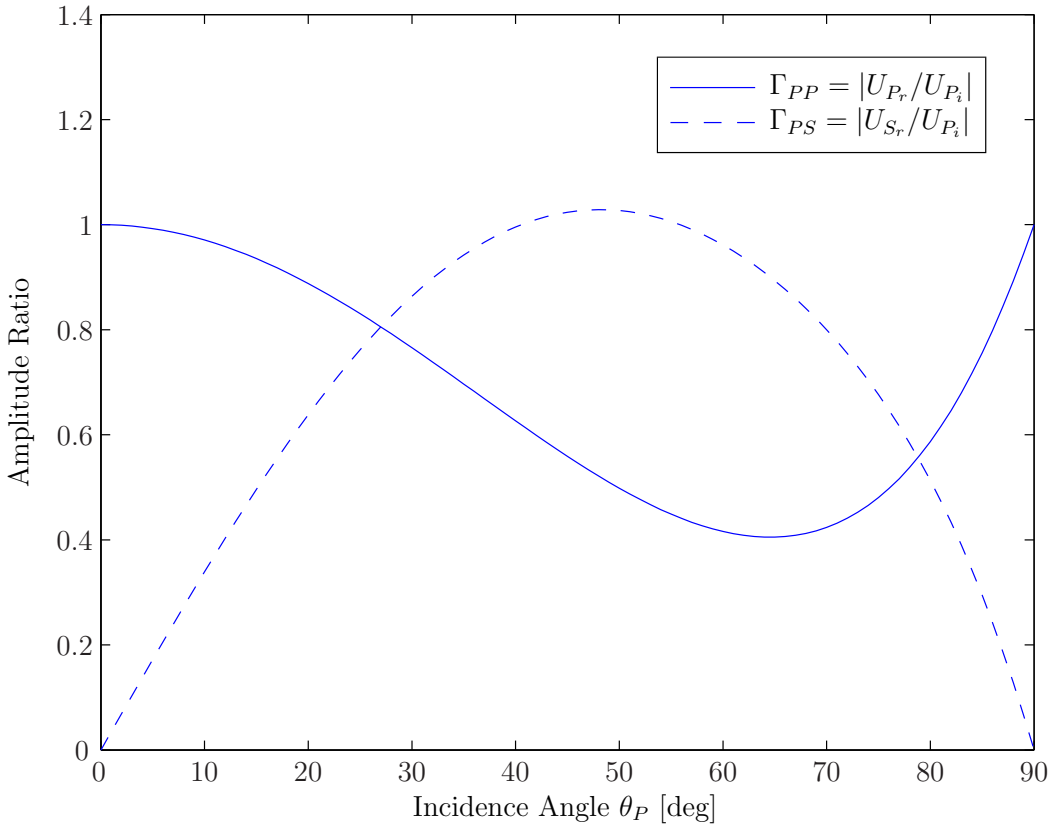

Figure 2.5: Linear Reflection Coefficients for an Incident P-Wave.

2.5.2.2 *Reflection of an Incident SV-Wave*

For the case of an incident SV-wave

$$\boldsymbol{u}_{S_i} = U_{S_i} \begin{bmatrix} \cos\theta_S \\ 0 \\ \sin\theta_S \end{bmatrix} e^{j(\omega t - k_S x \sin\theta_S + k_S z \cos\theta_S)}, \tag{2.41}$$

similar results can be obtained. At the free boundary, the incident SV-wave is reflected as a P-wave and an SV-wave. However, it is important to note that the reflected P-wave will only exist until a critical angle θ_{cr} is reached. The critical angle is given by

$$\theta_{cr} = \arcsin\left(\frac{k_P}{k_S}\right). \tag{2.42}$$

For incident angles $\theta_S > \theta_{cr}$, the incident SV-wave is totally reflected and the P-wave becomes a longitudinal surface wave decaying with depth. This can be understood by taking a look at the expression for the critical angle (2.42): For $\theta_S > \theta_{cr}$, we obtain $\sin\theta_P > 1$. It follows that $\cos\theta_P$ must be purely imaginary, and therefore it can be expressed as

$$\cos\theta_P = \sqrt{1 - \sin^2\theta_P} = \pm j\sqrt{\sin^2\theta_P - 1}. \tag{2.43}$$

For a P-wave of type (2.21), we obtain

$$\boldsymbol{u} = U\boldsymbol{d}\, e^{j(\omega t - k_P x \sin\theta_P + k_P z j\sqrt{\sin^2\theta_P - 1})} \tag{2.44}$$

$$= U\boldsymbol{d}\, e^{j(\omega t - k_P x \sin\theta_P)}\, e^{-k_P z\sqrt{\sin^2\theta_P - 1}} \tag{2.45}$$

which is the mathematical representation of a wave that travels in x-direction and decays in z-direction. Hence, for incidence angles $\theta_S > \theta_{cr}$, a P-wave that travels along the surface and decays with depth is obtained. Mode conversion of an incident SV-wave is illustrated in Fig.2.6.

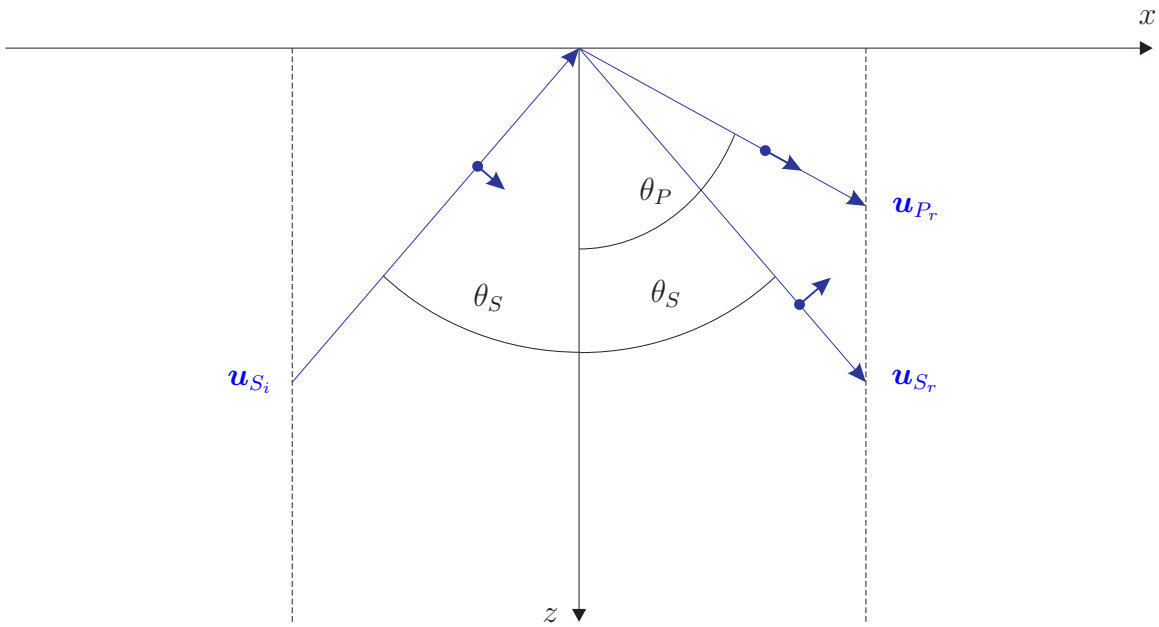

Figure 2.6: Mode Conversion of an Incident SV-Wave.

As before, the amplitudes U_{P_r} and U_{S_r} of the reflected waves can be derived using the boundary conditions. This leads to the *Fresnel* formulae

$$U_{P_r} = \frac{2\sqrt{\frac{\lambda+2\mu}{\mu}}\sin(2\theta_S)\cos(2\theta_S)}{\sin(2\theta_P)\sin(2\theta_S) + \frac{\lambda+2\mu}{\mu}\cos^2(2\theta_S)}\, U_{S_i} \tag{2.46}$$

$$U_{S_r} = -\frac{\sin(2\theta_P)\sin(2\theta_S) - \frac{\lambda+2\mu}{\mu}\cos^2(2\theta_S)}{\sin(2\theta_P)\sin(2\theta_S) + \frac{\lambda+2\mu}{\mu}\cos^2(2\theta_S)}\, U_{S_i}. \tag{2.47}$$

In Fig.2.7, the reflection coefficents

$$\Gamma_{SP} = \left|\frac{U_{P_r}}{U_{S_i}}\right|, \qquad \Gamma_{SS} = \left|\frac{U_{S_r}}{U_{S_i}}\right| \tag{2.48}$$

are shown for aluminum as a function of the incident angle θ_S.

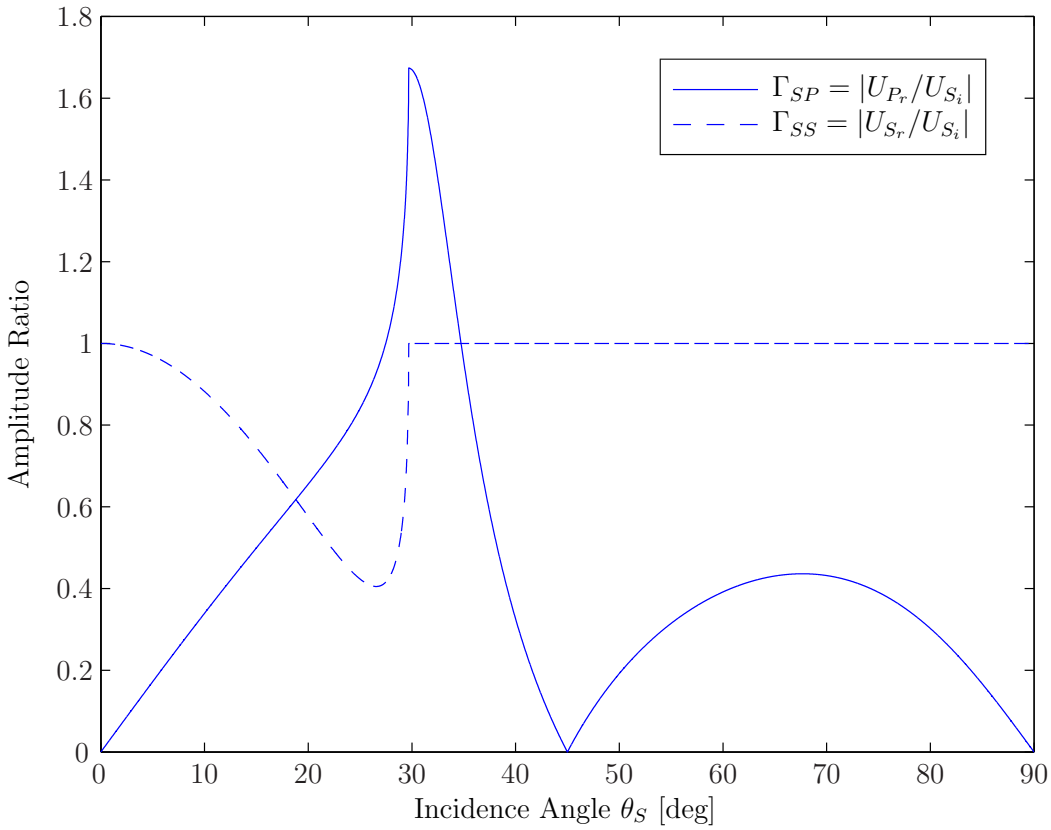

Figure 2.7: Linear Reflection Coefficients for an Incident SV-Wave.

CHAPTER III

NONLINEAR WAVE PROPAGATION

In this chapter, we extend our view to the case in which nonlinear effects are not negligible any longer. We have to keep in mind that we obtain the linear equations derived above in the case when we consider the nonlinear problem and neglect terms of quadratic and higher order. Considering geometric and material nonlinearities makes it necessary to deal with a couple of interesting effects, such as the generation of higher harmonic waves, as illustrated in Fig.3.1. The understanding of the generation of these waves is still at an early stage, and the same holds true for their experimental detection. Nevertheless, they prove to be very useful for nondestructive evaluation of materials. In particular, measurement of the nonlinear parameters such as the third-order elastic constants can be used to detect fatigue damage in the specimen at an early stage. Applying nonlinear techniques therefore enables us to detect endangered parts in the material before an actual crack appears. Kim et al. give an example of such a technique using nonlinear ultrasonic waves [16].

There is no exact analytical solution to the nonlinear equations of motion. However, the nonlinear boundary value problem that is affiliated with the propagation of waves in a nonlinear bounded medium can be decomposed into two linear boundary

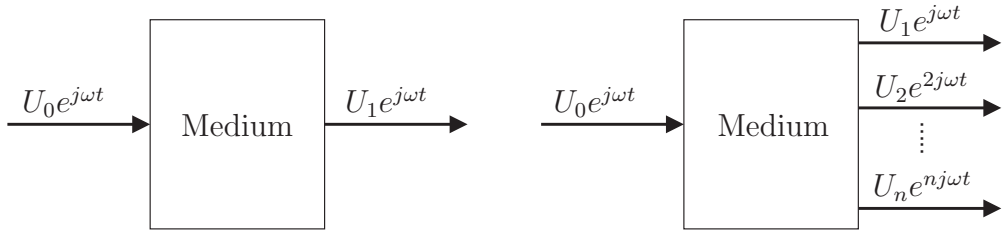

(a) Linear Framework. (b) Nonlinear Framework.

Figure 3.1: Wave Propagation in the Linear and Nonlinear Framework.

value problems using the perturbation method. This makes it possible to come up with a successive approximation of the solution, and this approach has been used frequently in the past [15, 27, 26, 8, 5].

The interaction of nonlinear elastic waves will also be explained in this chapter, since this process plays an important role in the generation of second harmonic waves in the bulk. Finally, the general solution to the equations of motion will be derived, which consists of a homogeneous and a particular solution.

3.1 Nonlinear Equations of Motion

In the linear framework, only considered infinitesimal deformation is considered. However, finite deformation and energy absorbing mechanisms in microscale can lead to nonlinear effects [13], which make it necessary to investigate the case of finite deformation. Finite deformation can be described from two different viewpoints: The Lagrangian formulation, which describes strain in the initial state, and the Eulerian formulation, which describes strain in the deformed state.

3.1.1 Equations of Motion

In the case of finite deformation, the Cauchy stress tensor cannot be applied any longer. Instead, the Piola-Kirchhoff stress tensors are used to express the stresses relative to the reference or initial configuration. The equations of motion in terms of the first Piola-Kirchhoff stress tensor $\boldsymbol{P}$ are given by

$$\rho\, \ddot{\boldsymbol{u}} = \nabla \boldsymbol{P} \tag{3.1}$$

or

$$\rho\, \frac{\partial^2 u_i}{\partial t^2} = \frac{\partial P_{ji}}{\partial a_j} \tag{3.2}$$

where a_j is the coordinate describing the reference state of the considered particle,

$$\{a_1, a_2, a_3\} = \{x, y, z\} \tag{3.3}$$

3.1.2 Piola-Kirchhoff Stress Tensors for an Isotropic Medium

The first Piola-Kirchhoff stress tensor $\boldsymbol{P}$ can be expressed in terms of the second Piola-Kirchhoff stress tensor $\boldsymbol{S}$ and the deformation gradient $\boldsymbol{F} = \boldsymbol{I} + \nabla \boldsymbol{u}$ with $\boldsymbol{I}$ being the second-order identity tensor,

$$\boldsymbol{P} = \boldsymbol{S} \cdot \boldsymbol{F}^T = \boldsymbol{S} \cdot (\boldsymbol{I} + \boldsymbol{u}\nabla) \tag{3.4}$$

or

$$P_{ij} = S_{ik}F_{kj} = S_{ik}(\delta_{kj} + u_{k,j}). \tag{3.5}$$

It is important to note that the first Piola-Kirchhoff stress tensor $\boldsymbol{P}$ is not symmetric. Many writers use the transpose of $\boldsymbol{P}$ to formulate the equations of motion [11, 22, 26], whereas in this work, we follow the definition by Malvern [18]. Now consider the second-order elastic constitutive law for an isotropic medium derived by Renton [21]

$$S_{ij} = \lambda E_{kk}\delta_{ij} + 2\mu E_{ij} + \delta_{ij}(\mathcal{C}E_{kk}E_{ll} + \mathcal{B}E_{kl}E_{lk}) + 2\mathcal{B}E_{kk}E_{ij} + \mathcal{A}E_{jk}E_{ki}. \tag{3.6}$$

$\mathcal{A}$, $\mathcal{B}$ and $\mathcal{C}$ are the third-order elastic constants (TOECs) introduced by Landau and Lifshitz [17] and E_{ij} is the Lagrangian strain tensor given by

$$E_{ij} = \frac{1}{2}(u_{i,j} + u_{j,i} + u_{k,i}u_{k,j}). \tag{3.7}$$

Note that there exist different forms of third-order elastic constants in the literature. Namely, one can find the constants introduced by Landau and Lifshitz, $\mathcal{A}, \mathcal{B}, \mathcal{C}$, those introduced by Murnaghan, l, m, n and in the standard tensor notation used by Brugger, C_{ijk}. The relations between the different constants are given in the book by Green [13]. Combining Eqs. (3.5), (3.6) and (3.7) leads to the final expression for the

first Piola-Kirchoff stress tensor in terms of the displacement u_i,

$$\begin{aligned} P_{ij} = \lambda \frac{\partial u_k}{\partial a_k}\delta_{ij} + \mu\left(\frac{\partial u_i}{\partial a_j} + \frac{\partial u_j}{\partial a_i}\right) \\ + \left(\frac{\lambda}{2}\frac{\partial u_k}{\partial a_l}\frac{\partial u_k}{\partial a_l} + \mathcal{C}\frac{\partial u_k}{\partial a_k}\frac{\partial u_l}{\partial a_l}\right)\delta_{ij} + \mathcal{B}\frac{\partial u_k}{\partial a_k}\frac{\partial u_i}{\partial a_j} + \frac{\mathcal{A}}{4}\frac{\partial u_i}{\partial a_k}\frac{\partial u_k}{\partial a_j} \\ + \frac{\mathcal{B}}{2}\left(\frac{\partial u_k}{\partial a_l}\frac{\partial u_k}{\partial a_l} + \frac{\partial u_k}{\partial a_l}\frac{\partial u_l}{\partial a_k}\right)\delta_{ij} + (\lambda + \mathcal{B})\frac{\partial u_k}{\partial a_k}\frac{\partial u_j}{\partial a_i} \\ + \left(\mu + \frac{\mathcal{A}}{4}\right)\left(\frac{\partial u_j}{\partial a_k}\frac{\partial u_i}{\partial a_k} + \frac{\partial u_k}{\partial a_j}\frac{\partial u_k}{\partial a_i} + \frac{\partial u_j}{\partial a_k}\frac{\partial u_k}{\partial a_i}\right). \end{aligned} \tag{3.8}$$

Note that this expression consists of a linear part that equals the expression for the Cauchy stress tensor (2.14) and a nonlinear part of second order in u_i. Hence, one can express P_{ij} as

$$P_{ij} = P_{ij}^L + P_{ij}^{NL} \tag{3.9}$$

with

$$P_{ij}^L = \lambda \frac{\partial u_k}{\partial a_k}\delta_{ij} + \mu\left(\frac{\partial u_i}{\partial a_j} + \frac{\partial u_j}{\partial a_i}\right) \tag{3.10}$$

$$\begin{aligned} P_{ij}^{NL} = \left(\frac{\lambda}{2}\frac{\partial u_k}{\partial a_l}\frac{\partial u_k}{\partial a_l} + \mathcal{C}\frac{\partial u_k}{\partial a_k}\frac{\partial u_l}{\partial a_l}\right)\delta_{ij} + \mathcal{B}\frac{\partial u_k}{\partial a_k}\frac{\partial u_i}{\partial a_j} + \frac{\mathcal{A}}{4}\frac{\partial u_i}{\partial a_k}\frac{\partial u_k}{\partial a_j} \\ + \frac{\mathcal{B}}{2}\left(\frac{\partial u_k}{\partial a_l}\frac{\partial u_k}{\partial a_l} + \frac{\partial u_k}{\partial a_l}\frac{\partial u_l}{\partial a_k}\right)\delta_{ij} + (\lambda + \mathcal{B})\frac{\partial u_k}{\partial a_k}\frac{\partial u_j}{\partial a_i} \\ + \left(\mu + \frac{\mathcal{A}}{4}\right)\left(\frac{\partial u_j}{\partial a_k}\frac{\partial u_i}{\partial a_k} + \frac{\partial u_k}{\partial a_j}\frac{\partial u_k}{\partial a_i} + \frac{\partial u_j}{\partial a_k}\frac{\partial u_k}{\partial a_i}\right). \end{aligned} \tag{3.11}$$

The equations of motion (3.2) can therefore be written as

$$\rho\,\frac{\partial^2 u_i}{\partial t^2} - \frac{\partial P_{ji}^L}{\partial a_j} = \frac{\partial P_{ji}^{NL}}{\partial a_j}, \tag{3.12}$$

with

$$\frac{\partial P_{ji}^{L}}{\partial a_j} = \lambda \frac{\partial^2 u_k}{\partial a_k \partial a_i} + \mu \left(\frac{\partial^2 u_i}{\partial a_j^2} + \frac{\partial^2 u_j}{\partial a_i \partial a_j} \right), \tag{3.13}$$

$$\begin{aligned} \frac{\partial P_{ji}^{NL}}{\partial a_j} = & \left(\mu + \frac{\mathcal{A}}{4} \right) \left(\frac{\partial^2 u_l}{\partial a_k^2} \frac{\partial u_l}{\partial a_i} + \frac{\partial^2 u_l}{\partial a_k^2} \frac{\partial u_i}{\partial a_l} + 2 \frac{\partial^2 u_i}{\partial a_k \partial a_l} \frac{\partial u_l}{\partial a_k} \right) \\ & + \left(\lambda + \mu + \frac{\mathcal{A}}{4} + \mathcal{B} \right) \left(\frac{\partial^2 u_l}{\partial a_i \partial a_k} \frac{\partial u_l}{\partial a_k} + \frac{\partial^2 u_k}{\partial a_l \partial a_k} \frac{\partial u_i}{\partial a_l} \right) \\ & + (\lambda + \mathcal{B}) \left(\frac{\partial^2 u_i}{\partial a_k^2} \frac{\partial u_l}{\partial a_l} \right) + (\mathcal{B} + 2\mathcal{C}) \left(\frac{\partial^2 u_k}{\partial a_i \partial a_k} \frac{\partial u_l}{\partial a_l} \right) \\ & + \left(\frac{\mathcal{A}}{4} + \mathcal{B} \right) \left(\frac{\partial^2 u_k}{\partial a_l \partial a_k} \frac{\partial u_l}{\partial a_i} + \frac{\partial^2 u_l}{\partial a_i \partial a_k} \frac{\partial u_k}{\partial a_l} \right). \end{aligned} \tag{3.14}$$

3.2 Perturbation Method

The equations of motion given by Eq.(3.12) together with the relevant boundary conditions represent a nonlinear boundary value problem (BVP). We can apply the perturbation method to derive an approximate solution to the problem. For the derivation of a second-order approximation, assume that the total displacement field can be written as

$$\boldsymbol{u} = \boldsymbol{u}^{(1)} + \boldsymbol{u}^{(2)}, \tag{3.15}$$

where $\boldsymbol{u}^{(1)}$ is called the primary solution and $\boldsymbol{u}^{(2)}$ is called the secondary solution. The primary solution is associated with the linear part of the BVP, whereas the secondary solution arises due to nonlinearities. However, for this approach to be valid, the perturbation condition

$$|\boldsymbol{u}^{(2)}| \ll |\boldsymbol{u}^{(1)}| \tag{3.16}$$

has to hold true. Eq. (3.16) implies that $\boldsymbol{u}^{(1)}$ is the dominant solution and $\boldsymbol{u}^{(2)}$ is a small correction to $\boldsymbol{u}^{(1)}$. We remind the reader that the perturbation method will result in an approximate solution, and it can only be applied if the perturbation condition is satisfied. However, for the generation of second harmonic waves,

experiments suggest that this is usually the case in most solid state materials. The generated second harmonic field is of much smaller amplitude than the primary wave field. Applying the perturbation series (3.15) to the equations of motion (3.12) results in

$$\rho \frac{\partial^2 u_i^{(1)}}{\partial t^2} + \rho \frac{\partial^2 u_i^{(2)}}{\partial t^2} - \frac{\partial P_{ji}^L(u_i^{(1)})}{\partial a_j} - \frac{\partial P_{ji}^L(u_i^{(2)})}{\partial a_j} = \frac{\partial P_{ji}^{NL}(u_i^{(1)} + u_i^{(2)})}{\partial a_j}. \tag{3.17}$$

The right hand side of this equation contains terms in $\boldsymbol{u}^{(1)} \cdot \boldsymbol{u}^{(1)}$, $\boldsymbol{u}^{(1)} \cdot \boldsymbol{u}^{(2)}$ and $\boldsymbol{u}^{(2)} \cdot \boldsymbol{u}^{(2)}$. However, due to the perturbation condition (3.16)

$$\left|\boldsymbol{u}^{(2)} \cdot \boldsymbol{u}^{(2)}\right| \ll \left|\boldsymbol{u}^{(1)} \cdot \boldsymbol{u}^{(2)}\right| \ll \left|\boldsymbol{u}^{(1)} \cdot \boldsymbol{u}^{(1)}\right|, \tag{3.18}$$

terms in $\boldsymbol{u}^{(2)}$ can be neglected. Thus, one obtains

$$\rho \frac{\partial^2 u_i^{(1)}}{\partial t^2} + \rho \frac{\partial^2 u_i^{(2)}}{\partial t^2} - \frac{\partial P_{ji}^L(u_i^{(1)})}{\partial a_j} - \frac{\partial P_{ji}^L(u_i^{(2)})}{\partial a_j} = \frac{\partial P_{ji}^{NL}(u_i^{(1)})}{\partial a_j}, \tag{3.19}$$

and this BVP can be decomposed into

$$\rho \frac{\partial^2 u_i^{(1)}}{\partial t^2} - \frac{\partial P_{ji}^L(u_i^{(1)})}{\partial a_j} = 0, \tag{3.20}$$

$$\rho \frac{\partial^2 u_i^{(2)}}{\partial t^2} - \frac{\partial P_{ji}^L(u_i^{(2)})}{\partial a_j} = \frac{\partial P_{ji}^{NL}(u_i^{(1)})}{\partial a_j}. \tag{3.21}$$

Hence, the nonlinear BVP (3.19) has been replaced by the linear homogeneous BVP (3.20) and the linear inhomogeneous BVP (3.21). Once the homogeneous BVP has been solved for the primary field $\boldsymbol{u}^{(1)}$, the forcing term on the right-hand side of the inhomogeneous BVP can be computed. Solving the inhomogeneous BVP yields the desired secondary solution $\boldsymbol{u}^{(2)}$.

As in the linear case, the curl of a P-wave field and the divergence of an SV-wave field vanish. This makes it possible to write the equations of motion as

$$\frac{\partial^2 u_i^{(1)}}{\partial t^2} - c_0^2 \frac{\partial^2 u_i^{(1)}}{\partial a_k \partial a_k} = 0, \tag{3.22}$$

$$\frac{\partial^2 u_i^{(2)}}{\partial t^2} - c_0^2 \frac{\partial^2 u_i^{(2)}}{\partial a_k \partial a_k} = \frac{1}{\rho} \frac{\partial P_{ji}^{NL}(u_i^{(1)})}{\partial a_j} \tag{3.23}$$

where c_0 is either the longitudinal wave speed c_P or the shear wave speed c_S.

Note that the outlined perturbation procedure can also be applied successively if one wants to compute higher order solutions $\boldsymbol{u}^{(3)}$, $\boldsymbol{u}^{(4)}$ and so on. As mentioned before, the amplitudes of the higher harmonics are orders of magnitude smaller, and therefore we will limit ourselves to the second order terms in this work. For more details on the perturbation method, the reader is referred to the book by Bender and Orszag [3].

The complete solution of the nonlinear boundary value problem is outlined in Fig.3.2.

3.3 Bulk Interaction of Elastic Waves

Whenever consider nonlinearities in an elastic solid are considered, interaction effects of the waves present in the bulk must be taken into account. In general, one can say that a wave can interact with itself (self-interaction) or two different waves can interact with each other (cross-interaction). In both cases, such an interaction will result in the generation of a new secondary wave. Which waves will be created depends on the types of the interacting waves (P-, SV- or SH-waves). Again, this is a purely nonlinear phenomenon and thus, the principle of linear superposition does not hold. There is no interaction of waves in an elastic solid if we restrict ourselves to a linear framework.

In the following, it will be clarified how different waves interact with each other. This plays an important role in determining the right-hand side of the linear inhomogeneous BVP (3.21).

As derived above, the right hand side of Eq.(3.21) can be given in terms of the

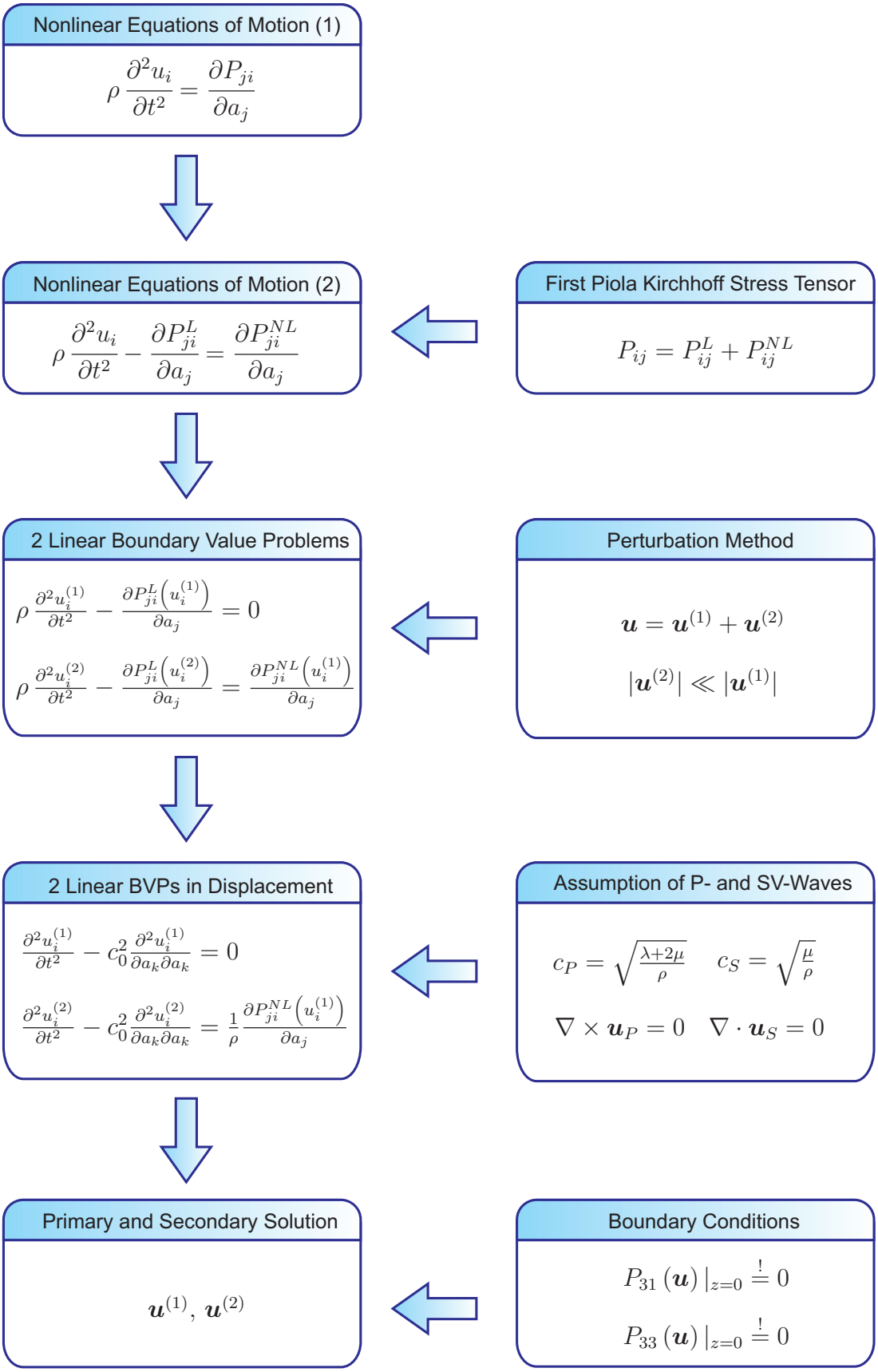

Figure 3.2: Solution Procedure for the Nonlinear BVP.

primary field $\boldsymbol{u}^{(1)}$ as

$$\begin{aligned}\frac{\partial P_{ji}^{NL}}{\partial a_j} &= \left(\mu+\frac{\mathcal{A}}{4}\right)\left(\frac{\partial^2 u_l^{(1)}}{\partial a_k^2}\frac{\partial u_l^{(1)}}{\partial a_i}+\frac{\partial^2 u_l^{(1)}}{\partial a_k^2}\frac{\partial u_i^{(1)}}{\partial a_l}+2\frac{\partial^2 u_i^{(1)}}{\partial a_k \partial a_l}\frac{\partial u_l^{(1)}}{\partial a_k}\right)\\ &+\left(\lambda+\mu+\frac{\mathcal{A}}{4}+\mathcal{B}\right)\left(\frac{\partial^2 u_l^{(1)}}{\partial a_i \partial a_k}\frac{\partial u_l^{(1)}}{\partial a_k}+\frac{\partial^2 u_k^{(1)}}{\partial a_l \partial a_k}\frac{\partial u_i^{(1)}}{\partial a_l}\right)\\ &+(\lambda+\mathcal{B})\left(\frac{\partial^2 u_i^{(1)}}{\partial a_k^2}\frac{\partial u_l^{(1)}}{\partial a_l}\right)+(\mathcal{B}+2\mathcal{C})\left(\frac{\partial^2 u_k^{(1)}}{\partial a_i \partial a_k}\frac{\partial u_l^{(1)}}{\partial a_l}\right)\\ &+\left(\frac{\mathcal{A}}{4}+\mathcal{B}\right)\left(\frac{\partial^2 u_k^{(1)}}{\partial a_l \partial a_k}\frac{\partial u_l^{(1)}}{\partial a_i}+\frac{\partial^2 u_l^{(1)}}{\partial a_i \partial a_k}\frac{\partial u_k^{(1)}}{\partial a_l}\right).\end{aligned} \tag{3.24}$$

Eq. (3.24) contains products of exponential terms. It is important to remember that we are only interested in the real part of every exponential term, since this part represents the physical wave. Let us consider the multiplication of the real parts of two complex exponentials,

$$\Re\left\{e^{j(\omega t-\boldsymbol{k}_I\boldsymbol{x})}\right\}\cdot\Re\left\{e^{j(\omega t-\boldsymbol{k}_{II}\boldsymbol{x})}\right\}. \tag{3.25}$$

The result of this multiplication is

$$\frac{1}{2}\left\{\cos\left(2\omega t-(\boldsymbol{k}_I+\boldsymbol{k}_{II})\boldsymbol{x}\right)\right\}+\cos\left((\boldsymbol{k}_I+\boldsymbol{k}_{II})\boldsymbol{x}\right)\}. \tag{3.26}$$

However, in this thesis we are only concerned about the time-dependent terms (harmonics), and thus the second cos term in (3.26) will be neglected. The remaining expression therefore is

$$\frac{1}{2}\left\{\cos\left(2\omega t-(\boldsymbol{k}_I+\boldsymbol{k}_{II})\boldsymbol{x}\right)\right\}. \tag{3.27}$$

Note that the term above is given in an exponential form,

$$\frac{1}{2}e^{j(2\omega t-(\boldsymbol{k}_I+\boldsymbol{k}_{II})\boldsymbol{x})}. \tag{3.28}$$

As in the case for the primary wave, this representation necessitates to keep in mind that only the real part of (3.28) represents the physical wave. If one considers the interaction between two primary waves of same frequency ω and amplitudes U_I and

U_{II}, wavenumbers k_I and k_{II}, it can be seen that the resulting right-hand side in Eq. (3.21) can be written as

$$\frac{1}{\rho}\nabla \boldsymbol{P}^{NL} = \beta^{bulk} U_I U_{II} e^{j(2\omega t - kx\sin\theta - kz\cos\theta)}\boldsymbol{d} \tag{3.29}$$

where β^{bulk} is a nonlinear parameter, k is the resulting wave number and $\boldsymbol{d}$ is the displacement vector. In the following sections, we will outline how to derive the nonlinear parameters β^{bulk} for different cases of interaction. The index *bulk* indicates that this nonlinear parameter is only due to bulk interaction, i.e. the boundary does not affect it. Note that the factor $\frac{1}{2}$ derived above is included in this parameter. For more information on the interaction of elastic waves, the work by Gol'dberg [11] and Jones and Kobett [15] is recommended. Due to the tedious algebra involved in the derivation process, MATHEMATICA [24] was used as a tool to simplify symbolic expressions. The expressions needed for the cases considered in Chapter 4 are given in the Appendix.

3.3.1 Self-Interaction

In the case of self-interaction, $\boldsymbol{u}^{(1)}$ will only consist of a single wave

$$\boldsymbol{u}^{(1)} = \boldsymbol{U}_I e^{j(\omega t - k_I x\sin\theta - k_I z\cos\theta)}, \tag{3.30}$$

where $\boldsymbol{U}_I$ represents the amplitude and k_I the wavenumber of the considered wave. Plugging this general form of a wave into Eq. (3.24) will result in

$$\begin{aligned}\nabla \boldsymbol{P}^{NL} = j\Bigg[&\left(\lambda + 2\mu + \frac{\mathcal{A}}{2} + \mathcal{B}\right)(\boldsymbol{U}_I\cdot\boldsymbol{U}_I)(\boldsymbol{k_I}\cdot\boldsymbol{k_I})\,\boldsymbol{k}_I \\ &+ (2\lambda + 4\mu + \mathcal{A} + 2\mathcal{B})(\boldsymbol{U}_I\cdot\boldsymbol{k}_I)(\boldsymbol{k}_I\cdot\boldsymbol{k}_I)\,\boldsymbol{U}_I \\ &+ \left(\frac{\mathcal{A}}{2} + 3\mathcal{B} + 2\mathcal{C}\right)(\boldsymbol{U}_I\cdot\boldsymbol{k}_I)(\boldsymbol{U}_I\cdot\boldsymbol{k}_I)\,\boldsymbol{k}_I\Bigg]\frac{1}{2}\,e^{j(2\omega t - 2k_I x\sin\theta - 2k_I z\cos\theta)}\end{aligned} \tag{3.31}$$

The wave vector of the generated second harmonic wave is given by

$$\boldsymbol{k} = 2\boldsymbol{k}_I. \tag{3.32}$$

In the follwing, expression (3.31) will be used to determine the parameters β^{bulk} corresponding to the self-interation of different waves.

3.3.1.1 Self-Interaction of a P-Wave

In order to determine the forcing term due to self-interaction of a P-wave, set

$$\boldsymbol{U}_I = U_P \begin{bmatrix} \sin\theta_P \\ 0 \\ \cos\theta_P \end{bmatrix}, \qquad \boldsymbol{k}_I = k_P \begin{bmatrix} \sin\theta_P \\ 0 \\ \cos\theta_P \end{bmatrix}. \tag{3.33}$$

After some simplifications, we obtain

$$\nabla \boldsymbol{P}^{NL} = jk_P^3(3\lambda + 6\mu + 2\mathcal{A} + 6\mathcal{B} + 2\mathcal{C})U_P^2 \begin{bmatrix} \sin\theta_P \\ 0 \\ \cos\theta_P \end{bmatrix} \frac{1}{2}\, e^{j(2\omega t - 2k_P x \sin\theta_P - 2k_P z\cos\theta_P)}, \tag{3.34}$$

and therefore the nonlinearity parameter for self-interaction of a P-wave is given by

$${}_P\beta_{PP}^{bulk} = \frac{jk_P^3}{2\rho}(3\lambda + 6\mu + 2\mathcal{A} + 6\mathcal{B} + 2\mathcal{C}) \tag{3.35}$$

The prior index P indicates that the nonlinearity parameter corresponds to a P-wave, which is determined by the displacement vector. The two posterior indices PP indicate that this nonlinearity parameter is caused by self-interaction of the primary wave $\boldsymbol{u}_P$. Note that the nonlinearity parameter could also be expressed using the Brugger constants,

$${}_P\beta_{PP}^{bulk} = \frac{jk_P^3}{2\rho}(3\lambda + 6\mu + 2\mathcal{A} + 6\mathcal{B} + 2\mathcal{C}) = \frac{jk_P^3}{2\rho}\frac{3c_{111} + c_{11}}{c_{11}}. \tag{3.36}$$

The fraction $\dfrac{3c_{111} + c_{11}}{c_{11}}$ is the well-known acoustic nonlinearity parameter for a longitudinal wave [23].

3.3.1.2 Self-Interaction of an SV-Wave

Accordingly, to determine the forcing term due to self-interaction of an SV-wave, set

$$\boldsymbol{U}_I = U_S \begin{bmatrix} \cos\theta_S \\ 0 \\ -\sin\theta_S \end{bmatrix}, \qquad \boldsymbol{k}_I = k_S \begin{bmatrix} \sin\theta_S \\ 0 \\ \cos\theta_S \end{bmatrix}. \tag{3.37}$$

After some simplifications, one obtains

$$\nabla \boldsymbol{P}^{NL} = jk_S^3 \left(\lambda + 2\mu + \frac{\mathcal{A}}{2} + \mathcal{B}\right) U_S^2 \begin{bmatrix} \sin\theta_S \\ 0 \\ \cos\theta_S \end{bmatrix} \frac{1}{2}\, e^{j(2\omega t - 2k_S x \sin\theta_S - 2k_S z \cos\theta_S)}, \tag{3.38}$$

and therefore the nonlinear parameter for self-interaction of an SV-wave is given by

$${}_P\beta_{SS}^{bulk} = \frac{jk_S^3}{2\rho}\left(\lambda + 2\mu + \frac{\mathcal{A}}{2} + \mathcal{B}\right) \tag{3.39}$$

Hence, the bulk interaction of an SV-wave with itself leads to a P-wave. There is no bulk nonlinearity corresponding to an SV wave, i.e.

$${}_S\beta_{SS}^{bulk} = 0. \tag{3.40}$$

3.3.2 Cross-Interaction

In the case of cross-interaction, the forcing term in Eq. (3.24) will become

$$
\begin{aligned}
\nabla \boldsymbol{P}^{NL} = j \Bigg[& \left(\mu + \frac{\mathcal{A}}{4}\right) (\boldsymbol{k}_{II} \cdot \boldsymbol{k}_{II}) (\boldsymbol{U}_I \cdot \boldsymbol{U}_{II}) \boldsymbol{k}_I + \left(\mu + \frac{\mathcal{A}}{4}\right) (\boldsymbol{k}_I \cdot \boldsymbol{k}_I) (\boldsymbol{U}_I \cdot \boldsymbol{U}_{II}) \boldsymbol{k}_{II} \\
& + \left(\mu + \frac{\mathcal{A}}{4}\right) (\boldsymbol{k}_I \cdot \boldsymbol{k}_I) (\boldsymbol{U}_I \cdot \boldsymbol{k}_{II}) \boldsymbol{U}_{II} + \left(\mu + \frac{\mathcal{A}}{4}\right) (\boldsymbol{k}_{II} \cdot \boldsymbol{k}_{II}) (\boldsymbol{U}_{II} \cdot \boldsymbol{k}_I) \boldsymbol{U}_I \\
& + 2\left(\mu + \frac{\mathcal{A}}{4}\right) (\boldsymbol{k}_I \cdot \boldsymbol{k}_{II}) (\boldsymbol{U}_I \cdot \boldsymbol{k}_{II}) \boldsymbol{U}_{II} + 2\left(\mu + \frac{\mathcal{A}}{4}\right) (\boldsymbol{k}_I \cdot \boldsymbol{k}_{II}) (\boldsymbol{U}_{II} \cdot \boldsymbol{k}_I) \boldsymbol{U}_I \\
& + \left(\lambda + \mu + \frac{\mathcal{A}}{4} + \mathcal{B}\right) (\boldsymbol{k}_I \cdot \boldsymbol{k}_{II}) (\boldsymbol{U}_I \cdot \boldsymbol{U}_{II}) \boldsymbol{k}_{II} + \left(\lambda + \mu + \frac{\mathcal{A}}{4} + \mathcal{B}\right) (\boldsymbol{k}_I \cdot \boldsymbol{k}_{II}) (\boldsymbol{U}_I \cdot \boldsymbol{U}_{II}) \boldsymbol{k}_I \\
& + \left(\lambda + \mu + \frac{\mathcal{A}}{4} + \mathcal{B}\right) (\boldsymbol{k}_I \cdot \boldsymbol{k}_{II}) (\boldsymbol{U}_I \cdot \boldsymbol{k}_I) \boldsymbol{U}_{II} + \left(\lambda + \mu + \frac{\mathcal{A}}{4} + \mathcal{B}\right) (\boldsymbol{k}_I \cdot \boldsymbol{k}_{II}) (\boldsymbol{U}_{II} \cdot \boldsymbol{k}_{II}) \boldsymbol{U}_I \\
& + (\lambda + \mathcal{B}) (\boldsymbol{k}_I \cdot \boldsymbol{k}_I) (\boldsymbol{U}_{II} \cdot \boldsymbol{k}_{II}) \boldsymbol{U}_I + (\lambda + \mathcal{B}) (\boldsymbol{k}_{II} \cdot \boldsymbol{k}_{II}) (\boldsymbol{U}_I \cdot \boldsymbol{k}_I) \boldsymbol{U}_{II} \\
& + (\mathcal{B} + 2\mathcal{C}) (\boldsymbol{U}_I \cdot \boldsymbol{k}_I) (\boldsymbol{U}_{II} \cdot \boldsymbol{k}_{II}) \boldsymbol{k}_{II} + (\mathcal{B} + 2\mathcal{C}) (\boldsymbol{U}_I \cdot \boldsymbol{k}_I) (\boldsymbol{U}_{II} \cdot \boldsymbol{k}_{II}) \boldsymbol{k}_I \\
& + \left(\frac{\mathcal{A}}{4} + \mathcal{B}\right) (\boldsymbol{U}_I \cdot \boldsymbol{k}_{II}) (\boldsymbol{U}_{II} \cdot \boldsymbol{k}_{II}) \boldsymbol{k}_I + \left(\frac{\mathcal{A}}{4} + \mathcal{B}\right) (\boldsymbol{U}_I \cdot \boldsymbol{k}_I) (\boldsymbol{U}_{II} \cdot \boldsymbol{k}_I) \boldsymbol{k}_{II} \\
& + \left(\frac{\mathcal{A}}{4} + \mathcal{B}\right) (\boldsymbol{U}_I \cdot \boldsymbol{k}_{II}) (\boldsymbol{U}_{II} \cdot \boldsymbol{k}_I) \boldsymbol{k}_I + \left(\frac{\mathcal{A}}{4} + \mathcal{B}\right) (\boldsymbol{U}_I \cdot \boldsymbol{k}_{II}) (\boldsymbol{U}_{II} \cdot \boldsymbol{k}_I) \boldsymbol{k}_{II} \Bigg] \\
& \cdot \frac{1}{2} e^{j(2\omega t - (k_I \sin\theta_I + k_{II} \sin\theta_{II})x - (k_I \cos\theta_I + k_{II} \cos\theta_{II})z)}
\end{aligned}
\tag{3.41}
$$

The wave vector of second harmonic waves generated by cross-interaction is given by

$$
\boldsymbol{k} = \boldsymbol{k}_I + \boldsymbol{k}_{II} \tag{3.42}
$$

Expression (3.41) can be used to obtain the bulk nonlinearity parameters β^{bulk} corresponding to the cross-interaction of two waves. Since the expression above is somewhat lengthy, MATHEMATICA was used to determine the exact expressions of the parameters. In the following, we explain the general procedure to obtain these parameters. The complete expressions for the interactions needed in Chapter 4 are given in the appendix.

3.3.2.1 Cross-Interaction of two P-Waves

Consider two P-waves of the same frequency propagating in two different directions,

$$\boldsymbol{U}_I = U_{P_I} \begin{bmatrix} \sin\theta_{P_I} \\ 0 \\ \cos\theta_{P_I} \end{bmatrix}, \qquad \boldsymbol{k}_{P_I} = k_{P_I} \begin{bmatrix} \sin\theta_{P_I} \\ 0 \\ \cos\theta_{P_I} \end{bmatrix} \tag{3.43}$$

and

$$\boldsymbol{U}_{II} = U_{P_{II}} \begin{bmatrix} \sin\theta_{P_{II}} \\ 0 \\ \cos\theta_{P_{II}} \end{bmatrix}, \qquad \boldsymbol{k}_{II} = k_{P_{II}} \begin{bmatrix} \sin\theta_{P_{II}} \\ 0 \\ \cos\theta_{P_{II}} \end{bmatrix} \tag{3.44}$$

No general solution is given here but instead we refer to the appendix. However, we point out that the cross-interaction of two P-waves in the bulk will always result in a second harmonic P-wave characterized by ${}_P\beta^{bulk}_{P_I P_{II}}$.

3.3.2.2 Cross-Interaction of two SV-Waves

Now consider two SV-waves of the same frequency propagating in two different directions,

$$\boldsymbol{U}_I = U_{S_I} \begin{bmatrix} \cos\theta_{S_I} \\ 0 \\ -\sin\theta_{S_I} \end{bmatrix}, \qquad \boldsymbol{k}_I = k_{S_I} \begin{bmatrix} \sin\theta_{S_I} \\ 0 \\ \cos\theta_{S_I} \end{bmatrix} \tag{3.45}$$

and

$$\boldsymbol{U}_{II} = U_{S_{II}} \begin{bmatrix} \cos\theta_{S_{II}} \\ 0 \\ -\sin\theta_{S_{II}} \end{bmatrix}, \qquad \boldsymbol{k}_{II} = k_{S_{II}} \begin{bmatrix} \sin\theta_{S_{II}} \\ 0 \\ \cos\theta_{S_{II}} \end{bmatrix} \tag{3.46}$$

As a result, the cross-interaction of two SV-waves in the bulk results in a second harmonic P-wave characterized by ${}_P\beta^{bulk}_{S_I S_{II}}$. As in the case of self-interaction of an SV-wave, there is no shear wave generated in the bulk,

$${}_S\beta^{bulk}_{S_I S_{II}} = 0. \tag{3.47}$$

3.3.2.3 Cross-Interaction of a P- and an SV-Wave

For the final case of cross-interaction of a P- and an SV-wave, assume two waves given by

$$\boldsymbol{U}_I = U_P \begin{bmatrix} \sin\theta_P \\ 0 \\ \cos\theta_P \end{bmatrix}, \qquad \boldsymbol{k}_P = k_P \begin{bmatrix} \sin\theta_P \\ 0 \\ \cos\theta_P \end{bmatrix} \tag{3.48}$$

and

$$\boldsymbol{U}_{II} = U_S \begin{bmatrix} \cos\theta_S \\ 0 \\ \sin\theta_S \end{bmatrix}, \qquad \boldsymbol{k}_{II} = k_S \begin{bmatrix} \sin\theta_S \\ 0 \\ \cos\theta_S \end{bmatrix}. \tag{3.49}$$

Again, we do not give the general result due to a lack of space but refer to the appendix. Note that the interaction of a P- and an SV-wave will result both in a second harmonic P-wave and a second harmonic SV-wave. The corresponding bulk parameters will be ${}_P\beta^{bulk}_{PS} (= {}_P\beta^{bulk}_{SP})$ and ${}_S\beta^{bulk}_{PS} (= {}_S\beta^{bulk}_{SP})$.

The self- and cross-interaction of the different elastic waves is illustrated in Fig. 3.3.

3.4 General Solution of the Equations of Motion

In the following section, a general solution to the equations of motion will be derived. This solution contains several unspecified constants, which will be determined in the next chapter for each specific problem. This solution follows the outline made by Zhou and al. [26]. However, the result will be different due to a different choice of parameters.

After application of the perturbation method and the right-hand side is replaced

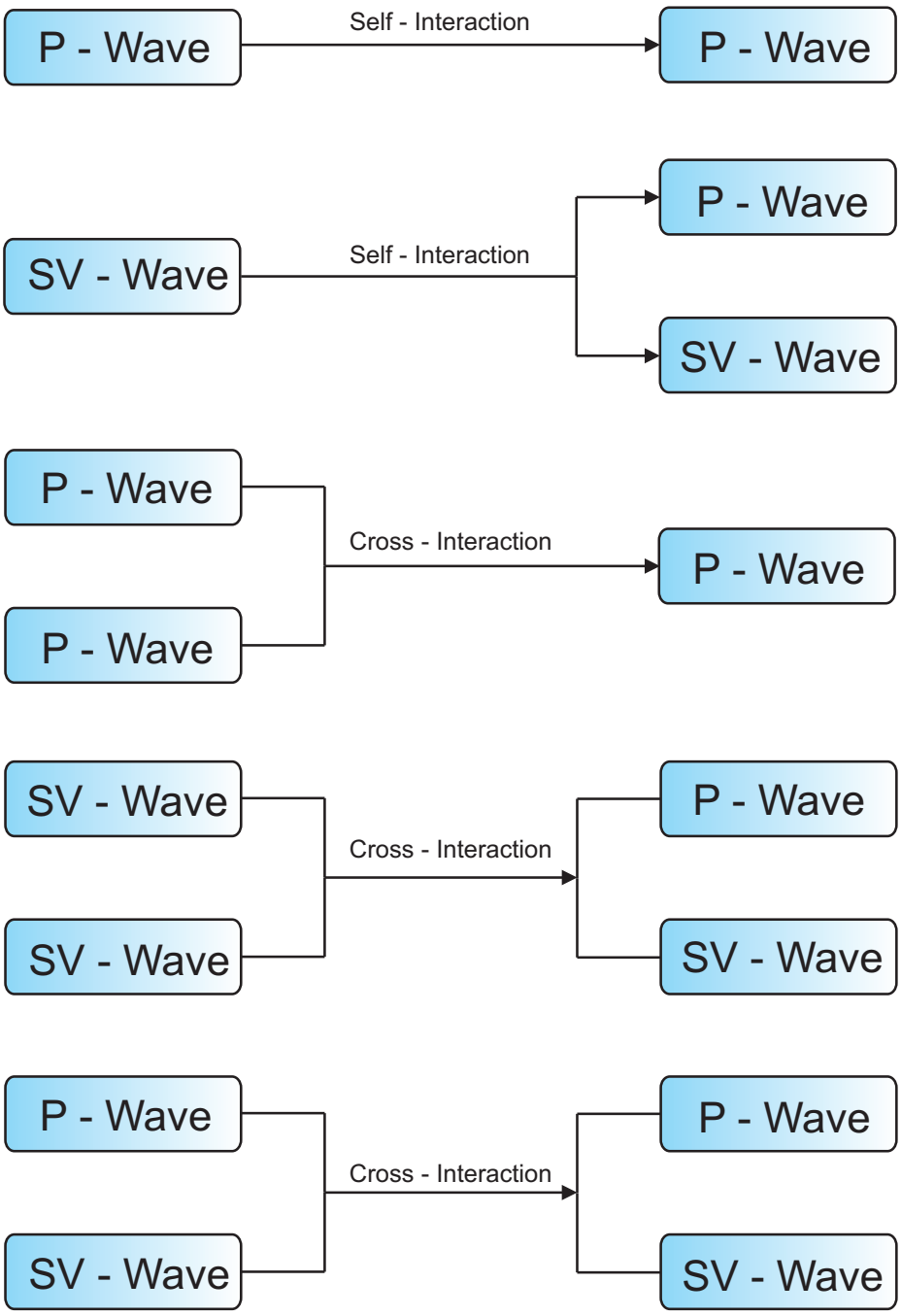

Figure 3.3: Self- and Cross-Interaction of Elastic Waves.

with (3.29). The resulting linear BVPs become

$$\frac{\partial^2 u_i^{(1)}}{\partial t^2} - c_0^2 \frac{\partial^2 u_i^{(1)}}{\partial a_k \partial a_k} = 0, \tag{3.50}$$

$$\frac{\partial^2 u_i^{(2)}}{\partial t^2} - c_0^2 \frac{\partial^2 u_i^{(2)}}{\partial a_k \partial a_k} = \beta^{bulk} U_I U_{II} e^{j(2\omega t - kx\sin\theta - kz\cos\theta)} d_i. \tag{3.51}$$

Using an ansatz, the linear homogeneous BVP (3.50) can easily be solved for the primary field $\boldsymbol{u}^{(1)}$ to be

$$\boldsymbol{u}^{(1)} = A e^{j(\omega t - k_0 x\sin\theta - k_0 z\cos\theta)} \boldsymbol{d}, \tag{3.52}$$

where A is an undetermined constant. In Chapter 4, it will be seen that the primary field caused by linear reflection of the incident P-wave also represents the solution to Eq. (3.50) and is of the form (3.52).

The solution to the inhomogeneous problem (3.51) is slightly more difficult. In the following, we will derive the solution to this problem which consists of a homogeneous solution and a particular solution.

3.4.1 Homogeneous Solution

Before we begin to derive the desired solution, we note that the left-hand side and the right-hand side of equation (3.51) should have the same kinf of displacement vector. As a consequence, it is sufficient to solve the scalar problem

$$\frac{\partial^2 u^{(2)}}{\partial t^2} - c_0^2 \frac{\partial^2 u^{(2)}}{\partial a_k \partial a_k} = \beta^{bulk} U_I U_{II} e^{j(2\omega t - kx\sin\theta - kz\cos\theta)}. \tag{3.53}$$

Using an ansatz similar as in the case of the primary solution $\boldsymbol{u}^{(1)}$, one obtains the homogeneous solution

$$u_{hom}^{(2)} = B e^{j(2\omega t - 2k_0 x\sin\theta - 2k_0 z\cos\theta)}, \tag{3.54}$$

where B is a constant to be determined.

3.4.2 Particular Solution

For the particular solution, use an ansatz

$$u_{part}^{(2)} = (Cx + Dz + E)\, e^{j(2\omega t - kx\sin\theta - kz\cos\theta)}. \tag{3.55}$$

Plugging this ansatz into the equations of motion leads to

$$\left[-4\omega^2 + c_0^2 k^2\right](Cx + Dz + E) + 2jc_0^2 kA\sin\theta + 2jc_0^2 kB\cos\theta = \beta^{bulk} U_I U_{II}. \tag{3.56}$$

Since the right-hand side of the latter equation does not contain any terms in x and z, the left-hand side cannot either. This leads to the two cases of *resonance* and *non-resonance*.

3.4.2.1 Non-Resonant Case

In the non-resonant case, it holds

$$k \neq 2k_0. \tag{3.57}$$

Thus, in order to satisfy Eq. (3.56),

$$C \stackrel{!}{=} 0 \quad \text{and} \quad D \stackrel{!}{=} 0. \tag{3.58}$$

The remainder of Eq. (3.56) can be solved for the constant E,

$$E = \frac{U_I U_{II} \beta^{bulk}}{c_0^2\,(k^2 - 4k_0^2)}. \tag{3.59}$$

The particular solution in the non-resonant case therefore becomes

$$u_{part}^{(2)} = \frac{U_I U_{II} \beta^{bulk}}{c_0^2\,(k^2 - 4k_0^2)} e^{j(2\omega t - kx\sin\theta - kz\cos\theta)}. \tag{3.60}$$

3.4.2.2 Resonant Case

In the resonant case, the resonance condition

$$k = 2k_0 \tag{3.61}$$

must be satisfied. Applying $\omega = c_0 k_0$ shows that this choice of k makes the terms in x and z vanish. There are three remaining constants, C, D, E, where C and D are related by the remainder of Eq. (3.56),

$$C = \beta^{bulk} \frac{U_I U_{II}}{4jk_0 c_0^2 \sin\theta} - \frac{\cos\theta}{\sin\theta} B. \tag{3.62}$$

This means

$$\begin{aligned} Cx + Dz + E &= \left(\beta^{bulk} \frac{U_I U_{II}}{4jk_0 c_0^2 \sin\theta} - \frac{\cos\theta}{\sin\theta} C \right) x + Dz + E \\ &= \frac{U_I U_{II}}{4jk_0 c_0^2} \left[\left(\frac{\beta^{bulk}}{\sin\theta} - \frac{4jk_0 c_0^2}{U_I U_{II}} \frac{\cos\theta}{\sin\theta} D \right) x + \frac{4jk_0 c_0^2}{U_I U_{II}} Dz \right] + E, \end{aligned} \tag{3.63}$$

and with the introduction of a new parameter β^{surf}

$$\beta^{surf} = \frac{\beta^{bulk}}{\sin^2\theta} - \frac{4jk_0 c_0^2}{U_I U_{II}} \frac{\cos\theta}{\sin\theta} D \tag{3.64}$$

we obtain

$$Cx + Dz + E = \frac{U_I U_{II}}{4jk_0 c_0^2} \left[\beta^{surf} \sin\theta x + \left(\frac{\beta^{bulk} - \beta^{surf} \sin^2\theta}{\cos\theta} \right) z \right] + E. \tag{3.65}$$

Hence, the particular solution in the case of resonance can be given as

$$u_{part}^{(2)} = \left\{ \frac{U_I U_{II}}{4jk_0 c_0^2} \left[\beta^{surf} \sin\theta\, x + \left(\frac{\beta^{bulk} - \beta^{surf} \sin^2\theta}{\cos\theta} \right) z \right] + E \right\} e^{j(2\omega t - 2k_0 x \sin\theta - 2k_0 z \cos\theta)}. \tag{3.66}$$

3.4.3 Complete Solution

It is now possible to give the complete solution consisting of the homogeneous solution and the particular solution.

3.4.3.1 Non-Resonant Case

In the non-resonant case, $k \neq 2k_0$ holds and the solution is given by

$$\begin{aligned} u^{(2)} = &\frac{U_I U_{II} \beta^{bulk}}{c_0^2 (k^2 - 4k_0^2)} e^{j(2\omega t - kx \sin\theta - kz \cos\theta)} \\ &+ \gamma^{surf} e^{j(2\omega t - 2k_0 x \sin\theta - 2k_0 z \cos\theta)} \end{aligned} \tag{3.67}$$

with

$$\gamma^{surf} = B. \tag{3.68}$$

However, note that the part

$$\gamma^{surf} e^{j(2\omega t - 2k_0 x \sin\theta - 2k_0 z \cos\theta)} \tag{3.69}$$

does not satisfy Snell's law for angles θ corresponding to waves generated by cross-interaction. Therefore, this part of the solution is excluded. The same result is achieved if one keeps this part and applies the boundary conditions. It can be seen, that these parts must vanish, because there will be no matching exponential terms.

3.4.3.2 Resonant Case

For $k = 2k_0$, the complete solution is given by

$$\begin{aligned} u^{(2)} = \frac{U_I U_{II}}{4jk_0 c_0^2} \left[\beta^{surf} \sin\theta\, x + \left(\frac{\beta^{bulk} - \beta^{surf} \sin^2\theta}{\cos\theta} \right) z \right] e^{j(2\omega t - 2k_0 x \sin\theta - 2k_0 z \cos\theta)} \\ + \gamma^{surf} e^{j(2\omega t - 2k_0 x \sin\theta - 2k_0 z \cos\theta)}. \end{aligned} \tag{3.70}$$

The parameter γ^{surf} is the amplitude of the part of the solution that is not growing with x and z. It is given by

$$\gamma^{surf} = B + E. \tag{3.71}$$

Since the part

$$\gamma^{surf} e^{j(2\omega t - 2k_0 x \sin\theta - 2k_0 z \cos\theta)} \tag{3.72}$$

now satisfies Snell's law, it does not vanish in general.

Note that the parameters β^{surf} and γ^{surf} can only be determined by applying the boundary conditions, which have not yet been considered. Their indices *surf* will remind the reader of this in the following.

Notice that there is a substantial difference in the two solutions: While the solution in the case of resonance is accumulating with growing x and z, the non-resonant solution does not show this feature. As a matter of fact, second harmonic waves that are growing with propagation distance have been observed in many experiments [16, 20]. The accumulating second harmonic is of great interest to the field of non-destructive evaluation, since it is often easier to measure than the second harmonic with constant (very small) amplitude.

3.5 Boundary Conditions

The general solution for the equations of motion given above is not yet unique since there are unknown constants β^{surf} and γ^{surf}. These can only be determined for specific boundary conditions. Again, the perturbation method will be applied to these boundary conditions.

In general, the stress is given by the Piola-Kirchhoff stress tensor given above. For the case of a free surface , the boundary conditions are given by

$$P_{31}|_{z=0} \stackrel{!}{=} 0 \quad \text{and} \quad P_{33}|_{z=0} \stackrel{!}{=} 0. \tag{3.73}$$

Assuming the solution to be of the form

$$\boldsymbol{u} = \boldsymbol{u}^{(1)} + \boldsymbol{u}^{(2)} \tag{3.74}$$

we obtain

$$P_{31}\left(\boldsymbol{u}^{(1)} + \boldsymbol{u}^{(2)}\right)|_{z=0} = P_{31}^{L}\left(\boldsymbol{u}^{(1)}\right)|_{z=0} + P_{31}^{NL}\left(\boldsymbol{u}^{(1)}\right)|_{z=0} + P_{31}^{L}\left(\boldsymbol{u}^{(2)}\right)|_{z=0} \tag{3.75}$$

and

$$P_{33}\left(\boldsymbol{u}^{(1)} + \boldsymbol{u}^{(2)}\right)|_{z=0} = P_{33}^{L}\left(\boldsymbol{u}^{(1)}\right)|_{z=0} + P_{33}^{NL}\left(\boldsymbol{u}^{(1)}\right)|_{z=0} + P_{33}^{L}\left(\boldsymbol{u}^{(2)}\right)|_{z=0} \tag{3.76}$$

where the inequalities

$$\left|\boldsymbol{u}^{(2)} \cdot \boldsymbol{u}^{(2)}\right| \ll \left|\boldsymbol{u}^{(1)} \cdot \boldsymbol{u}^{(2)}\right| \ll \left|\boldsymbol{u}^{(1)} \cdot \boldsymbol{u}^{(1)}\right| \tag{3.77}$$

have been used. The linear stresses in $\boldsymbol{u^{(1)}}$ satisfy the linear boundary conditions given by Eqs. (2.34) and (2.35),

$$P_{31}^{L}\left(\boldsymbol{u}^{(1)}\right)|_{z=0} = \sigma_{31}\left(\boldsymbol{u}^{(1)}\right)|_{z=0} = 0 \tag{3.78}$$

$$P_{33}^{L}\left(\boldsymbol{u}^{(1)}\right)|_{z=0} = \sigma_{33}\left(\boldsymbol{u}^{(1)}\right)|_{z=0} = 0. \tag{3.79}$$

The final conditions for the free boundary under perturbation are therefore given by

$$P_{31}^{L}\left(\boldsymbol{u}^{(2)}\right)|_{z=0} = -P_{31}^{NL}\left(\boldsymbol{u}^{(1)}\right)|_{z=0} \tag{3.80}$$

and

$$P_{33}^{L}\left(\boldsymbol{u}^{(2)}\right)|_{z=0} = -P_{33}^{NL}\left(\boldsymbol{u}^{(1)}\right)|_{z=0}. \tag{3.81}$$

CHAPTER IV

SECOND HARMONIC GENERATION AT A FREE BOUNDARY

With the theoretical background given in the last chapters, we can now approach the problem of the generation of second harmonic waves under presence of a free boundary. We will separately consider the case of an incident P-wave and an incident SV-wave. These cases are both of great interest for actual experiments. Using the general solution given above, we will give expressions for all involved waves. Then we will apply the boundary conditions in order to determine the unknown constants, which will lead to the complete solution.

Once the complete solution to this problem is known, we will investigate how the boundary influences the generation of the second harmonic waves. We will then discuss the accumulation behavior of the created second harmonics and which incident angles allow an easy measurement of the second harmonics. These results make it possible to choose an experimental setup that could measure nonlinearities in an efficient and practical way, since we only need access to one surface.

For the numerical studies in this chapter, we choose aluminum as our medium, since its behavior is well understood and its material properties are well known. For our purposes, we assume aluminum to be isotropic. The material properties for aluminum are taken from [19]. The values are given in Tables 4.1. For the numerical study, we assume an incident ultrasonic wave of frequency $f = 5\,\mathrm{MHz}$, amplitude $U_{P_i} = 1 \cdot 10^{-10}\,\mathrm{m}$ or, in the case of an incident SV-wave, $U_{S_i} = 1 \cdot 10^{-10}\,\mathrm{m}$. The specimen we consider has a thickness of $L = 0.2\,\mathrm{m}$.

Table 4.1: Material Properties of Aluminum.

ρ	c_P	c_S	λ	μ	$\mathcal{A}$	$\mathcal{B}$	$\mathcal{C}$
$2700\,\mathrm{kg/m^3}$	$6320\,\mathrm{m/s}$	$3130\,\mathrm{m/s}$	$54.9\,\mathrm{GPa}$	$26.5\,\mathrm{GPa}$	$-320\,\mathrm{GPa}$	$-200\,\mathrm{GPa}$	$-190\,\mathrm{GPa}$

Table 4.2: Parameters Used for Numerical Analysis.

Amplitude U_{P_i}	Frequency f	Thickness of Specimen
$1 \cdot 10^{-10}\,\mathrm{m}$	$5\,\mathrm{MHz}$	$0.2\,\mathrm{m}$

4.1 Incidence of a P-Wave

In this section, we consider an obliquely incident P-wave, its linear reflection at a free boundary and the generated secondary field. The complete solution for this case is given and the primary and secondary wave fields are presented.

4.1.1 Problem Setup for Oblique Incidence

Assume our medium to be isotropic and infinite in the $x-$ and $y-$direction and of finite thickness L in $z-$direction. Now let a P-wave of amplitude U_{P_i} be incident under an incidence angle θ_P,

$$\boldsymbol{u}_{P_i} = U_{P_i} \begin{bmatrix} \sin\theta_P \\ 0 \\ \cos\theta_P \end{bmatrix} e^{j(\omega t - k_P x \sin\theta_P + k_P z \cos\theta_P)}. \tag{4.1}$$

This wave could be excited using a longitudinal wave source located at $x = -L\tan\theta_P$, $z = L$, causing a displacement field

$$\boldsymbol{f}(t) = U_{P_i} \begin{bmatrix} \sin\theta_P \\ 0 \\ \cos\theta_P \end{bmatrix} e^{j(\omega t - k_P x \sin\theta_P + k_P z \cos\theta_P - \phi)} \tag{4.2}$$

where ϕ is a phase shift determined by the exact location of the source. The boundary conditions are determined by a stress-free surface at $z = 0$. Also see Fig. 4.1 for the problem setup.

4.1.2 Primary Wave Field

As shown in Section 2.5, mode conversion at the free boundary leads to simultaneous occurrence of a reflected P-wave and a reflected SV-wave. Their reflection angles are determined by Snell's law (2.32), and the amplitudes of the linearly reflected waves can be computed using Fresnel's formulae, (2.38) and (2.39). Then, the primary field is given by

$$\begin{aligned} \boldsymbol{u}^{(1)} = U_{P_i} \begin{bmatrix} \sin\theta_P \\ 0 \\ -\cos\theta_P \end{bmatrix} \quad & e^{j(\omega t - k_P x \sin\theta_P + k_P z \cos\theta_P)} \\ + U_{P_r} \begin{bmatrix} \sin\theta_P \\ 0 \\ \cos\theta_P \end{bmatrix} \quad & e^{j(\omega t - k_P x \sin\theta_P - k_P z \cos\theta_P)} \\ + U_{S_r} \begin{bmatrix} \cos\theta_S \\ 0 \\ -\sin\theta_S \end{bmatrix} \quad & e^{j(\omega t - k_S x \sin\theta_S - k_S z \cos\theta_S)} \end{aligned} \tag{4.3}$$

and illustrated in Fig. 4.1. In Fig. 4.2, show the amplitudes of the primary waves in aluminum are shown. Note that the presented absolute values result from the Fresnel formulae (2.38) and (2.39) using the parameters given in Tables 4.1 and 4.2.

4.1.3 Secondary Wave Field

The secondary wave field is caused by self- and cross-interactions of the primary waves. If one assumes an incident linear P-wave as illustrated above, one obtains the secondary wave field

$$\begin{aligned} \boldsymbol{u}^{(2)} = & {}_P\boldsymbol{u}^{(2)}_{P_iP_i} + {}_P\boldsymbol{u}^{(2)}_{P_iP_r} + {}_P\boldsymbol{u}^{(2)}_{P_iS_r} + {}_S\boldsymbol{u}^{(2)}_{P_iS_r} + {}_P\boldsymbol{u}^{(2)}_{P_rP_r} \\ & + {}_P\boldsymbol{u}^{(2)}_{P_rS_r} + {}_S\boldsymbol{u}^{(2)}_{P_rS_r} + {}_S\boldsymbol{u}^{(2)}_{S_rS_r} + {}_P\boldsymbol{u}^{(2)}_{S_rS_r}. \end{aligned} \tag{4.4}$$

Note that the index on the left side of each wave indicates its type (P for a longitudinal wave, S for a shear vertical wave), whereas the other indices on the righ side are showing which primary waves generate the secondary wave under consideration. If these two indices are the same, e.g. ${}_P\boldsymbol{u}^{(2)}_{P_iP_i}$, the wave is created by self-interaction.

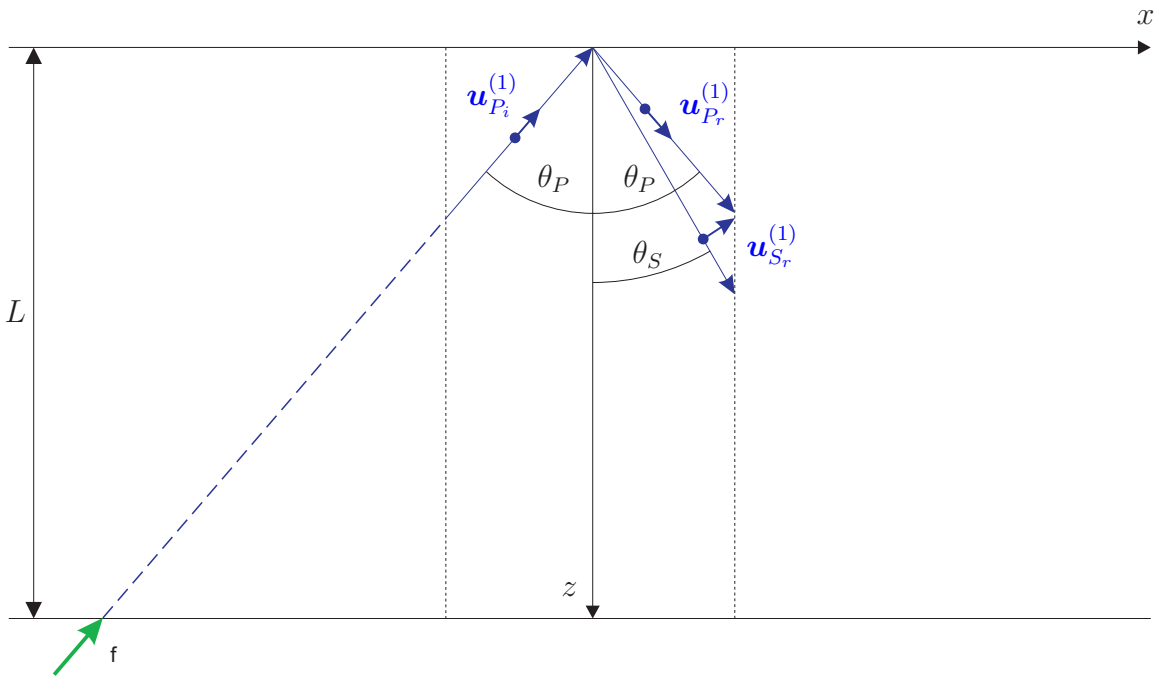

Figure 4.1: Primary Wave Field for an Incident P-Wave.

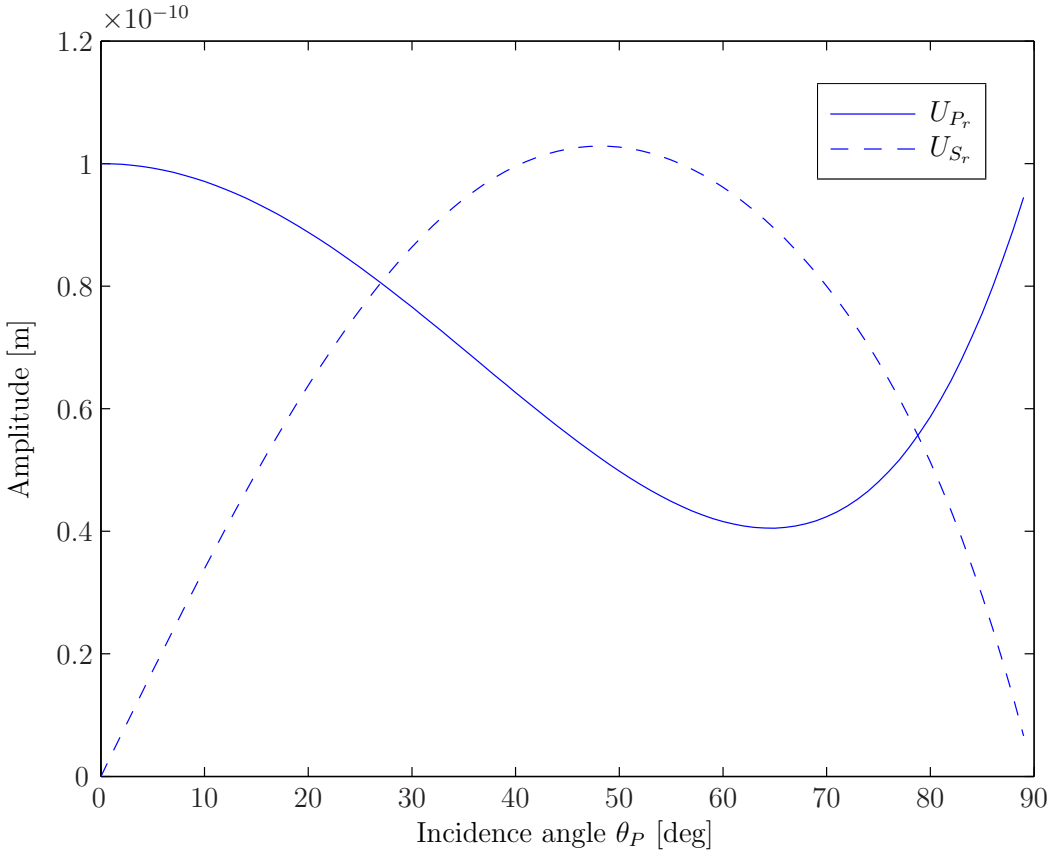

Figure 4.2: Absolute Values of U_{P_r} and U_{S_r} in Aluminum.

If the indices are different, e.g. ${}_S\boldsymbol{u}^{(2)}_{P_iS_r}$, the wave is caused by cross-interaction. For each of the waves given in Eq. (4.4), one can find an explicit term according to the solution procedure given in Section 3.4.3. These terms are given in Appendix B.1, and the secondary field is illustrated in Fig. 4.3. The reader is also referred to Table 4.3 for details each secondary wave.

The wave vectors $\boldsymbol{k}$ of the generated waves are determined by the wave vectors of the generating primary waves. For example, for the case of the second harmonic wave generated by the incident P-wave and the reflected SV-wave, this means

$$\boldsymbol{k}_{P_iS_r} = \boldsymbol{k}_{P_i} + \boldsymbol{k}_{S_r}, \tag{4.5}$$

or in component for using the angles given in Fig. 4.3,

$$k_{P_iS_r} \begin{bmatrix} \sin\Psi \\ 0 \\ \cos\Psi \end{bmatrix} = k_P \begin{bmatrix} \sin\theta_P \\ 0 \\ -\cos\theta_P \end{bmatrix} + k_S \begin{bmatrix} \sin\theta_S \\ 0 \\ \cos\theta_S \end{bmatrix}. \tag{4.6}$$

In a similar way, one obtains

$$\boldsymbol{k}_{P_rS_r} = \boldsymbol{k}_{P_r} + \boldsymbol{k}_{S_r}, \tag{4.7}$$

or

$$k_{P_rS_r} \begin{bmatrix} \sin\Phi \\ 0 \\ \cos\Phi \end{bmatrix} = k_P \begin{bmatrix} \sin\theta_P \\ 0 \\ \cos\theta_P \end{bmatrix} + k_S \begin{bmatrix} \sin\theta_S \\ 0 \\ \cos\theta_S \end{bmatrix}, \tag{4.8}$$

as well as

$$\boldsymbol{k}_{P_iP_r} = \boldsymbol{k}_{P_i} + \boldsymbol{k}_{P_r}, \tag{4.9}$$

or

$$k_{P_iP_r} \begin{bmatrix} 1 \\ 0 \\ 0 \end{bmatrix} = k_P \begin{bmatrix} \sin\theta_P \\ 0 \\ -\cos\theta_P \end{bmatrix} + k_P \begin{bmatrix} \sin\theta_P \\ 0 \\ \cos\theta_P \end{bmatrix}. \tag{4.10}$$

The angles Ψ and Φ can be determined using Eqs. (4.5) and (4.7),

$$\Psi = \arctan\left(\frac{2k_P \sin\theta_P}{k_S \cos\theta_S - k_P \cos\theta_P}\right), \tag{4.11}$$

$$\Phi = \arctan\left(\frac{2k_P \sin\theta_P}{k_S \cos\theta_S + k_P \cos\theta_P}\right). \tag{4.12}$$

The wave numbers can be derived from Eqs. (4.5), (4.7) and (4.9),

$$k_{P_iS_r} = \sqrt{(2k_P \sin\theta_P)^2 + (k_S \cos\theta_S - k_P \cos\theta_P)^2}, \tag{4.13}$$

$$k_{P_rS_r} = \sqrt{(2k_P \sin\theta_P)^2 + (k_S \cos\theta_S + k_P \cos\theta_P)^2}, \tag{4.14}$$

$$k_{P_iP_r} = 2k_P \sin\theta_P. \tag{4.15}$$

Note that once the angles of propagation are known, one can also use Snell's law to compute the wavenumbers,

$$k_{P_iS_r} = 2k_P \frac{\sin\theta_P}{\sin\Psi}, \tag{4.16}$$

$$k_{P_rS_r} = 2k_P \frac{\sin\theta_P}{\sin\Phi}. \tag{4.17}$$

Now consider the wave vectors for the waves generated by self-interaction of the reflected waves. For the secondary P-wave generated by self-interaction of the incident P-wave, we obtain

$$\boldsymbol{k}_{P_iP_i} = 2\boldsymbol{k}_{P_i}, \tag{4.18}$$

or

$$k_{P_iP_i} \begin{bmatrix} \sin\theta_P \\ 0 \\ -\cos\theta_P \end{bmatrix} = 2k_P \begin{bmatrix} \sin\theta_P \\ 0 \\ -\cos\theta_P \end{bmatrix}. \tag{4.19}$$

Similarly,

$$\boldsymbol{k}_{P_rP_r} = 2\boldsymbol{k}_{P_r}, \tag{4.20}$$

or

$$k_{P_rP_r}\begin{bmatrix}\sin\theta_P\\0\\\cos\theta_P\end{bmatrix}=2k_P\begin{bmatrix}\sin\theta_P\\0\\\cos\theta_P\end{bmatrix} \tag{4.21}$$

and

$$\boldsymbol{k}_{S_rS_r}=2\boldsymbol{k}_{S_r}, \tag{4.22}$$

or

$$k_{S_rS_r}\begin{bmatrix}\sin\theta_S\\0\\\cos\theta_S\end{bmatrix}=2k_S\begin{bmatrix}\sin\theta_S\\0\\\cos\theta_S\end{bmatrix}. \tag{4.23}$$

The resulting wavenumbers can easily be obtained from Eqs. (4.19) to (4.23),

$$k_{P_iP_i}=2k_P, \tag{4.24}$$

$$k_{P_rP_r}=2k_P, \tag{4.25}$$

$$k_{S_rS_r}=2k_S. \tag{4.26}$$

Note that these are the case of internal resonance, and waves generated by self-interaction will generally show a linear growth in the second order approximation.

4.1.4 Complete Solution

The general expression for the secondary wave field (4.4) is not unique since it contains unknown constants. The unknown constants are ${}_P\beta^{surf}_{P_rP_r}$, ${}_S\beta^{surf}_{S_rS_r}$, ${}_P\gamma^{surf}_{P_rP_r}$ and ${}_S\gamma^{surf}_{S_rS_r}$. Note that ${}_P\gamma^{surf}_{P_iP_i}$ is given by the initial conditions, i.e. the location of the source at $z=L$. This leads to the expression for ${}_P\boldsymbol{u}^{(2)}_{P_iP_i}$ given in Appendix B.1.

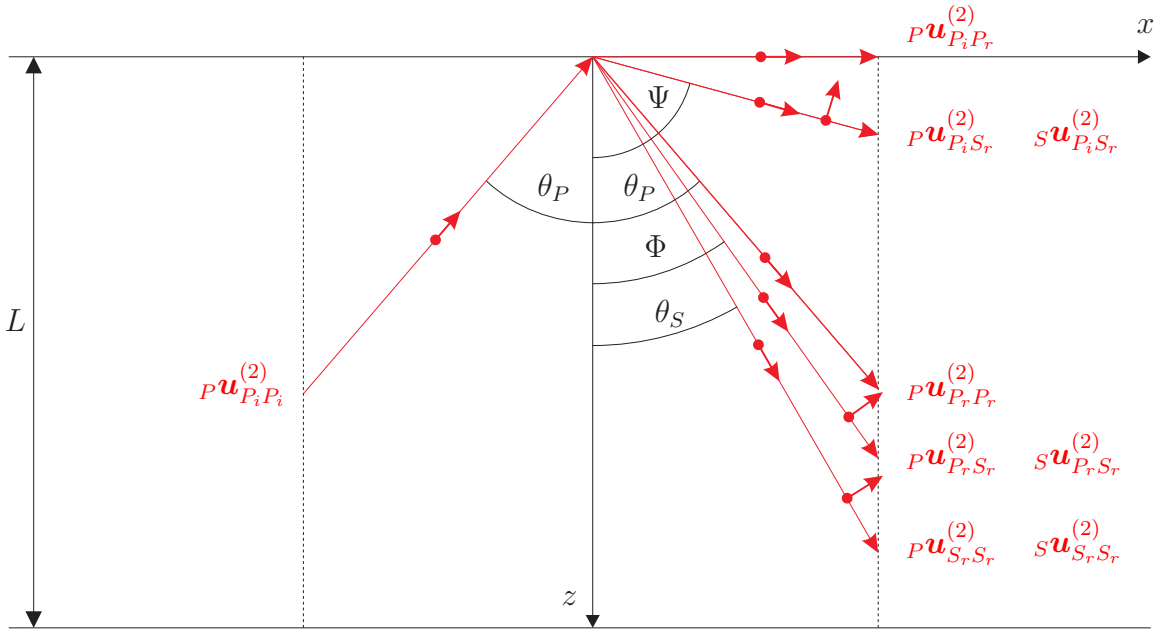

Figure 4.3: Secondary Wave Field for an Incident P-Wave.

Table 4.3: Secondary Waves for P-Wave Incidence.

Interaction	Wave	Generated by	Wave Number	Resonance	Angle
$_P\boldsymbol{u}^{(2)}_{P_iP_i}$	Self	$\boldsymbol{u}^{(1)}_{P_i}$	$2k_P$	yes	θ_P
$_P\boldsymbol{u}^{(2)}_{P_iP_r}$	Cross	$\boldsymbol{u}^{(1)}_{P_i}, \boldsymbol{u}^{(1)}_{P_r}$	$k_{P_iP_r}$	no	90°
$_P\boldsymbol{u}^{(2)}_{P_iS_r}$	Cross	$\boldsymbol{u}^{(1)}_{P_i}, \boldsymbol{u}^{(1)}_{S_r}$	$k_{P_iS_r}$	no	Ψ
$_S\boldsymbol{u}^{(2)}_{P_iS_r}$	Cross	$\boldsymbol{u}^{(1)}_{P_i}, \boldsymbol{u}^{(1)}_{S_r}$	$k_{P_iS_r}$	no	Ψ
$_P\boldsymbol{u}^{(2)}_{P_rP_r}$	Self	$\boldsymbol{u}^{(1)}_{P_r}$	$2k_P$	yes	θ_P
$_P\boldsymbol{u}^{(2)}_{P_rS_r}$	Cross	$\boldsymbol{u}^{(1)}_{P_r}, \boldsymbol{u}^{(1)}_{S_r}$	$k_{P_rS_r}$	no	Φ
$_S\boldsymbol{u}^{(2)}_{P_rS_r}$	Cross	$\boldsymbol{u}^{(1)}_{P_r}, \boldsymbol{u}^{(1)}_{S_r}$	$k_{P_rS_r}$	no	Φ
$_P\boldsymbol{u}^{(2)}_{S_rS_r}$	Self	$\boldsymbol{u}^{(1)}_{S_r}, \boldsymbol{u}^{(1)}_{S_r}$	$2k_S$	no	θ_S
$_S\boldsymbol{u}^{(2)}_{S_rS_r}$	Self	$\boldsymbol{u}^{(1)}_{S_r}$	$2k_S$	yes	θ_S

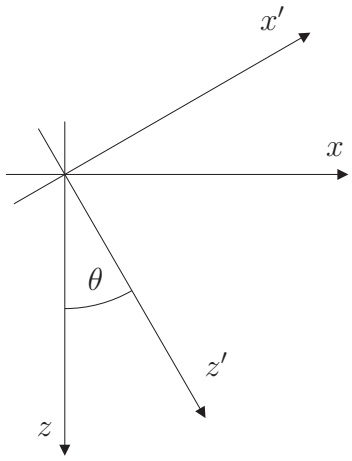

Figure 4.4: Rotation of the Coordinate System.

Additionally, the surface parameter ${}_P\beta^{surf}_{P_iP_i}$ can be expressed in terms of the bulk nonlinearity ${}_P\beta^{bulk}_{P_iP_i}$ because we assume the incident wave to originate far from the boundary at $z = 0$,

$$ {}_P\beta^{surf}_{P_iP_i} = {}_P\beta^{bulk}_{P_iP_i}. \tag{4.27}$$

This becomes clear, if one rotates the coordinate system such that the newly introduced x'-coordinate coincides with the direction of propagation, as illustrated in Fig. 4.4. In the new coordinates, the amplitude of the particular solution in the case of resonance becomes

$$ u^{(2)} = \frac{U_I U_{II}}{4jk_0c_0^2}\left[\beta^{bulk}x' + \left(\beta^{bulk} - \beta^{surf}\right)\frac{\sin\theta}{\cos\theta}z'\right]. \tag{4.28}$$

Now, if one assumes that a plane wave travels in an infinite medium, there is no component that is growing with the z'-coordinate. This can only be satisfied for

$$ \beta^{surf} = \beta^{bulk}. \tag{4.29}$$

In the following, this result will be important for the incident waves. Assuming this wave to originate far from the boundary, Eq. (4.29) can be applied in the case of both the incident P- and the incident SV-wave. In the next step, the two boundary conditions

$$ P_{31}^{L}\left(\boldsymbol{u}^{(2)}\right)|_{z=0} = -P_{31}^{NL}\left(\boldsymbol{u}^{(1)}\right)|_{z=0} \tag{4.30}$$

and

$$P_{33}^{L}\left(\boldsymbol{u}^{(2)}\right)|_{z=0} = -P_{33}^{NL}\left(\boldsymbol{u}^{(1)}\right)|_{z=0} \tag{4.31}$$

are applied to the primary and secondary fields using

$$\frac{\partial P_{ji}^{L}}{\partial a_j}\left(\boldsymbol{u}^{(2)}\right) = \lambda\frac{\partial^2 u_k^{(2)}}{\partial a_k \partial a_i} + \mu\left(\frac{\partial^2 u_i^{(2)}}{\partial a_j^2} + \frac{\partial^2 u_j^{(2)}}{\partial a_i \partial a_j}\right), \tag{4.32}$$

$$\begin{aligned}\frac{\partial P_{ji}^{NL}}{\partial a_j}\left(\boldsymbol{u}^{(1)}\right) = {} & \left(\mu + \frac{\mathcal{A}}{4}\right)\left(\frac{\partial^2 u_l^{(1)}}{\partial a_k^2}\frac{\partial u_l^{(1)}}{\partial a_i} + \frac{\partial^2 u_l^{(1)}}{\partial a_k^2}\frac{\partial u_i^{(1)}}{\partial a_l} + 2\frac{\partial^2 u_i^{(1)}}{\partial a_k \partial a_l}\frac{\partial u_l^{(1)}}{\partial a_k}\right) \\ & + \left(\lambda + \mu + \frac{\mathcal{A}}{4} + \mathcal{B}\right)\left(\frac{\partial^2 u_l^{(1)}}{\partial a_i \partial a_k}\frac{\partial u_l^{(1)}}{\partial a_k} + \frac{\partial^2 u_k^{(1)}}{\partial a_l \partial a_k}\frac{\partial u_i^{(1)}}{\partial a_l}\right) \\ & + (\lambda + \mathcal{B})\left(\frac{\partial^2 u_i^{(1)}}{\partial a_k^2}\frac{\partial u_l^{(1)}}{\partial a_l}\right) + (\mathcal{B} + 2\mathcal{C})\left(\frac{\partial^2 u_k^{(1)}}{\partial a_i \partial a_k}\frac{\partial u_l^{(1)}}{\partial a_l}\right) \\ & + \left(\frac{\mathcal{A}}{4} + \mathcal{B}\right)\left(\frac{\partial^2 u_k^{(1)}}{\partial a_l \partial a_k}\frac{\partial u_l^{(1)}}{\partial a_i} + \frac{\partial^2 u_l^{(1)}}{\partial a_i \partial a_k}\frac{\partial u_k^{(1)}}{\partial a_l}\right).\end{aligned} \tag{4.33}$$

Evaluating the boundary conditions at $z = 0$ yields two equations. However, the left-hand sides of Eqs. (4.30) and (4.31) contain terms in x, whereas all terms of $P_{31}^{NL}\left(\boldsymbol{u}^{(1)}\right)|_{z=0}$ and $P_{33}^{NL}\left(\boldsymbol{u}^{(1)}\right)|_{z=0}$ are independent of x. As a consequence, we obtain two homogeneous equations in terms containing x and two equations without x-dependency. Thus, there are four equations containing four unknowns, and the problem has a definite solution. Since the equations in x only contain the unknowns ${}_P\beta_{P_rP_r}^{surf}$ and ${}_S\beta_{S_rS_r}^{surf}$, we solve for them first. After some tedious algebraic manipulations, the equations

$${}_P\beta_{P_rP_r}^{surf} = \frac{\sin(2\theta_P)\sin(2\theta_S) - \frac{\lambda+2\mu}{\mu}\cos^2(2\theta_S)}{\sin(2\theta_P)\sin(2\theta_S) + \frac{\lambda+2\mu}{\mu}\cos^2(2\theta_S)}\frac{U_{P_i}^2}{U_{P_r}^2}\,{}_P\beta_{P_iP_i}^{bulk} \tag{4.34}$$

and

$${}_S\beta_{S_rS_r}^{surf} = \frac{2\sqrt{\frac{\lambda+2\mu}{\mu}}\sin(2\theta_P)\cos(2\theta_S)}{\sin(2\theta_P)\sin(2\theta_S) + \frac{\lambda+2\mu}{\mu}\cos^2(2\theta_S)}\frac{U_{P_i}^2}{U_{S_r}^2}\,{}_P\beta_{P_iP_i}^{bulk} \tag{4.35}$$

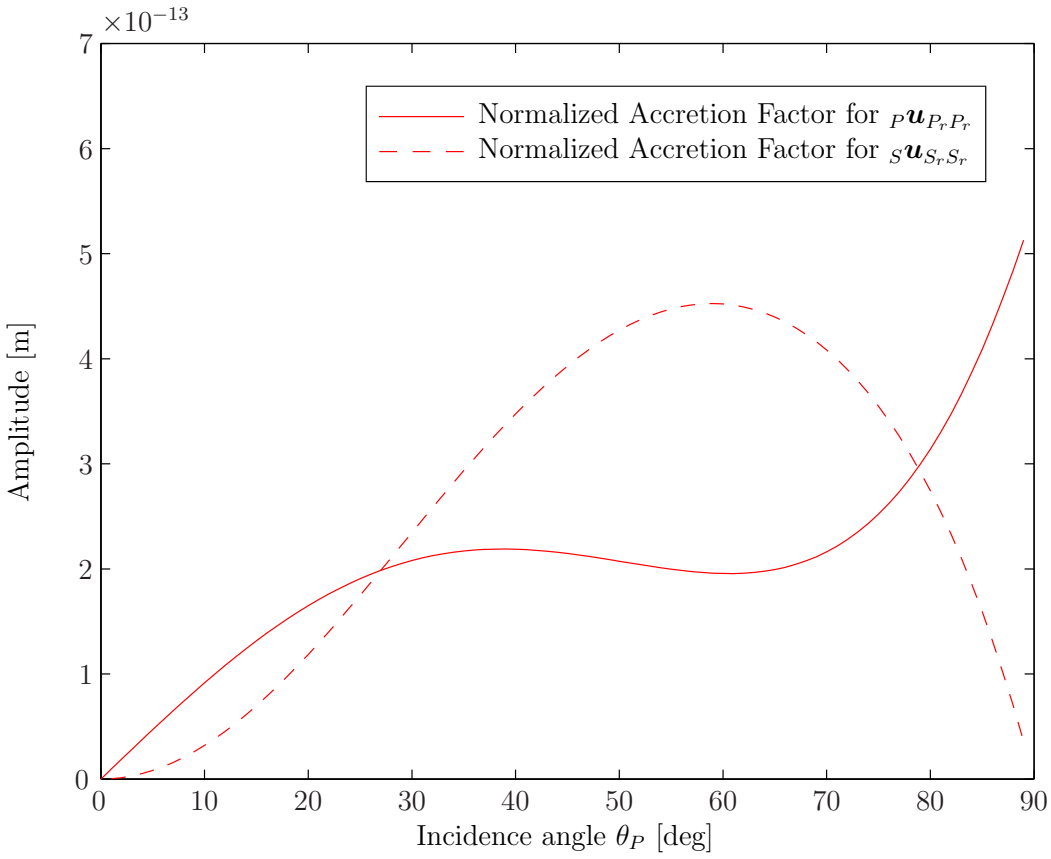

Figure 4.5: Nonlinear Accretion Factors for an Incident P-Wave in Aluminum.

are obtained. Note that these expressions are similar to the Fresnel formulae (2.38) and (2.39). In Fig. 4.5, the normalized accumulation factors

$$\left| \frac{U_{P_r}^2}{4jk_P c_P^2} \sin(\theta_P)\, {}_P\beta_{P_rP_r}^{surf} \right| \tag{4.36}$$

and

$$\left| \frac{U_{S_r}^2}{4jk_S c_S^2} \sin(\theta_S)\, {}_S\beta_{S_rS_r}^{surf} \right| \tag{4.37}$$

are shown for different incidence angles θ_P in aluminum.

Since the parameters ${}_P\beta_{P_rP_r}^{surf}$ and ${}_S\beta_{S_rS_r}^{surf}$ are determined, one can proceed by solving the remaining two equations (without x-dependency) for ${}_P\gamma_{P_rP_r}$ and ${}_S\gamma_{S_rS_r}$. These two constants represent the amplitudes of the non-accumulating parts of the second harmonics generated by self-interaction. Zhou and Shui [26] call these waves the freely

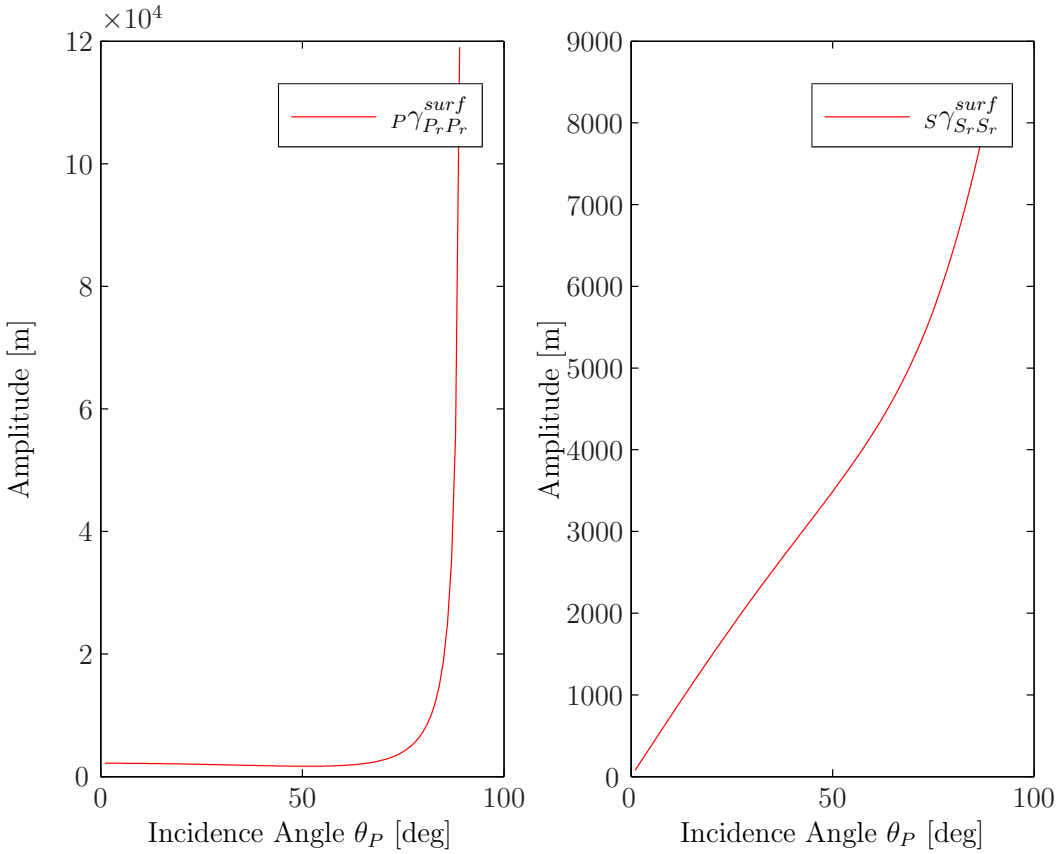

Figure 4.6: Absolute Values of ${}_P\gamma^{surf}_{P_rP_r}$ and ${}_S\gamma^{surf}_{S_rS_r}$ in Aluminum.

propagating waves, because they are determined by the homogeneous solution of the equation of motion without any excitation terms, in contrast to the accumulating terms which are caused by the forcing terms as can be seen in Section 3.4. Since there is no short analytical expressions for ${}_P\gamma_{P_rP_r}$ and ${}_S\gamma_{S_rS_r}$ as in the case for ${}_P\beta^{surf}_{P_rP_r}$ and ${}_S\beta^{surf}_{S_rS_r}$, the remaining equations are solved numerically and the obtained values are plotted for different incident angles. These plots are shown on a linear scale in Fig. 4.6. Fig. 4.7 shows these constants plotted on a logarithmic scale in the same way as in [25] and [26].

4.1.5 Second Harmonic Amplitudes

With the solution to the secondary wave field being known, one can perform a numerical simulation of an actual experiment to gain physical insight into how the amplitudes

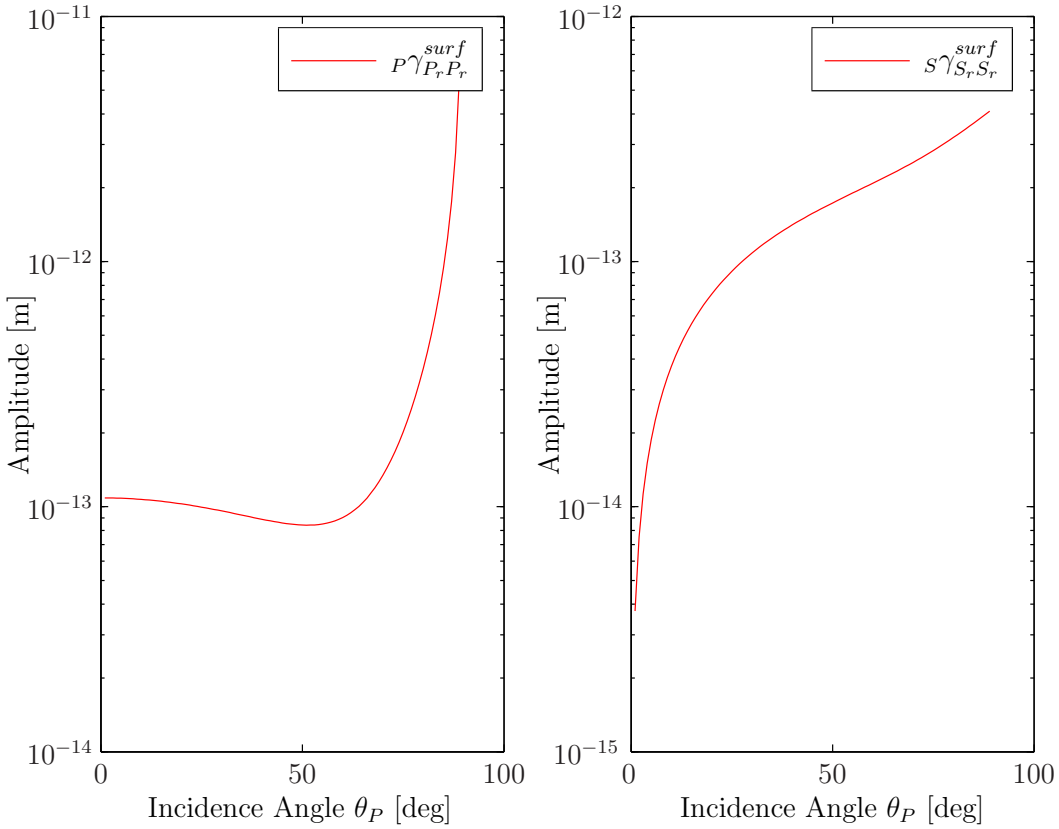

Figure 4.7: Absolute Values of ${}_P\gamma^{surf}_{P_rP_r}$ and ${}_S\gamma^{surf}_{S_rS_r}$ in Aluminum on a Logarithmic Scale.

of the second harmonic waves behave for different angles of incidence. In general, second harmonics with large amplitudes are desirable for practical applications, because they can be detected with a better signal-to-noise ratio. However, when choosing an experimental setup, we also have to take some other aspects into consideration, such as the inherent damping (attenuation and diffraction) of the propagating waves. Additionally, one has to keep in mind that our solution is an approximation obtained by applying the perturbation method. As a consequence, the chosen approach will only be valid as long as the perturbation condition (3.16) is satisfied. In order to overcome this drawback, Ginsberg and Shu [22] only use the perturbation method to obtain qualitative information on the solution. Then, they compute the solution applying the method of characteristics, which is explained in the book by Bender and Orszag [3]. Our approach has the advantage of conceptual simplicity and straightforwardness, and since we are only interested in the behavior of the wave field in a region close to the wave source, the present result can be considered to be sufficiently precise.

In the following, it will be investigated how the second harmonics develop with increasing propagation distance. A focus will be put on the secondary waves generated by self-interaction, since all other waves have much smaller amplitudes. The considered waves are of particular interest for measurements, because they show the accumulation feature, i.e. these waves have increasing amplitudes. The shown amplitudes were obtained by plotting the amplitudes (which are a function of both the $x-$ and $z-$ coordinate as a function of the $x-$ coordinate. Table 4.4 shows the amplitudes of all second harmonics that can be measured after reflection for an incident angle of $\theta_P = 50°$. We clearly see that the two waves generated by self-interaction that satisfy the resonance condition ($_P\boldsymbol{u}^{(2)}_{P_rP_r}$, $_S\boldsymbol{u}^{(2)}_{S_rS_r}$) have much larger amplitudes than all other waves.

Table 4.4: Amplitudes of Second Harmonics after Reflection at $z = L$.

Secondary Wave	Resonance	Amplitude
${}_P\boldsymbol{u}^{(2)}_{P_iP_r}$	no	$2.76 \cdot 10^{-17}\,\mathrm{m}$
${}_P\boldsymbol{u}^{(2)}_{P_iS_r}$	no	$4.90 \cdot 10^{-16}\,\mathrm{m}$
${}_S\boldsymbol{u}^{(2)}_{P_iS_r}$	no	$3.50 \cdot 10^{-17}\,\mathrm{m}$
${}_P\boldsymbol{u}^{(2)}_{P_rP_r}$	yes	$4.22 \cdot 10^{-14}\,\mathrm{m}$
${}_P\boldsymbol{u}^{(2)}_{P_rS_r}$	no	$5.00 \cdot 10^{-17}\,\mathrm{m}$
${}_S\boldsymbol{u}^{(2)}_{P_rS_r}$	no	$8.86 \cdot 10^{-17}\,\mathrm{m}$
${}_P\boldsymbol{u}^{(2)}_{S_rS_r}$	no	$4.10 \cdot 10^{-17}\,\mathrm{m}$
${}_S\boldsymbol{u}^{(2)}_{S_rS_r}$	yes	$1.73 \cdot 10^{-13}\,\mathrm{m}$

If one wants to know how the amplitudes of the second harmonic waves develop with propagation distance, specific rays of wavefronts have to be followed. On a ray, the 2-dimensional problem can be reduced to a one-dimensional problem since one coordinate can be expressed in terms of the other, as long as we follow the ray. For the second harmonic ${}_P\boldsymbol{u}^{(2)}_{P_iP_i}$, this yields

$$z = -\frac{x}{\tan\theta_P}. \tag{4.38}$$

For the wave ${}_P\boldsymbol{u}^{(2)}_{P_rP_r}$, use

$$z = \frac{x}{\tan\theta_P} \tag{4.39}$$

and for ${}_S\boldsymbol{u}^{(2)}_{S_rS_r}$

$$z = \frac{x}{\tan\theta_S} \tag{4.40}$$

holds true. As a result, the amplitudes along the rays can be expressed as

$$\left|{}_P\boldsymbol{u}^{(2)}_{P_iP_i}\right| = \left|\frac{U^2_{P_i}}{4jk_Pc^2_P}{}_P\beta^{bulk}_{P_iP_i}\left(\frac{x}{\sin\theta_P}+\frac{L}{\cos\theta_P}\right)\right|, \tag{4.41}$$

$$\left|{}_P\boldsymbol{u}^{(2)}_{P_rP_r}\right| = \left|\frac{U^2_{P_r}}{4jk_Pc^2_P}{}_P\beta^{bulk}_{P_rP_r}\left(\frac{x}{\sin\theta_P}+{}_P\gamma^{surf}_{P_rP_r}\right)\right|, \tag{4.42}$$

$$\left|{}_S\boldsymbol{u}^{(2)}_{S_rS_r}\right| = \left|{}_S\gamma^{surf}_{S_rS_r}\right|. \tag{4.43}$$

Note that the expression for ${}_S\boldsymbol{u}^{(2)}_{S_rS_r}$ is constant. This is caused by the fact that there is no bulk nonlinearity for an SV-wave. Hence, the second harmonic SV-wave does not grow along the ray, although we have ${}_S\beta^{surf}_{S_rS_r} \neq 0$. Now we can plot the amplitudes of the second harmonics over the x-coordinate for different incidence angles. This is done in Figs. 4.9 to 4.12 for aluminum. The plot demonstrates how the second harmonic ${}_P\boldsymbol{u}^{(2)}_{P_iP_i}$ increases in a linear fashion from an amplitude of 0 at $z = L$ ($x = -L\tan\theta_P$) to its maximum at $z = 0$ ($x = 0$). The reflected second harmonic P-wave ${}_P\boldsymbol{u}^{(2)}_{P_rP_r}$ decreases from its maximum at $z = 0$ ($x = 0$) to its minimum at $z = L$ ($x = L\tan\theta_P$). The reflected second harmonic SV-wave ${}_S\boldsymbol{u}^{(2)}_{S_rS_r}$ is constant along the ray we follow, i.e. a ray from $z = 0$ and $x = 0$ to $z = L$ and $x = L\tan\theta_S$.

Since the source and the receiver can only be attached to the surface at $z = L$, only the amplitudes of the waves at this specific location are of interest. In Fig. 4.8, a possible setup of transducers is shown. *Transducer 1* will launch the incident P-wave into the material, *Transducer 2* will measure the reflected second harmonic P-wave ${}_P\boldsymbol{u}^{(2)}_{P_rP_r}$ and *Transducer 3* will measure the reflected SV second harmonic ${}_S\boldsymbol{u}^{(2)}_{S_rS_r}$. The measured amplitudes are shown in Figs. 4.9 to 4.12 for incidence angles of 10°, 30°, 50° and 70°. Note that for all shown angles, the amplitude of the SV-wave ${}_S\boldsymbol{u}^{(2)}_{S_rS_r}$ is greater than the amplitude of the reflected P-wave ${}_P\boldsymbol{u}^{(2)}_{P_rP_r}$. It also can be seen that a greater incidence angle θ_P results in larger amplitudes. This is reasonable, since a larger incidence angle causes a longer propagation distance. Hence, the second harmonic amplitudes become larger. However, we have to keep in mind that large incidence angles come with a number of disadvantages. First of all, the length of the

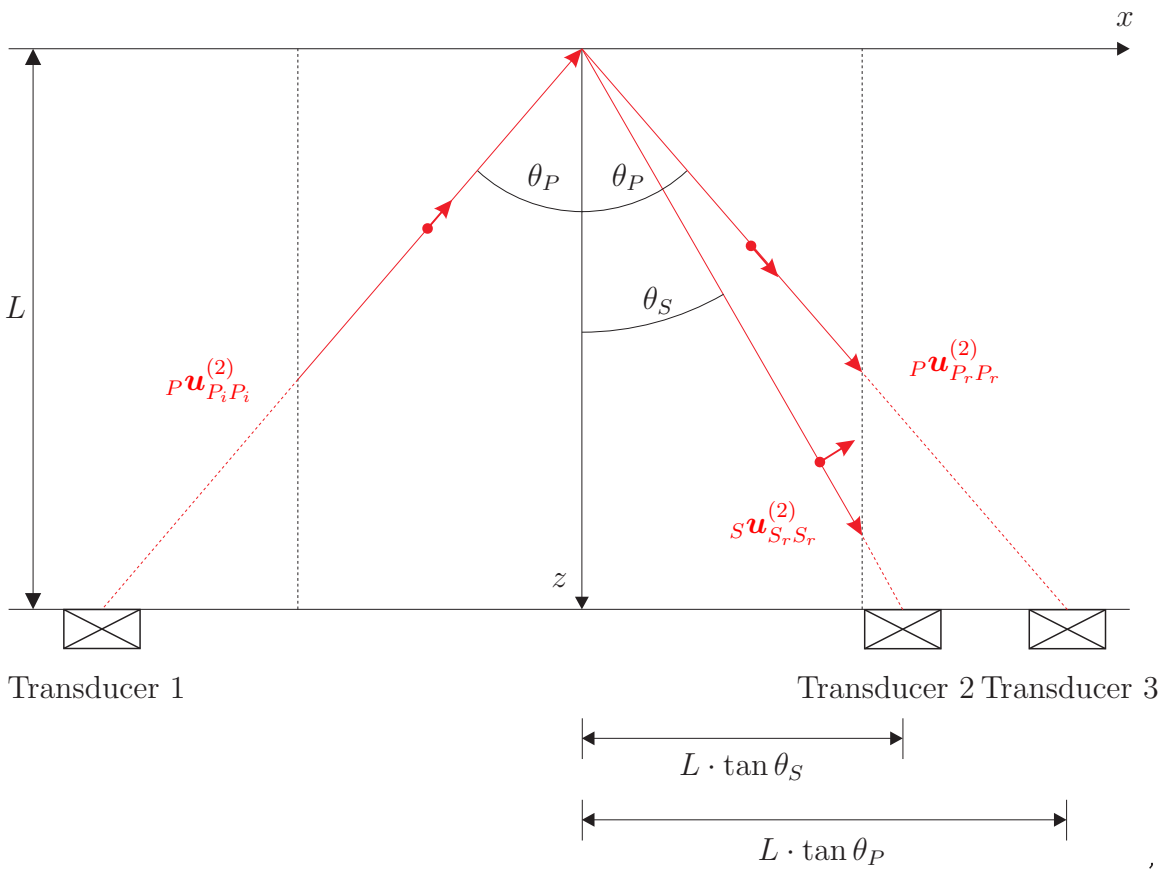

Figure 4.8: Measurement of Reflected Second Harmonics for P-Wave Incidence.

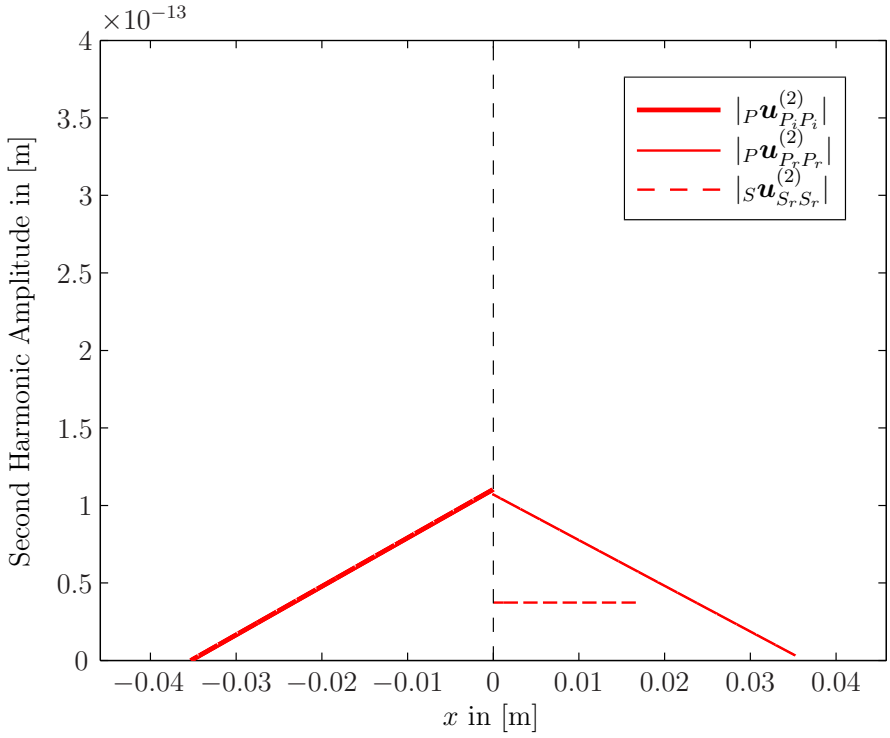

Figure 4.9: Second Harmonic Amplitudes for $\theta_P = 10°$.

specimen considered depends on the incidence angle. If this length is too long in an actual NDE experiment, one can only say that a defect or an area of higher fatigue is somewhere in this large area. The smaller the angle is, the smaller is the considered section of our specimen. Consequently, a small angle is preferable for an effective detection of defects.

4.1.6 Second Harmonic Amplitudes for Increased TOECs

So far, only an undamaged specimen has been considered. However, the idea of NDT is to detect flaws and, more recently, areas of high fatigue. As mentioned before, the third order elastic constants $\mathcal{A}, \mathcal{B}$ and $\mathcal{C}$ are very sensitive to changes in the microstructure of the material. Therefore, a state of high fatigue will cause an increase in these values. As a consequence, the nonlinear parameters β will change, and the overall result will be an increase in the amplitudes of the second harmonic waves [6]. Hence, if we measure an increase in the second harmonic amplitudes, we can

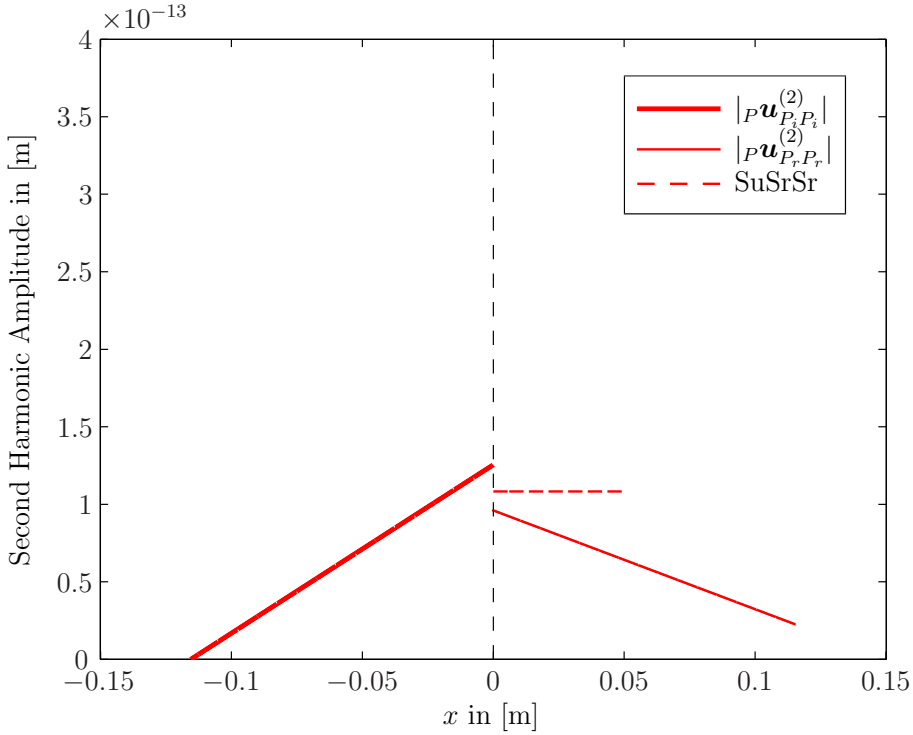

Figure 4.10: Second Harmonic Amplitudes for $\theta_P = 30°$.

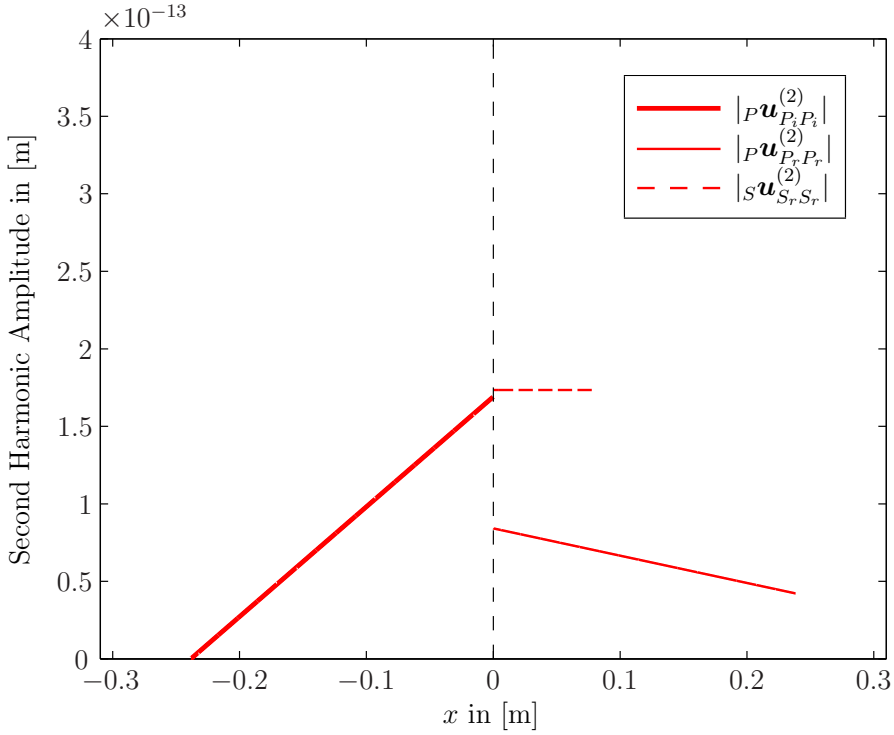

Figure 4.11: Second Harmonic Amplitudes for $\theta_P = 50°$.

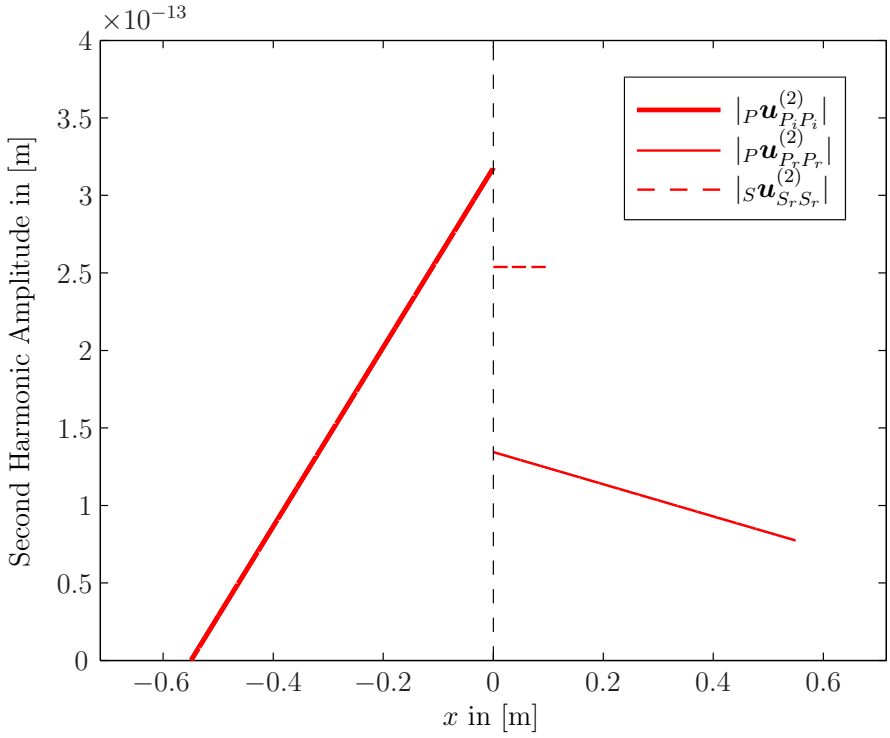

Figure 4.12: Second Harmonic Amplitudes for $\theta_P = 70°$.

conclude that the nonlinear parameter has changed and the tested area is subject to increased fatigue damage. For details on the influence of fatigue on the microstructure of elastic solids, the work by Cantrell and Yost [7] is recommended. Herrmann et al. have investigated the influence of fatigue on the nonlinear parameter in a nickel-base superalloy [14]. They show that the nonlinear parameter of an aluminum specimen subject to fatigue cycles will increase. The quantitative relationship between applied fatigue and change in the elastic constants is beyond the scope of this thesis. We will assumean increase in the third order elastic constants by 30%, and illustrate how the simulated second harmonic amplitudes increase with this change. For quantitative statements concerning the relationship between the elastic constants and the change in second harmonic amplitudes, more research is certainly needed. For the new third

order elastic constants, assume

$$\mathcal{A}^{fatigue} = 1.3 \cdot \mathcal{A} \tag{4.44}$$

$$\mathcal{B}^{fatigue} = 1.3 \cdot \mathcal{B} \tag{4.45}$$

$$\mathcal{C}^{fatigue} = 1.3 \cdot \mathcal{C}, \tag{4.46}$$

where $\mathcal{A}^{fatigue}, \mathcal{B}^{fatigue}$ and $\mathcal{C}^{fatigue}$ represent the increased third order elastic constants. Again, it is pointed out that this increase in nonlinearity is fairly arbitrary with the main purpose of illustrating how the measurement of second harmonic waves can be used to detect fatigue in the material.

In Fig. 4.13 we compare the amplitudes of the reflected second harmonic waves ${}_P\boldsymbol{u}^{(2)}_{P_iP_i}$, ${}_P\boldsymbol{u}^{(2)}_{P_rP_r}$ and ${}_P\boldsymbol{u}^{(2)}_{P_rP_r}$ for the original values of $\mathcal{A}, \mathcal{B}, \mathcal{C}$ with the amplitudes of the same waves for the increased TOECs, $\mathcal{A}^{fatigue}$, $\mathcal{B}^{fatigue}$, $\mathcal{C}^{fatigue}$. It can clearly be seen that the increase in the TOECs causes an increase in the second harmonic amplitudes. The increase is around 30%. Note that the increase in the third order elastic constants causes an increase in the bulk parameters , β^{bulk} (see the bulk parameters given Appendix A.1), which in turn causes an increase in the second harmonic amplitudes.

4.1.7 Normal Incidence

For $\theta_P = 0$ one obtains the interesting case of normal incidence. This case is much easier to analyze, and therefore its solution can be used to get some insight in order to understand the more complex problem of an obliquely incident wave. The conceptual simplicity of this particular case is caused by a smaller number of waves that contribute to the problem. Consider the Fresnel equations (2.38) and (2.39). For the case of normal incidence, set $\theta_P = 0$. Thus, the Fresnel equations reduce to

$$U_{P_r} = -U_{P_i} \tag{4.47}$$

$$U_{S_r} = 0. \tag{4.48}$$

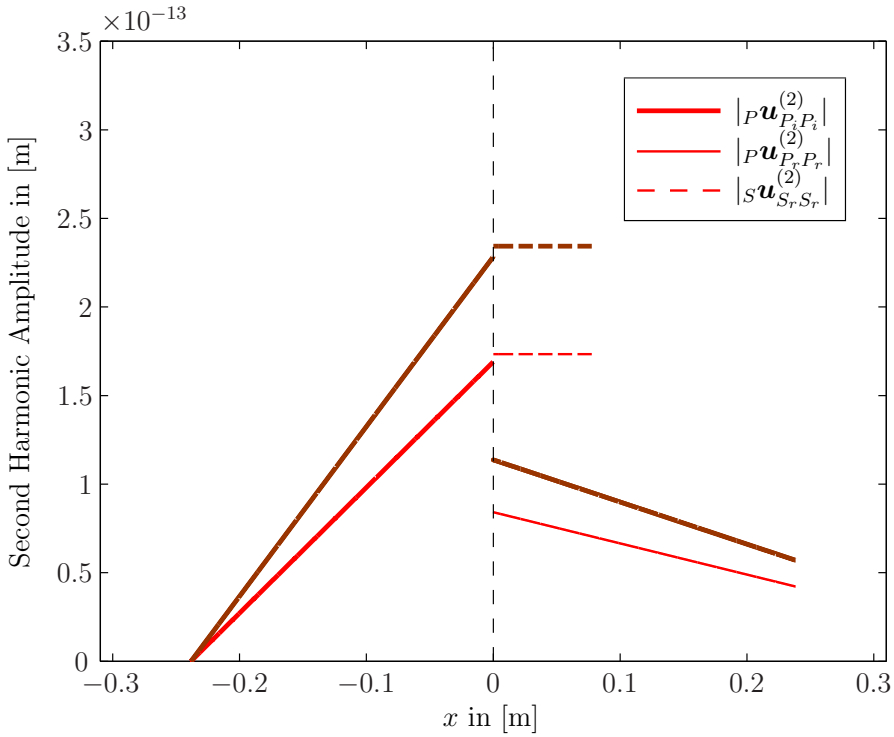

Figure 4.13: Second Harmonic Amplitudes for $\theta_P = 50°$. Shown are both the amplitudes for the original third order elastic constants $\mathcal{A}$, $\mathcal{B}$, $\mathcal{C}$, and the amplitudes for the third order elastic constants increased by 30%. It can be seen that these amplitudes are also increased by about 30%. Note that the propagation distance is the same in both cases.

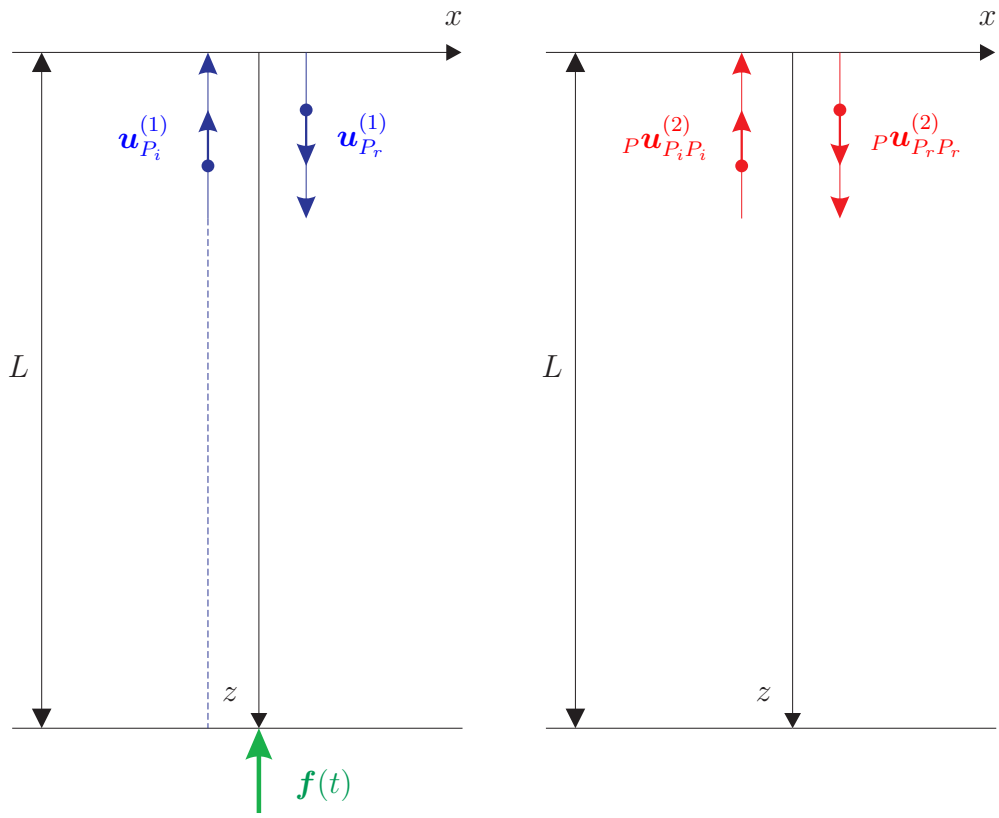

(a) Primary Field. (b) Secondary Field.

Figure 4.14: Wave Fields for Normal P-Wave Incidence.

This means that the incident P-wave is only reflected as a P-wave. There is no reflected SV-wave. This results in the simple primary wave field illustrated in Fig. 14(a).

Mathematically, the primary field is represented by

$$\boldsymbol{u}^{(1)} = U_{P_i} \begin{bmatrix} 0 \\ 0 \\ -1 \end{bmatrix} e^{j(\omega t + k_P z)} + U_{P_r} \begin{bmatrix} 0 \\ 0 \\ 1 \end{bmatrix} e^{j(\omega t - k_P z)}. \tag{4.49}$$

The secondary field consists of an accumulating P-wave generated by self-interaction of the incident P-wave, and an accumulating P-wave generated by self-interaction of the reflected P-wave. The secondary field is illustrated in Fig. 14(b). There is no cross-interaction between the two primary P-waves, which can be seen by calculating

the bulk parameter,

$$ {}_P\beta^{bulk}_{P_iP_r} = 0. \tag{4.50} $$

For normal incidence, a 1-D problem is obtained. As a consequence, the general solution obtained in Section 3.4 takes a simpler form. There is no β^{surf}. The influence of the boundary is inherent in the parameter γ^{surf}, which represents the amplitude of the freely propagating second harmonic P-wave caused by self-interaction of the reflected P-wave. The secondary field is therefore given by

$$ \begin{aligned} \boldsymbol{u}^{(2)} &= \frac{U^2_{P_i}}{4jk_pc^2_P}\,{}_P\beta^{bulk}_{P_iP_i}(L-z)e^{j(2\omega t+2k_Pz)}\begin{bmatrix}0\\0\\-1\end{bmatrix} \\ &+\left[\frac{U^2_{P_r}}{4jk_pc^2_P}\,{}_P\beta^{bulk}_{P_rP_r}z + {}_P\gamma^{surf}_{P_rP_r}\right]e^{j(2\omega t-2k_Pz)}\begin{bmatrix}0\\0\\1\end{bmatrix} \quad . \end{aligned} \tag{4.51} $$

Since we only consider a 1-D problem, we only have one boundary condition to determine the remaining unknown constant ${}_P\gamma^{surf}_{P_rP_r}$. This boundary condition is given by

$$ P^L_{33}\left(\boldsymbol{u}^{(2)}\right)|_{z=0} = -P^{NL}_{33}\left(\boldsymbol{u}^{(1)}\right)|_{z=0}, \tag{4.52} $$

which means that the normal stress at the free surface has to vanish. After some algebraic manipulations, one obtains

$$ {}_P\gamma^{surf}_{P_rP_r} = \frac{1}{8k^2_Pc^2_P}\left[(2jk_PL-1)U^2_{P_i}\,{}_P\beta^{bulk}_{P_iP_i} - U^2_{P_r}\,{}_P\beta^{bulk}_{P_rP_r}\right] \tag{4.53} $$

and with

$$ {}_P\beta^{bulk}_{P_rP_r} = {}_P\beta^{bulk}_{P_iP_i}, \tag{4.54} $$

$$ U^2_{P_r} = U^2_{P_i} \tag{4.55} $$

one obtains

$$ {}_P\gamma^{surf}_{P_rP_r} = \frac{U^2_{P_i}}{4k^2_Pc^2_P}\,{}_P\beta^{bulk}_{P_iP_i}\left(jk_PL-1\right). \tag{4.56} $$

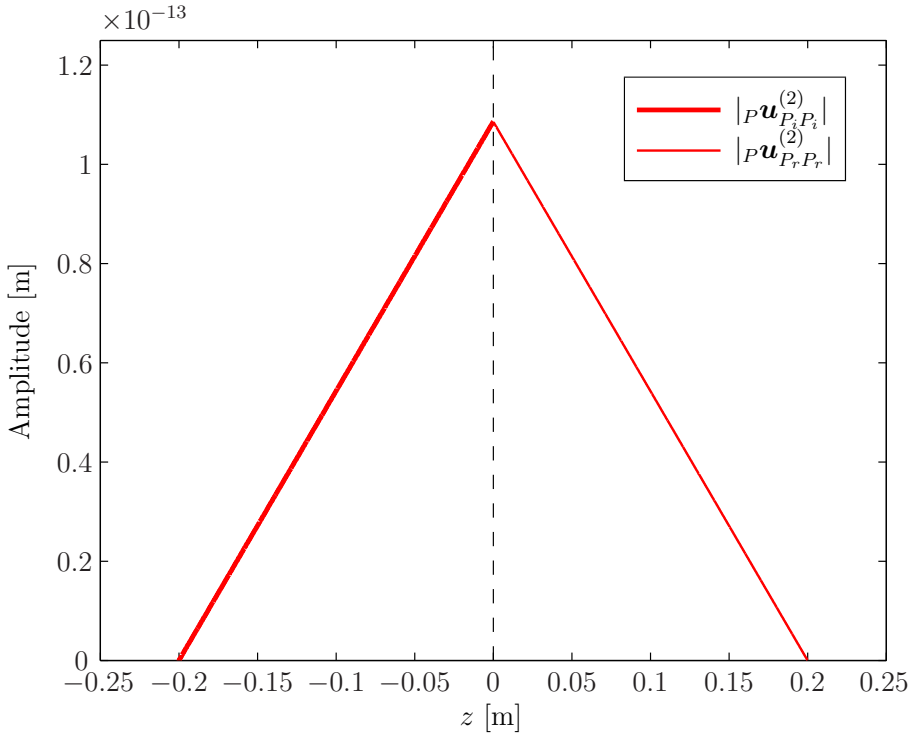

Figure 4.15: Second Harmonic Amplitudes for Normal Incidence of a P-Wave.

Now the amplitudes of the second harmonic waves can be plotted as a function of the z-coordinate. The increase and decrease of the second harmonics is shown in Fig. 4.15.

It can be seen that ${}_P\boldsymbol{u}^{(2)}_{P_iP_i}$, the second harmonic caused by self-interaction of the incident P-wave, grows linearly as it propagates from $z = L$ to $z = 0$. At $z = 0$, its amplitude reaches a maximum. In contrast, ${}_P\boldsymbol{u}^{(2)}_{P_rP_r}$ decreases from its maximum at $z = 0$ to an amplitude of 0 at $z = L$.

Note that the amplitudes of the second harmonic waves are now plotted as a function of the coordinate z, since there is no x-dependency as in the case of oblique incidence. Fig. 4.15 shows that although the second harmonic wave field increases from $z = L$ to $z = 0$, the measured amplitude at $z = L$ is zero. This is due to the reflection at the free boundary which causes the second harmonic field to decrease linearly, contrary to the increase before reflection. As a consequence, normal incidence of a P-wave cannot be used to measure second harmonics in reflection mode. However,

normal incidence can still be useful if both surfaces can be accessed. In this case, the second harmonic field can be measured at $z = 0$, where it has obtained its maximum.

For more information on the case of normal incidence, we refer to the research done by Braun [4, 5]. In these works, not only a free, but also a rigid boundary is investigated. The resulting plots for the free boundary are in agreement with the results presented in this thesis.

4.2 Incidence of an SV-Wave

4.2.1 Problem Setup for Oblique Incidence

The setup is the same as in the case of an incident P-wave. However, the incidence wave is now of SV-type. As in the previous case, mode conversion will occur which determines the primary field. Self- and cross-interaction of the primary waves and the influence of the boundary will lead to the secondary field. However, as outlined in Section 2, the reflected P-wave will not occur for every incidence angle θ_S. For $\theta_S > \theta_{cr}$, the P-wave will become a longitudinal surface wave that decays with depth. As a consequence, the secondary field will also show different behaviors below and above the critical angle. The incident SV-wave has an amplitude U_{S_i} and an incidence angle θ_S,

$$\boldsymbol{u}_{S_i} = U_{S_i} \begin{bmatrix} \cos\theta_S \\ 0 \\ \sin\theta_S \end{bmatrix} e^{j(\omega t - k_S x \sin\theta_S + k_S z \cos\theta_S)}. \tag{4.57}$$

Note that this wave could be excited using a shear wave source located at $x = -L\tan\theta_S$, $z = L$, producing a displacement field

$$\boldsymbol{f}(t) = U_{S_i} \begin{bmatrix} \cos\theta_S \\ 0 \\ \sin\theta_S \end{bmatrix} e^{j(\omega t - k_S x \sin\theta_S + k_S z \cos\theta_S - \phi)} \tag{4.58}$$

where ϕ is a phase shift determined by the exact location of the source. Again, the boundary conditions are determined by a stress-free surface at $z = 0$. The problem setup for the incident SV-wave is illustrated in Fig.4.16.

4.2.2 Primary Wave Field

As shown in Section 2.5, mode conversion that occurs at the free boundary leads to a reflected P-wave and a reflected SV-wave. The reflection angles are determined by Snell's law (2.32), and the amplitudes of the linearly reflected waves can be computed using Fresnel's formulas, (2.38) and (2.39). The primary field is given by

$$\begin{aligned} \boldsymbol{u}^{(1)} = U_{S_i} \begin{bmatrix} \cos\theta_S \\ 0 \\ \sin\theta_S \end{bmatrix} \quad & e^{j(\omega t - k_S x \sin\theta_S + k_S z \cos\theta_S)} \\ + U_{P_r} \begin{bmatrix} \sin\theta_P \\ 0 \\ \cos\theta_P \end{bmatrix} \quad & e^{j(\omega t - k_P x \sin\theta_P - k_P z \cos\theta_P)} \\ + U_{S_r} \begin{bmatrix} \cos\theta_S \\ 0 \\ -\sin\theta_S \end{bmatrix} \quad & e^{j(\omega t - k_S x \sin\theta_S - k_S z \cos\theta_S)} \end{aligned} \tag{4.59}$$

and illustrated in Fig.4.16. In Fig.4.17, the amplitudes of the primary waves in aluminum are shown. These amplitudes can be obtained using the Fresnel formulas (2.38) and (2.39) and the parameters given in Tables 4.1 and 4.2.

4.2.3 Secondary Wave Field

The secondary wave field is again caused by self- and cross-interactions of the primary waves. If one assumes an incident SV-wave as illustrated above, the secondary wave field

$$\begin{aligned} \boldsymbol{u}^{(2)} = & {}_P\boldsymbol{u}^{(2)}_{S_iS_i} + {}_P\boldsymbol{u}^{(2)}_{S_iS_r} + {}_P\boldsymbol{u}^{(2)}_{P_rP_r} + {}_P\boldsymbol{u}^{(2)}_{P_rS_r} \\ & + {}_S\boldsymbol{u}^{(2)}_{P_rS_r} + {}_S\boldsymbol{u}^{(2)}_{S_rS_r} + {}_P\boldsymbol{u}^{(2)}_{S_rS_r}. \end{aligned} \tag{4.60}$$

is obtained. This representation of the secondary field is justified as follows. The incident SV-wave will cause a second harmonic P-wave, ${}_P\boldsymbol{u}^{(2)}_{S_iS_i}$. It will not cause any SV-wave, because ${}_S\beta^{bulk}_{S_iS_i} = 0$ and ${}_S\beta^{surf}_{S_iS_i} = {}_S\beta^{bulk}_{S_iS_i}$ for a wave originating far from the boundary. After reflection, self-interaction of the reflected P-wave leads to

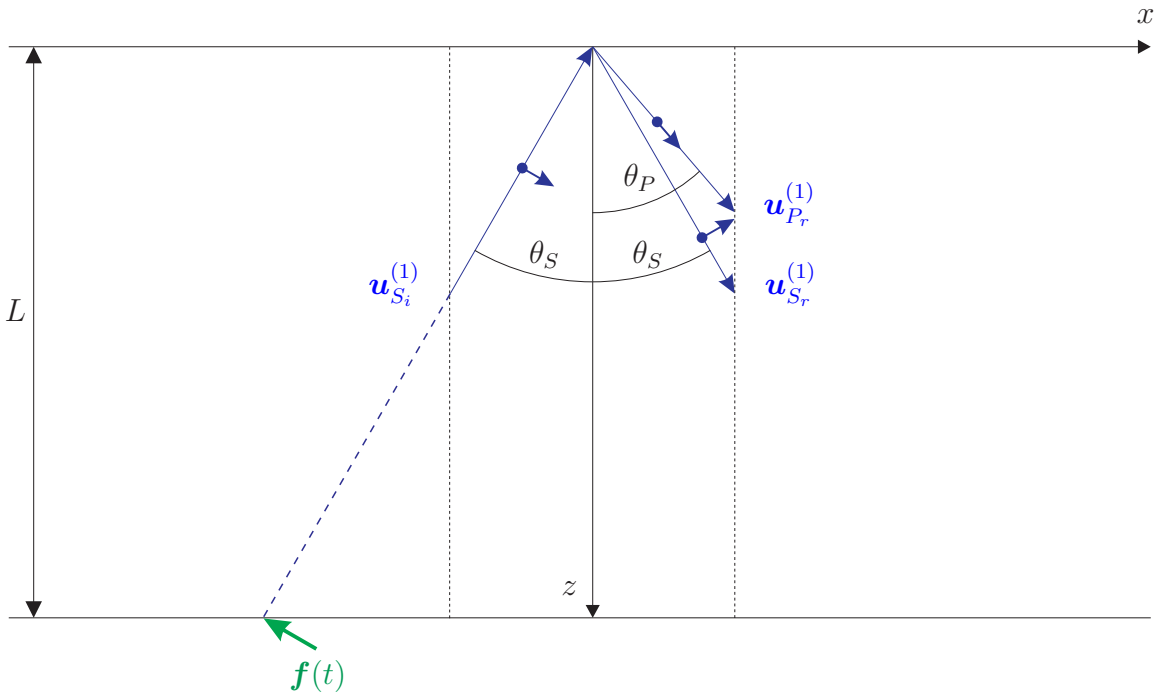

Figure 4.16: Primary Wave Field for an Incident SV-Wave.

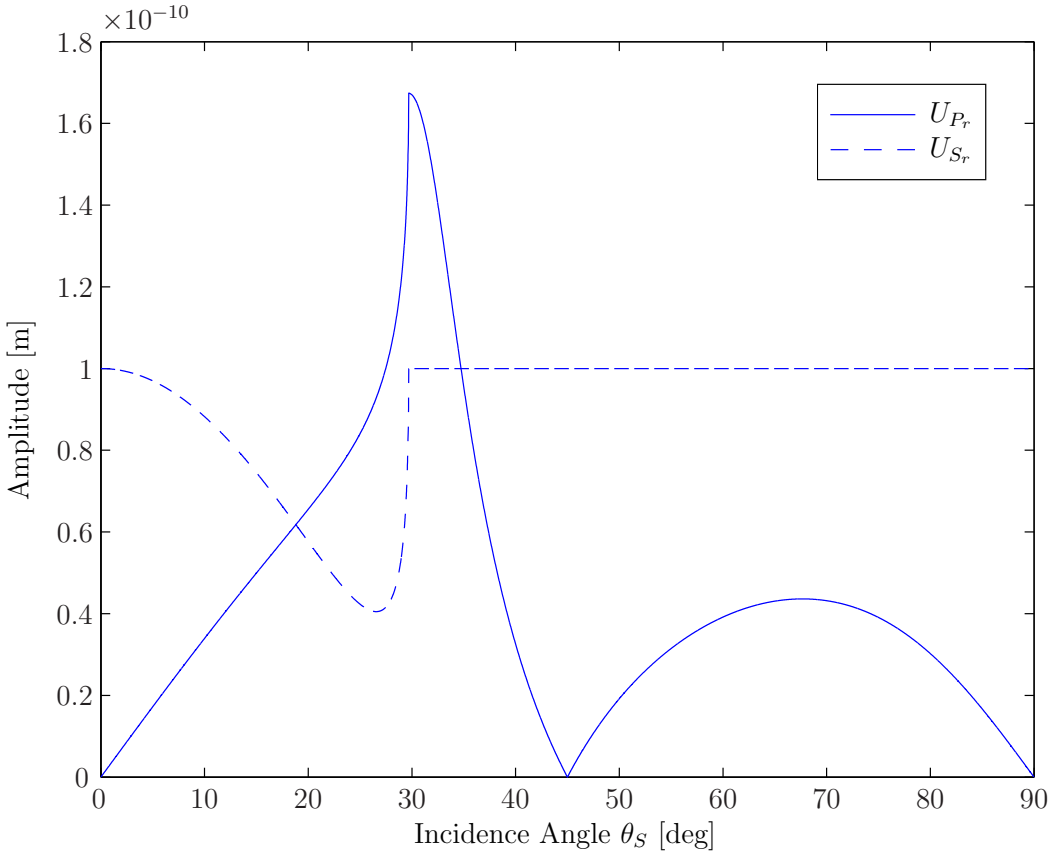

Figure 4.17: Absolute Values of U_{P_r} and U_{S_r} in Aluminum.

${}_P\boldsymbol{u}^{(2)}_{P_rP_r}$, self-interaction of the reflected SV-wave causes ${}_S\boldsymbol{u}^{(2)}_{S_rS_r}$ and ${}_S\boldsymbol{u}^{(2)}_{S_rS_r}$. Cross-interaction of the reflected P- and SV-wave leads to ${}_P\boldsymbol{u}^{(2)}_{P_rS_r}$ and ${}_S\boldsymbol{u}^{(2)}_{P_rS_r}$. Note that cross-interaction of the incident SV-wave and the reflected P-wave can be neglected since these waves have a wave vector that points out of the medium. However, in the case of two layered media, the waves resulting from this cross-interaction must be considered, since the generated second harmonic waves will travel in the second medium. For the case of two media, we refer to the work of Zhou and Shui [26]. For each of the waves given in Eq. (4.60), a complete expression is given in Appendix B.2. A summary of these waves can also be found in Table 4.5.

The wave vectors $\boldsymbol{k}$ of the generated waves are determined by the wave vectors of the generating primary waves as it was done for the incident P-wave. The angle Φ can be determined using Eq. (4.9), which leads to

$$\Phi = \arctan\left(\frac{2k_S \sin\theta_S}{k_S\cos\theta_S + k_P\cos\theta_P}\right). \tag{4.61}$$

The required wave numbers can be derived as,

$$k_{S_iS_r} = 2k_S\sin\theta_S, \tag{4.62}$$

$$k_{P_rS_r} = \sqrt{(2k_P\sin\theta_P)^2 + (k_S\cos\theta_S + k_P\cos\theta_P)^2}. \tag{4.63}$$

Again, Snell's law can be used to compute the wavenumbers, e.g.

$$k_{P_rS_r} = 2k_S\frac{\sin\theta_S}{\sin\Phi}. \tag{4.64}$$

Now consider the wave vectors for the waves generated by self-interaction of the reflected waves. For the P-wave generated by self-interaction of the incident SV-wave, one obtains

$$\boldsymbol{k}_{S_iS_i} = 2\boldsymbol{k}_S, \tag{4.65}$$

or

$$k_{S_iS_i}\begin{bmatrix}\sin\theta_S\\0\\-\cos\theta_S\end{bmatrix}=2k_S\begin{bmatrix}\sin\theta_S\\0\\-\cos\theta_S\end{bmatrix}. \tag{4.66}$$

Similarly,

$$\boldsymbol{k}_{S_rS_r}=2\boldsymbol{k}_S, \tag{4.67}$$

or

$$k_{S_rS_r}\begin{bmatrix}\sin\theta_S\\0\\\cos\theta_S\end{bmatrix}=2k_S\begin{bmatrix}\sin\theta_S\\0\\\cos\theta_S\end{bmatrix} \tag{4.68}$$

and

$$\boldsymbol{k}_{P_rP_r}=2\boldsymbol{k}_P, \tag{4.69}$$

or

$$k_{P_rP_r}\begin{bmatrix}\sin\theta_P\\0\\\cos\theta_P\end{bmatrix}=2k_P\begin{bmatrix}\sin\theta_P\\0\\\cos\theta_P\end{bmatrix}. \tag{4.70}$$

The resulting wavenumbers can easily be obtained from Eqs. (4.66) to (4.70),

$$k_{S_iS_i}=2k_S, \tag{4.71}$$

$$k_{S_rS_r}=2k_S, \tag{4.72}$$

$$k_{P_rP_r}=2k_P. \tag{4.73}$$

Note that these are the cases of internal resonance, and waves generated by self-interaction will generally show the feature of accumulation with propagation distance.

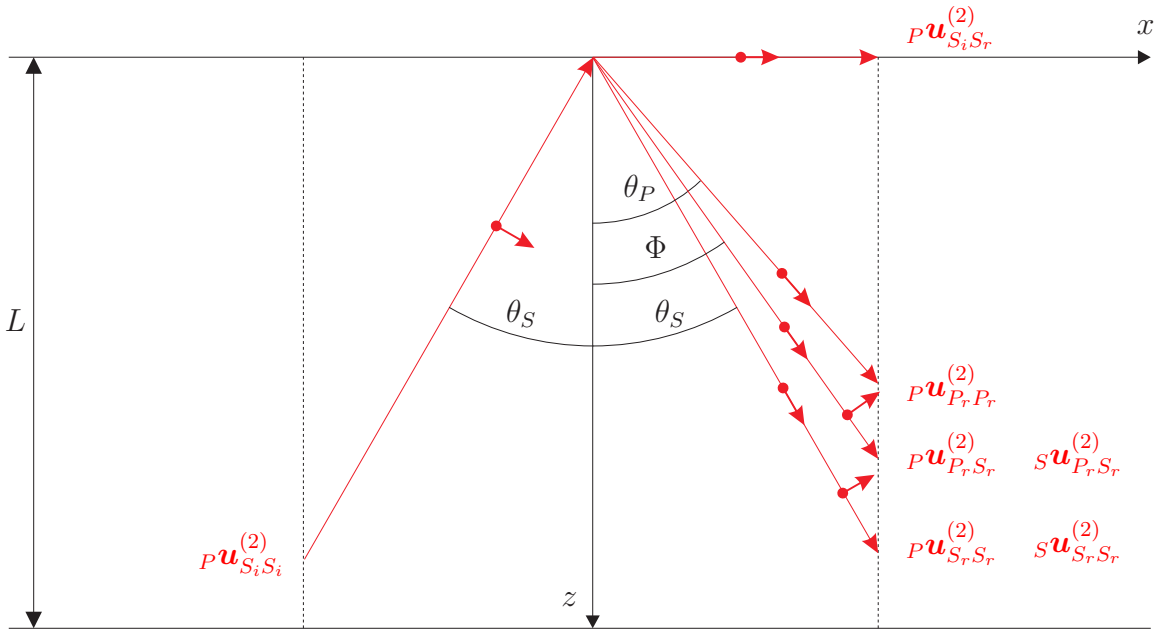

Figure 4.18: Secondary Wave Field for an Incident SV-Wave.

Table 4.5: Secondary Waves for SV-Wave Incidence.

Wave	Interaction	Generated by	Wave Number	Resonance	Angle
$_P\boldsymbol{u}^{(2)}_{S_iS_i}$	Self	$\boldsymbol{u}^{(1)}_{S_i}$	$2k_S$	no	θ_S
$_P\boldsymbol{u}^{(2)}_{S_iS_r}$	Cross	$\boldsymbol{u}^{(1)}_{S_i}, \boldsymbol{u}^{(1)}_{S_r}$	$k_{S_iS_r}$	no	90°
$_P\boldsymbol{u}^{(2)}_{P_rP_r}$	Self	$\boldsymbol{u}^{(1)}_{P_r}$	$2k_P$	yes	θ_P
$_P\boldsymbol{u}^{(2)}_{P_rS_r}$	Cross	$\boldsymbol{u}^{(1)}_{P_r}, \boldsymbol{u}^{(1)}_{S_r}$	$k_{P_rS_r}$	no	Φ
$_S\boldsymbol{u}^{(2)}_{P_rS_r}$	Cross	$\boldsymbol{u}^{(1)}_{P_r}, \boldsymbol{u}^{(1)}_{S_r}$	$k_{P_rS_r}$	no	Φ
$_P\boldsymbol{u}^{(2)}_{S_rS_r}$	Self	$\boldsymbol{u}^{(1)}_{S_r}, \boldsymbol{u}^{(1)}_{S_r}$	$2k_S$	no	θ_S
$_S\boldsymbol{u}^{(2)}_{S_rS_r}$	Self	$\boldsymbol{u}^{(1)}_{S_r}$	$2k_S$	yes	θ_S

4.2.4 Complete Solution

The secondary wave field still contains unknown constants ${}_P\beta^{surf}_{P_rP_r}$, ${}_S\beta^{surf}_{S_rS_r}$, ${}_P\gamma^{surf}_{P_rP_r}$ and ${}_S\gamma^{surf}_{S_rS_r}$. Note that

$$ {}_S\beta^{surf}_{S_iS_i} = {}_S\beta^{bulk}_{S_iS_i} = 0. \tag{4.74}$$

Again, we choose

$$ {}_S\gamma^{surf}_{S_iS_i} = 0 \tag{4.75}$$

as initial condition. We still have a free boundary as a boundary condition,

$$ P^L_{31}\left(\boldsymbol{u}^{(2)}\right)|_{z=0} = -P^{NL}_{31}\left(\boldsymbol{u}^{(1)}\right)|_{z=0} \tag{4.76}$$

and

$$ P^L_{33}\left(\boldsymbol{u}^{(2)}\right)|_{z=0} = -P^{NL}_{33}\left(\boldsymbol{u}^{(1)}\right)|_{z=0}, \tag{4.77}$$

where the perturbation method has been applied. Again, this leads to a total of four equations, two equations in x and two without x-dependency. Since the equations in x do not contain any unknowns except ${}_P\beta^{surf}_{P_rP_r}$ and ${}_S\beta^{surf}_{S_rS_r}$, they are solved first. However, since ${}_S\beta^{bulk}_{S_iS_i} = 0$, there is only the trivial solution

$$ {}_P\beta^{surf}_{P_rP_r} = 0, {}_S\beta^{surf}_{S_rS_r} = 0. \tag{4.78}$$

Also see Fig.4.19.

With ${}_P\beta^{surf}_{P_rP_r}$ and ${}_S\beta^{surf}_{S_rS_r}$ being known, one can proceed and solve for ${}_P\gamma^{surf}_{P_rP_r}$ and ${}_S\gamma^{surf}_{S_rS_r}$. This has been done numerically for aluminum. Fig.4.20 shows these constants for different incidence angles θ_S. In Fig.4.21, the same constants are shown on a logarithmic scale.

4.2.5 Second Harmonic Amplitudes

As in the case of an incident P-wave, we are interested in the behavior of the second harmonic amplitudes. What makes the present case particularly interesting is the

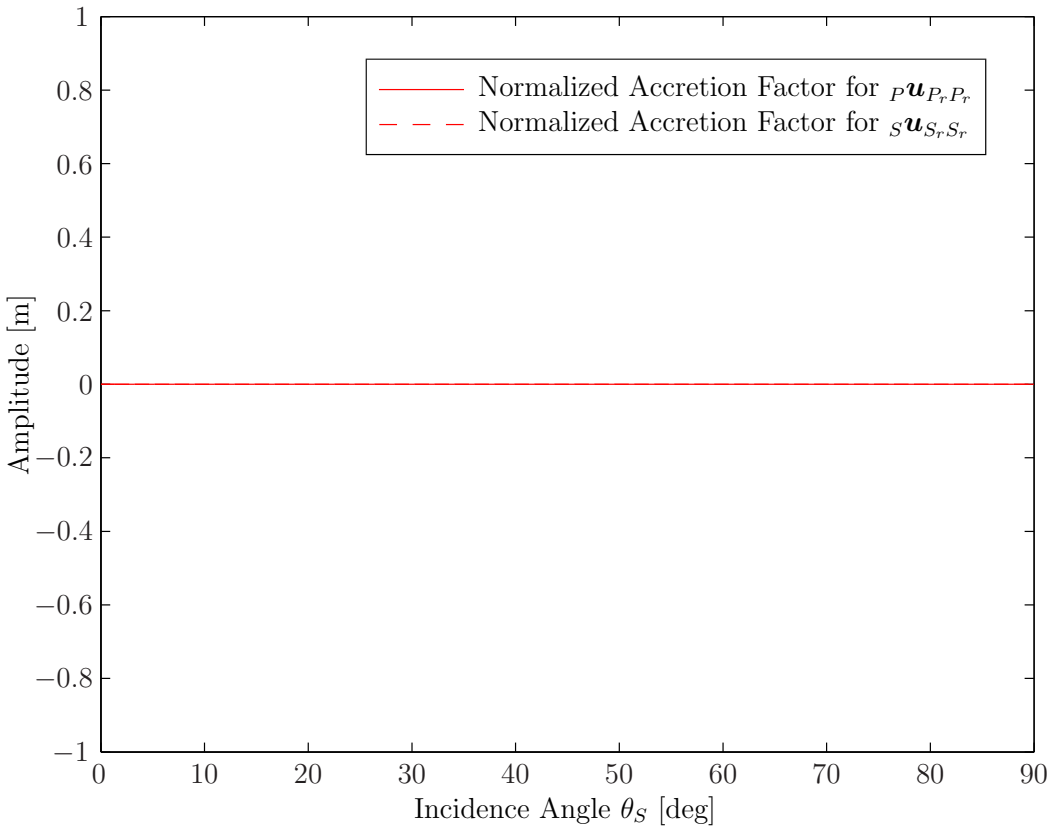

Figure 4.19: Nonlinear Accretion Factors for an Incident SV-Wave in Aluminum.

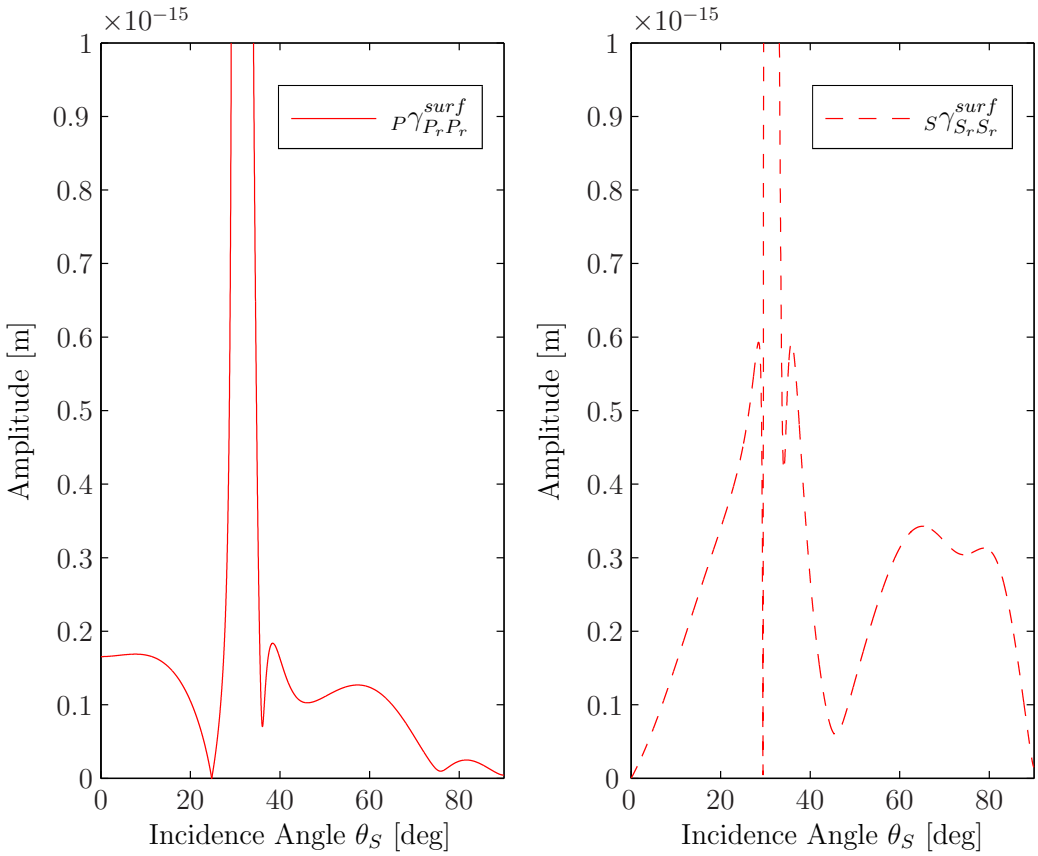

Figure 4.20: Absolute values of ${}_P\gamma^{surf}_{P_rP_r}$ and ${}_S\gamma^{surf}_{S_rS_r}$ in Aluminum.

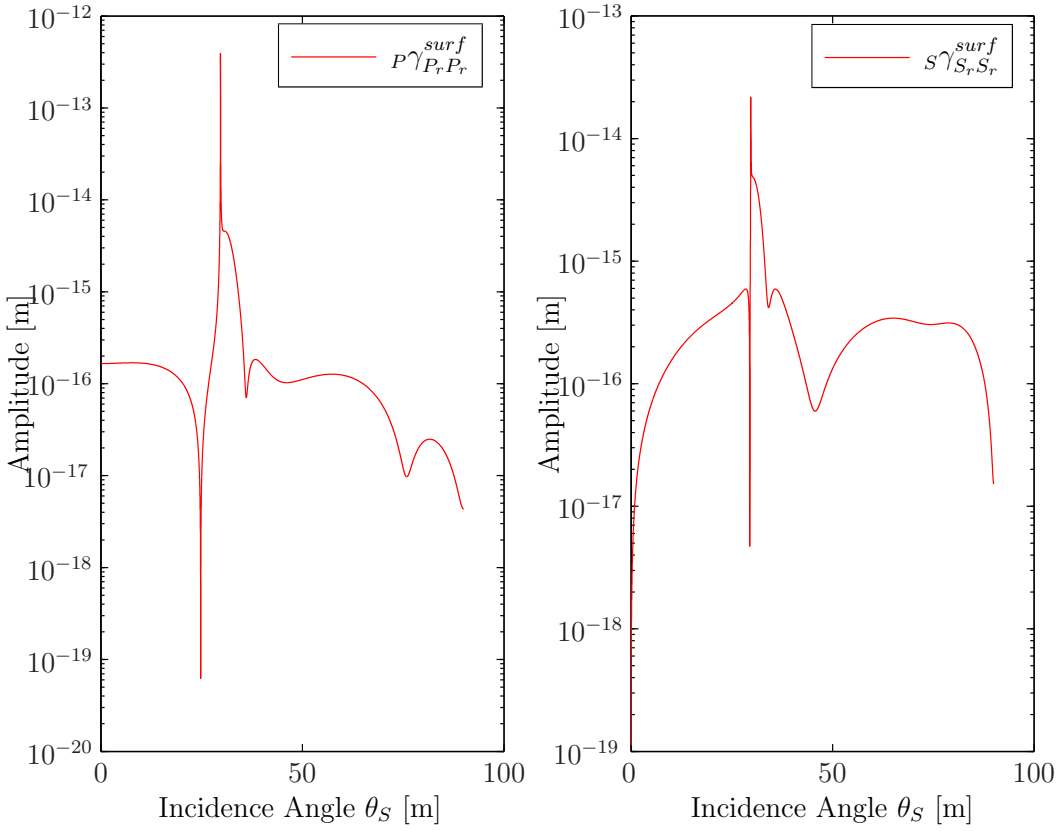

Figure 4.21: Absolute values of ${}_P\gamma^{surf}_{P_rP_r}$ and ${}_S\gamma^{surf}_{S_rS_r}$, Logarithmic Scale.

critical angle, θ_{cr}. Above this angle, there is no more reflected P-wave. Instead, there is a longitudinal surface wave. This wave travels along the boundary and decays with depth. In general, this wave is not very useful for the NDE experiment under consideration. Nevertheless, surface waves (and Rayleigh waves in particular) prove useful for long range surface inspection. Since there is no reflected P-wave above the critical angle, there is also no second harmonic ${}_P\boldsymbol{u}^{(2)}_{P_rP_r}$. If we plot the amplitudes of the second harmonics caused by self-interaction, namely ${}_P\boldsymbol{u}^{(2)}_{P_rP_r}$ and ${}_S\boldsymbol{u}^{(2)}_{S_rS_r}$, along their rays, we will see this effect clearly. Along the rays, it holds

$$z = \frac{x}{\tan\theta_P} \tag{4.79}$$

for ${}_P\boldsymbol{u}^{(2)}_{P_rP_r}$ and

$$z = \frac{x}{\tan\theta_S} \tag{4.80}$$

for ${}_S\boldsymbol{u}^{(2)}_{S_rS_r}$. Taking this into account, the amplitudes of the considered second harmonics below the critical angle are given by

$$\left|{}_P\boldsymbol{u}^{(2)}_{P_rP_r}\right| = \left|\frac{U_{P_r}^2}{4jk_Pc_P^2}\,{}_P\beta^{bulk}_{P_rP_r}\left(\frac{x}{\sin\theta_P} + {}_P\gamma^{surf}_{P_rP_r}\right)\right|, \tag{4.81}$$

$$\left|{}_S\boldsymbol{u}^{(2)}_{S_rS_r}\right| = \left|{}_S\gamma^{surf}_{S_rS_r}\right|. \tag{4.82}$$

Note that the expression for ${}_S\boldsymbol{u}^{(2)}_{S_rS_r}$ is constant. Above the critical angle, we may only consider ${}_S\boldsymbol{u}^{(2)}_{S_rS_r}$, because the longitudinal surface wave is decaying exponentially with depth. The expressions above become

$$\left|{}_P\boldsymbol{u}^{(2)}_{P_rP_r}\right| = \left|\frac{U_{P_r}^2}{4jk_Pc_P^2}\,{}_P\beta^{bulk}_{P_rP_r}\left(\frac{x}{\sin\theta_P} + {}_P\gamma^{surf}_{P_rP_r}\right)e^{-k_Pz\sqrt{\sin^2\theta_P-1}}\right|, \tag{4.83}$$

$$\left|{}_S\boldsymbol{u}^{(2)}_{S_rS_r}\right| = \left|{}_S\gamma^{surf}_{S_rS_r}\right|. \tag{4.84}$$

Hence, no significant amplitude of ${}_P\boldsymbol{u}^{(2)}_{P_rP_r}$ can be measured at $z = L$. The only wave that remains interesting for an NDE experiment is ${}_S\boldsymbol{u}^{(2)}_{S_rS_r}$. In Fig.4.22, we show the measurement of the second harmonics caused by self-interaction below the critical

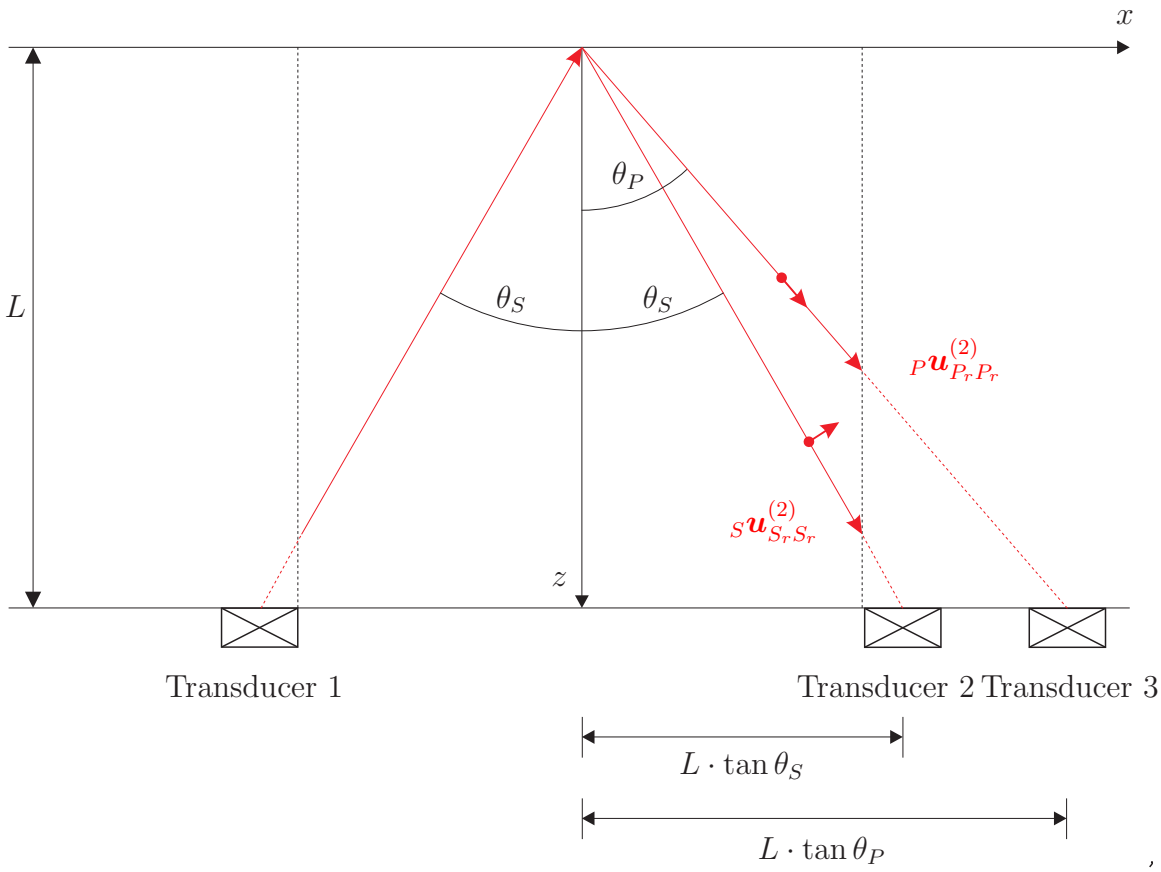

Figure 4.22: Measurement of Reflected Second Harmonics for SV-Wave Incidence, $\theta_S < \theta_{cr}$.

angle. Fig.4.23 shows the case above the critical angle, where $_P\boldsymbol{u}^{(2)}_{P_rP_r}$ has become a longitudinal surface wave. It can be observed that the amplitudes above the critical angle are much smaller. Below the critical angle, the reflected second harmonic P-wave has the largest amplitude. Since this wave does not exist above the critical angle, a measurement setup with an incidence angle below the critical angle seems appropriate.

Figs.4.24 and 4.26 show the amplitudes of the considered second harmonics for $\theta_S = 10°$ and $\theta_S = 20°$. Figures 4.25 and 4.25 show the amplitudes right before and after the reflection. For the given material parameters, the critical angle is

$$\theta_{cr} = 29.7°. \tag{4.85}$$

In Figs.4.28 and 4.29, we show the amplitudes for incident angles above the critical

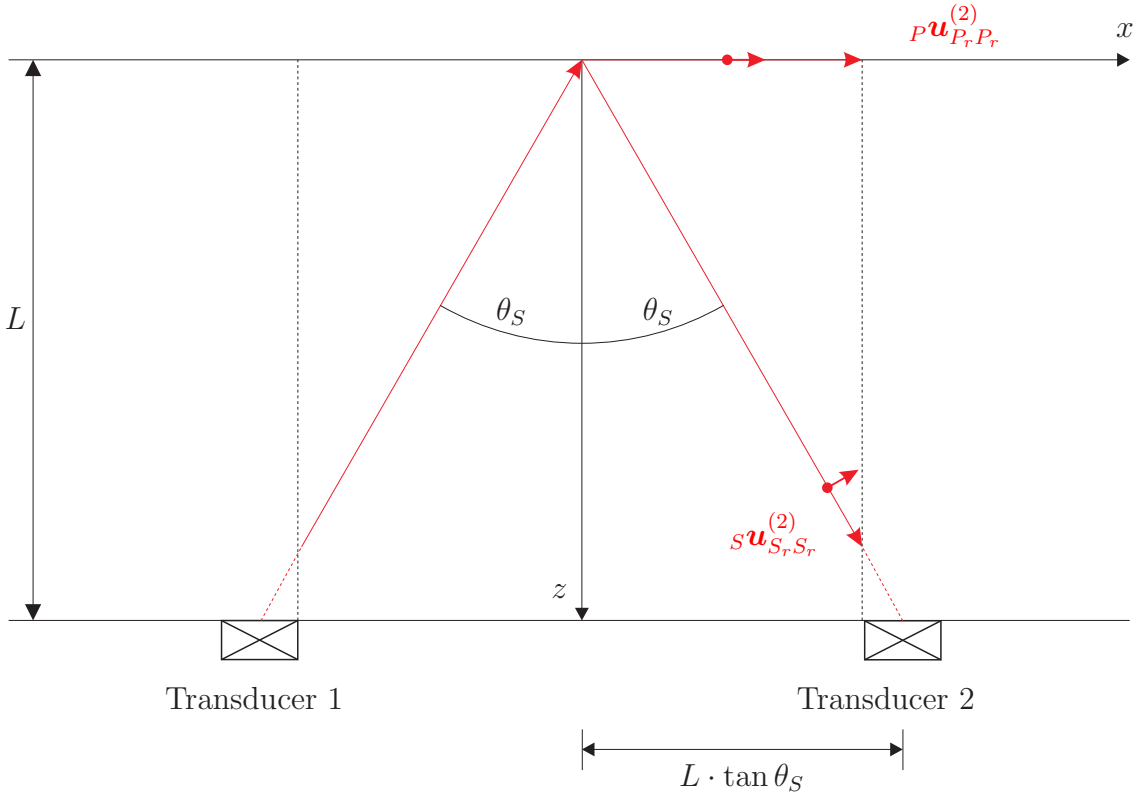

Figure 4.23: Measurement of Reflected Second Harmonics for SV-Wave Incidence, $\theta_S > \theta_{cr}$.

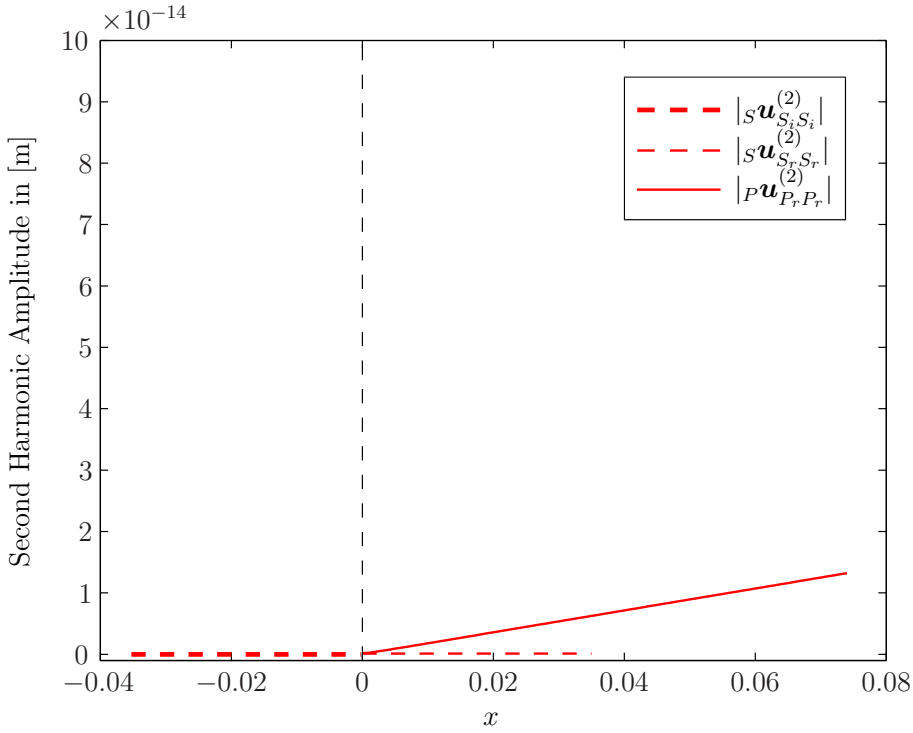

Figure 4.24: Second Harmonic Amplitudes for $\theta_P = 10°$.

angle, namely $\theta_S = 50°$ and $\theta_S = 70°$.

4.2.6 Normal Incidence

The case of normal incidence of an SV-wave is a simplification of the case considered above. Since the SV-wave is now propagating perpendicular to the surface, the SV-wave is totally reflected as an SV-wave. The setup for normal incidence is shown in Fig.30(a).

For the primary field, the amplitudes can be calculated using the Fresnel formulae,

$$U_{S_r} = U_{S_i}, \tag{4.86}$$

$$U_{P_r} = 0. \tag{4.87}$$

Therefore, the primary field can be expressed as

$$\boldsymbol{u}^{(1)} = U_{S_i} \begin{bmatrix} 1 \\ 0 \\ 0 \end{bmatrix} e^{j(\omega t + k_S z)} + U_{S_r} \begin{bmatrix} 1 \\ 0 \\ 0 \end{bmatrix} e^{j(\omega t - k_S z)}. \tag{4.88}$$

The secondary field is made up by a second harmonic P-wave caused by self-interaction of the incident SV-wave, and a reflected second harmonic P-wave caused by self-interaction of the reflected first harmonic SV-wave. Also see Fig. 30(b). No second harmonic SV-waves will be generated. This results in the secondary field

$$\begin{aligned} \boldsymbol{u}^{(2)} = & \frac{U_{S_i}^2}{c_P^2(4k_S^2 - 4k_P^2)} {}_P\beta_{S_iS_i}^{bulk} e^{j(2\omega t + 2k_S z)} + \begin{bmatrix} 0 \\ 0 \\ -1 \end{bmatrix} \\ & \left[\frac{U_{S_r}^2}{c_P^2(4k_S^2 - 4k_P^2)} {}_P\beta_{S_rS_r}^{bulk} \right] e^{j(2\omega t - 2k_S z)} \begin{bmatrix} 0 \\ 0 \\ 1 \end{bmatrix} + {}_P\gamma_{S_rS_r}^{surf} e^{j(2\omega t - 2k_P z)} \begin{bmatrix} 0 \\ 0 \\ 1 \end{bmatrix} . \end{aligned} \tag{4.89}$$

Note that there are actually three P-waves: One propagating in negative z-direction with wavenumber $2k_S$, one propagating in positive z-direction with wavenumber $2k_S$

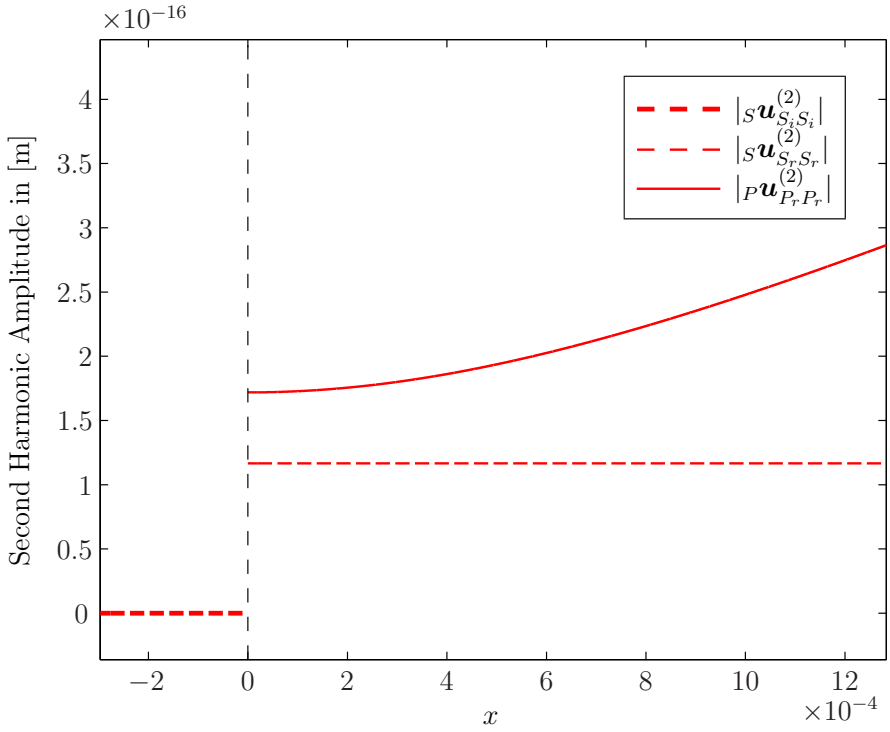

Figure 4.25: Second Harmonic Amplitudes for $\theta_P = 10°$, zoomed in.

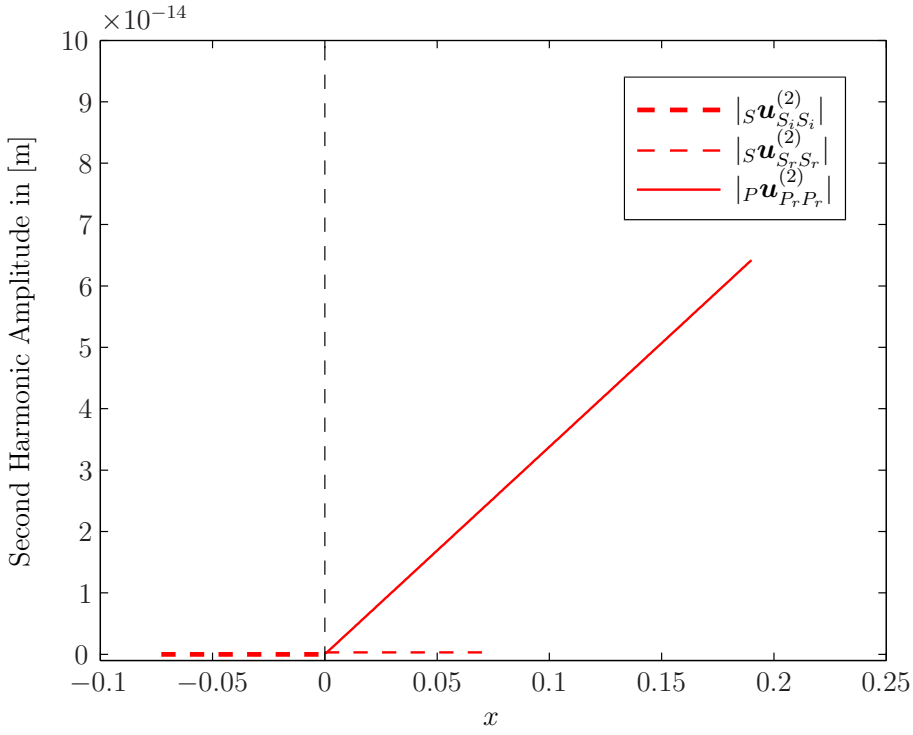

Figure 4.26: Second Harmonic Amplitudes for $\theta_P = 20°$.

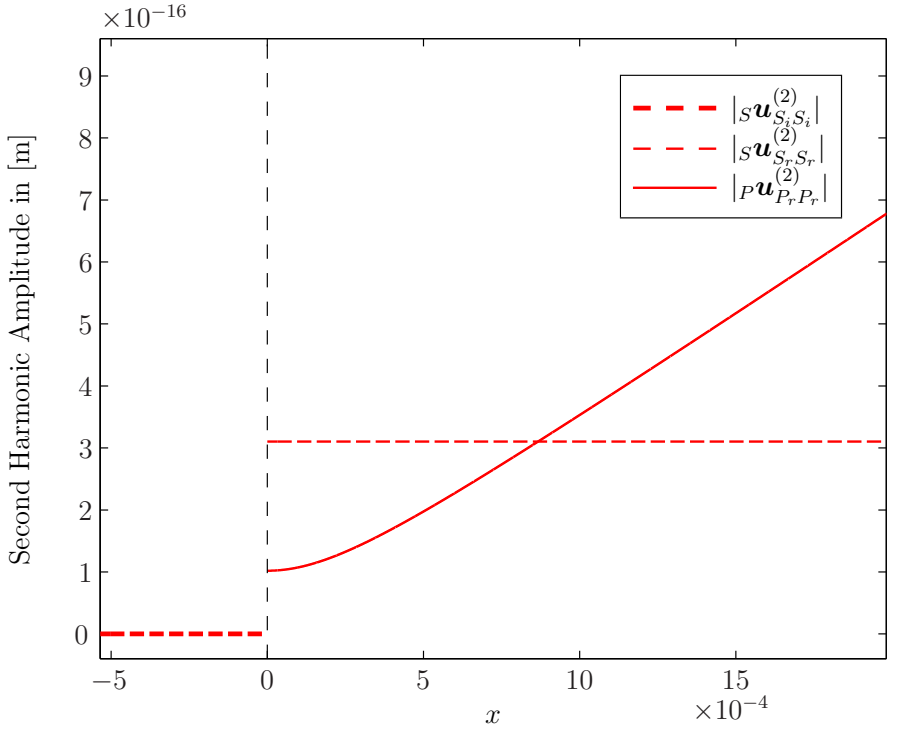

Figure 4.27: Second Harmonic Amplitudes for $\theta_P = 20°$, zoomed in.

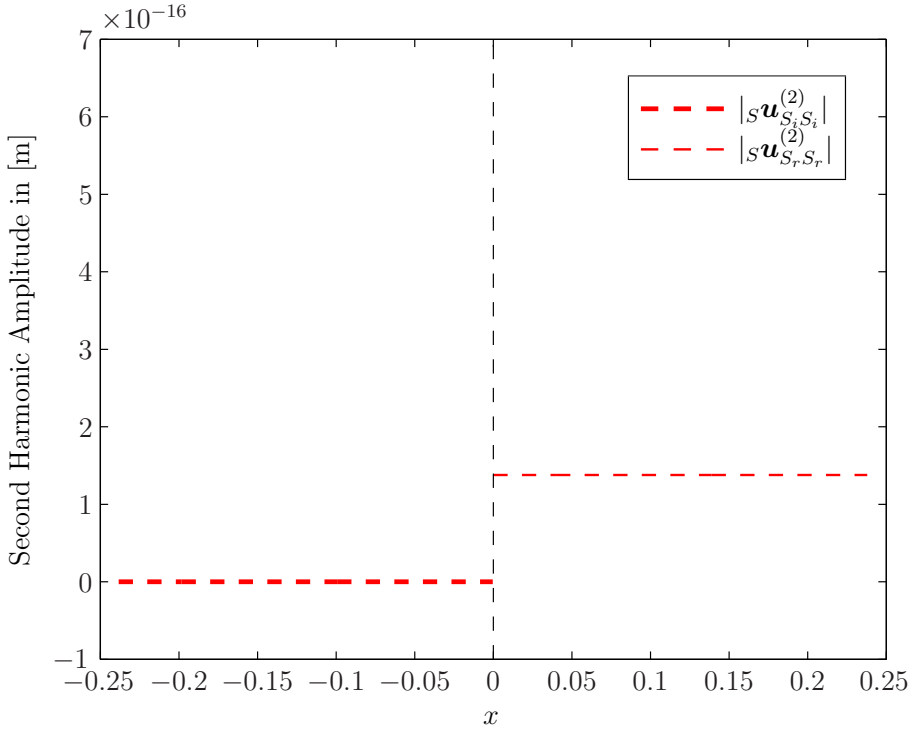

Figure 4.28: Second Harmonic Amplitudes for $\theta_P = 50°$.

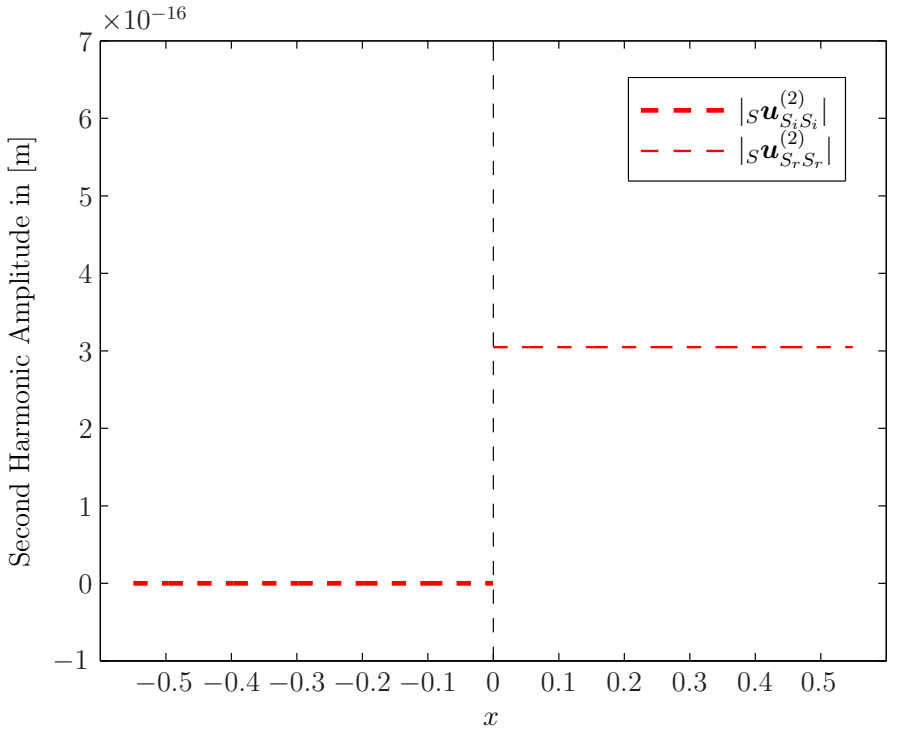

Figure 4.29: Second Harmonic Amplitudes for $\theta_P = 70°$.

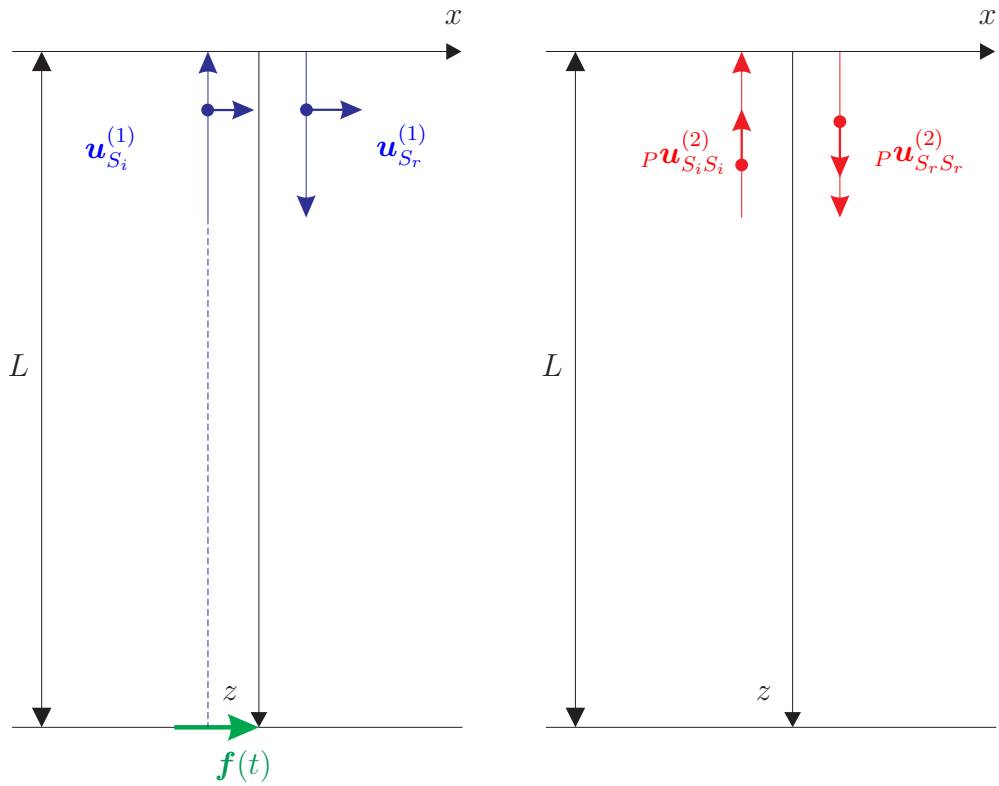

(a) Primary Field.

(b) Secondary Field.

Figure 4.30: Wave Fields for Normal SV-Wave Incidence.

and finally, another P-wave propagating in the positive z-direction with wavenumber $2k_P$. Note that none of these waves show the feature of accumulation. Applying the boundary condition,

$$P_{33}^{L}\left(\boldsymbol{u}^{(2)}\right)|_{z=0} = -P_{33}^{NL}\left(\boldsymbol{u}^{(1)}\right)|_{z=0}, \tag{4.90}$$

we can determine the remaining unknown ${}_P\gamma_{S_rS_r}^{surf}$,

$${}_P\gamma_{S_rS_r}^{surf} = -\frac{k_S}{k_P}\frac{U_{S_i}^2}{c_P^2(4k_S^2-4k_P^2)}{}_P\beta_{S_iS_i}^{bulk} - \frac{k_S}{k_P}\frac{U_{S_r}^2}{c_P^2(4k_S^2-4k_P^2)}{}_P\beta_{S_rS_r}^{bulk}. \tag{4.91}$$

Using

$$U_{S_r} = U_{S_i} \tag{4.92}$$

and

$${}_P\beta_{S_rS_r}^{bulk} = {}_P\beta_{S_iS_i}^{bulk} \tag{4.93}$$

we obtain

$${}_P\gamma_{S_rS_r}^{surf} = -2\frac{k_S}{k_P}\frac{U_{S_i}^2}{c_P^2(4k_S^2-4k_P^2)}{}_P\beta_{S_iS_i}^{bulk}. \tag{4.94}$$

Now the amplitudes of the second harmonics can be plotted. Note that there are only P-waves with constant amplitudes, as Fig.4.31 indicates. There are two reflected second harmonic P-waves, one of them represesnts the homogeneous solution while the other one represents the particular solution. Also note that all waves have small amplitudes of order 10^{-16} or smaller. Therefore, normal incidence of an SV-wave seems not useful for second harmonic generation.

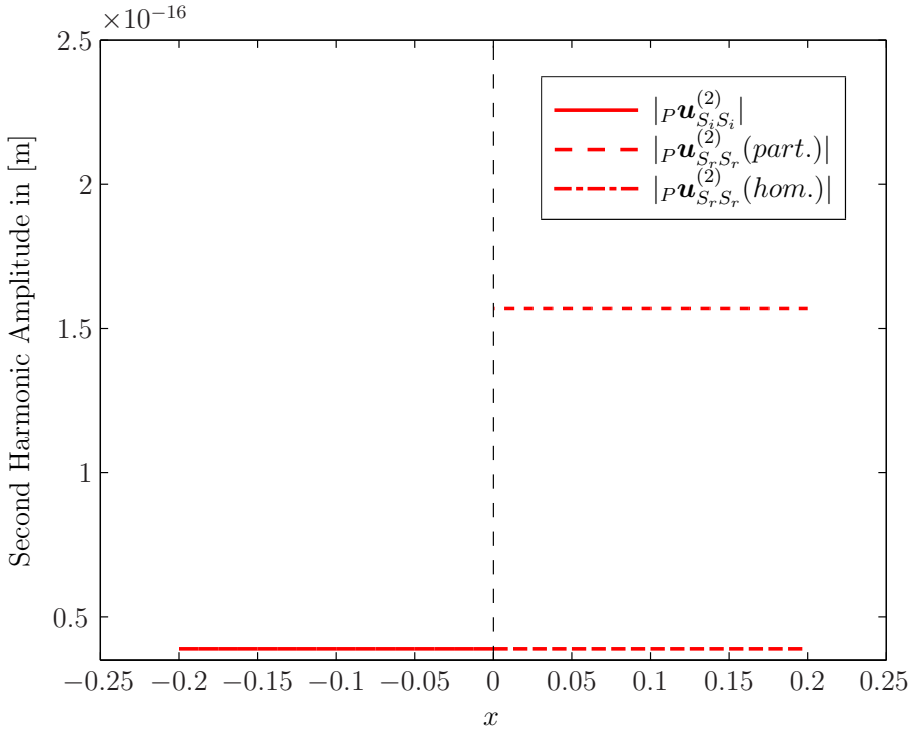

Figure 4.31: Second Harmonic Amplitudes for Normal Incidence of an SV-Wave.

CHAPTER V

CONCLUSIONS AND OUTLOOK

5.1 Conclusions

The objective of this study is to analyze the generation of second harmonic waves under the presence of a free boundary. A summary of the theory of linear wave propagation has been given, with a focus on reflection of waves at a free boundary. The nonlinear interaction of two primary bulk waves has been investigated. It has been shown that there are two ways in which the primary waves can interact: self-interaction and cross-interaction. Assuming a stress-free boundary, the nonlinear equations of motion have been solved using the perturbation method. This shows that there are two general types of solution:

1. The resonant case. In this case, the generated second harmonic waves show the feature of accumulation, i.e. these waves grow in a linear fashion with propagation distance. It has been shown that the resonant case can only occur for second harmonic waves caused by self-interaction due to the requirement of phase speed matching. Secondary waves caused by cross-interaction cannot satisfy the resonance condition due to the lac of phase speed matching.

2. The non-resonant case. In this case, the generated waves have a constant amplitude.

The situation of an incident P- and an incident SV-wave has been analyzed. For both incident waves, the primary and secondary fields have been derived and unknown constants have been determined by applying the boundary conditions. It was seen that the secondary field is significantly influenced by the free boundary. The behavior

of the second harmonic amplitudes with propagation distance has been illustrated. The results show that only the waves that satisfy the resonance condition are of interest for measurements, because all other waves have vanishing amplitudes. Even the accumulating waves have amplitudes of three to four orders of magnitude smaller than the primary waves.

The degenerate case of normal incidence has also been presented. It has become clear that normal incidence is not useful for the measurement of second harmonic waves if only one surface is accessible. We therefore recommend the setup of oblique incidence for one-sided measurements. It was seen that the incidence angle has crucial influence on the obtained second harmonic amplitudes. In general, a greater incidence angle will result in higher amplitudes, but at the same time, greater incidence angles have disadvantages. In particular, a large incidence angle makes the area under inspection large, and from our measurements, we can only conclude that a defect is somewhere within this large area. As a consequence, choosing the incidence angle is a trade-off between high harmonic amplitudes and area under inspection.

As a conclusion, one can say that oblique incidence of P- and SV-waves and their reflection at a free boundary proves useful for the generation of second harmonic waves.

5.2 Outlook

In this thesis, we have restricted ourselves to a purely analytical investigation and a numerical simulation. The results of this work indicate that the setup of obliquely incident waves and their reflection at a free boundary could have potential for applications in the field of nondestructive evaluation. However, experiments have to be conducted in order to prove the existence of the waves that have been predicted in this work. Such experiments will be challenging, since the second harmonic waves have very small amplitudes, and nonlinearities caused by the measurement equipment

could make it difficult to obtain good results. However, since an actual NDE application is the desired outcome of this research, such experiments will be essential to evaluate the feasibility of the suggested one-sided measurement setup. At the same time, further theoretical investigations are needed to affirm the results obtained in this work. We remind the reader that the solution was obtained by applying the perturbation method, therefore the derived solution is rather an approximation of the solution. Different approaches should be applied, and the results from these approaches should be compared to the results given in this thesis.

Therefore, future research should be focused both on theory and experiments, and we have to keep in mind that only the combination of the both fields will result in an actual benefit.

APPENDIX A

BULK NONLINEARITY PARAMETERS

A.1 β^{bulk} *Parameters for P-Wave Incidence*

$$ {}_P\beta^{bulk}_{P_iP_i} = j\frac{k_P^3}{2\rho}\left(3\lambda + 6\mu + 2\mathcal{A} + 6\mathcal{B} + 2\mathcal{C}\right) \tag{A.1} $$

$$ {}_P\beta^{bulk}_{P_rP_r} = j\frac{k_P^3}{2\rho}\left(3\lambda + 6\mu + 2\mathcal{A} + 6\mathcal{B} + 2\mathcal{C}\right) \tag{A.2} $$

$$ {}_P\beta^{bulk}_{S_rS_r} = j\frac{k_S^3}{2\rho}\left(\lambda + 2\mu + \frac{\mathcal{A}}{2} + \mathcal{B}\right) \tag{A.3} $$

$$ {}_S\beta^{bulk}_{S_rS_r} = 0 \tag{A.4} $$

$$ \begin{aligned} {}_P\beta^{bulk}_{P_iP_r} = j\frac{k_P^3}{2\rho}[&3\lambda + 3\mu + \mathcal{A} + 6\mathcal{B} + 4\mathcal{C} - (2\lambda + 6\mu + 2\mathcal{A} + 4\mathcal{B})\cos(2\theta_P) \\ &+ (\lambda + 3\mu + \mathcal{A} + 2\mathcal{B})\cos(4\theta_P)]\sin(\theta_P) \end{aligned} \tag{A.5} $$

$$ \begin{aligned} {}_P\beta^{bulk}_{P_iS_r} = \frac{jk_Pk_S}{8\rho}\Big[\big\{ &-2k_P(\lambda+\mu)\cos(\theta_P) + k_S(4\lambda + 8\mu + 2\mathcal{A} + 4\mathcal{B})\cos(\theta_S) \\ &+ (\lambda + 3\mu + \mathcal{A} + 2\mathcal{B})(-k_S\cos(2\theta_P + \theta_S) - 3k_P\cos(\theta_P + 2\theta_S) \\ &+ k_P\cos(3\theta_P + 2\theta_S) + k_S\cos(2\theta_P + 3\theta_S))\big\}\sin(\Psi) \\ &- \big\{2k_P(\lambda+\mu)\sin(\theta_P) + k_S(4\lambda + 8\mu + 2\mathcal{A} + 4\mathcal{B})\sin(\theta_S) \\ &+ (\lambda + 3\mu + \mathcal{A} + 2\mathcal{B})(k_S\sin(2\theta_P + \theta_S) - 3k_P\sin(\theta_P + 2\theta_S) \\ &- k_P\sin(3\theta_P + 2\theta_S) + k_S\sin(2\theta_P + 3\theta_S))\big\}\cos(\Psi)\Big] \end{aligned} \tag{A.6} $$

$$
\begin{aligned}
{}_S\beta^{bulk}_{P_iS_r} = \frac{jk_Pk_S}{8\rho}\Big[\big\{ &-2k_P(\lambda+\mu)\cos(\theta_P) + k_S(4\lambda+8\mu+2\mathcal{A}+4\mathcal{B})\cos(\theta_S) \\
&+ (\lambda+3\mu+\mathcal{A}+2\mathcal{B})(-k_S\cos(2\theta_P+\theta_S) - 3k_P\cos(\theta_P+2\theta_S) \\
&+ k_P\cos(3\theta_P+2\theta_S) + k_S\cos(2\theta_P+3\theta_S))\big\}\cos(\Psi) \\
&- \big\{2k_P(\lambda+\mu)\sin(\theta_P) + k_S(4\lambda+8\mu+2\mathcal{A}+4\mathcal{B})\sin(\theta_S) \\
&+ (\lambda+3\mu+\mathcal{A}+2\mathcal{B})(k_S\sin(2\theta_P+\theta_S) - 3k_P\sin(\theta_P+2\theta_S) \\
&- k_P\sin(3\theta_P+2\theta_S) + k_S\sin(2\theta_P+3\theta_S))\big\}\sin(\Psi)\Big]
\end{aligned}
\tag{A.7}
$$

$$
\begin{aligned}
{}_P\beta^{bulk}_{P_rS_r} = \frac{jk_Pk_S}{8\rho}\Big[&2k_P(\lambda+\mu)\sin(\Phi-\theta_P) \\
&+ k_S(\lambda+3\mu+\mathcal{A}+2\mathcal{B})\sin(\Phi+2\theta_P-3\theta_S) \\
&+ k_P(3\lambda+9\mu+3\mathcal{A}+6\mathcal{B})\sin(\Phi+\theta_P-2\theta_S) \\
&+ k_S(4\lambda+8\mu+2\mathcal{A}+4\mathcal{B})\sin(\Phi-\theta_S) \\
&- k_S(\lambda+3\mu+\mathcal{A}+2\mathcal{B})\sin(\Phi-2\theta_P+\theta_S) \\
&- k_P(\lambda+3\mu+\mathcal{A}+2\mathcal{B})\sin(\Phi-3\theta_P+2\theta_S)\Big]
\end{aligned}
\tag{A.8}
$$

$$
\begin{aligned}
{}_S\beta^{bulk}_{P_rS_r} = \frac{jk_Pk_S}{8\rho}\Big[&2k_P(\lambda+\mu)\cos(\Phi-\theta_P) \\
&+ k_S(\lambda+3\mu+\mathcal{A}+2\mathcal{B})\cos(\Phi+2\theta_P-3\theta_S) \\
&+ k_P(3\lambda+9\mu+3\mathcal{A}+6\mathcal{B})\cos(\Phi+\theta_P-2\theta_S) \\
&+ k_S(4\lambda+8\mu+2\mathcal{A}+4\mathcal{B})\cos(\Phi-\theta_S) \\
&- k_S(\lambda+3\mu+\mathcal{A}+2\mathcal{B})\cos(\Phi-2\theta_P+\theta_S) \\
&- k_P(\lambda+3\mu+\mathcal{A}+2\mathcal{B})\cos(\Phi-3\theta_P+2\theta_S)\Big]
\end{aligned}
\tag{A.9}
$$

A.2 β^{bulk} *Parameters for SV-Wave Incidence*

$$ {}_S\beta^{bulk}_{S_iS_i} = 0 \tag{A.10}$$

$$ {}_P\beta^{bulk}_{S_iS_i} = j\frac{k_S^3}{2\rho}\left(\lambda + 2\mu + \frac{\mathcal{A}}{2} + \mathcal{B}\right) \tag{A.11}$$

$$ {}_P\beta^{bulk}_{P_rP_r} = j\frac{k_P^3}{2\rho}\left(3\lambda + 6\mu + 2\mathcal{A} + 6\mathcal{B} + 2\mathcal{C}\right) \tag{A.12}$$

$$ {}_P\beta^{bulk}_{S_rS_r} = j\frac{k_S^3}{2\rho}\left(\lambda + 2\mu + \frac{\mathcal{A}}{2} + \mathcal{B}\right) \tag{A.13}$$

$$ {}_S\beta^{bulk}_{S_rS_r} = 0 \tag{A.14}$$

$$ {}_S\beta^{bulk}_{S_iS_r} = 0 \tag{A.15}$$

$$\begin{aligned} {}_P\beta^{bulk}_{S_iP_r} = \frac{jk_Pk_S}{8\rho}\Big[\big\{ &-2k_P(\lambda+\mu)\cos(\theta_P) + k_S(4\lambda + 8\mu + 2\mathcal{A} + 4\mathcal{B})\cos(\theta_S) \\ &+ (\lambda + 3\mu + \mathcal{A} + 2\mathcal{B})(-k_S\cos(2\theta_P + \theta_S) - 3k_P\cos(\theta_P + 2\theta_S) \\ &+ k_P\cos(3\theta_P + 2\theta_S) + k_S\cos(2\theta_P + 3\theta_S))\big\}\sin(\Psi) \\ &+ \big\{2k_P(\lambda+\mu)\sin(\theta_P) + k_S(4\lambda + 8\mu + 2\mathcal{A} + 4\mathcal{B})\sin(\theta_S) \\ &+ (\lambda + 3\mu + \mathcal{A} + 2\mathcal{B})(k_S\sin(2\theta_P + \theta_S) - 3k_P\sin(\theta_P + 2\theta_S) \\ &- k_P\sin(3\theta_P + 2\theta_S) + k_S\sin(2\theta_P + 3\theta_S))\big\}\cos(\Psi)\Big] \end{aligned} \tag{A.16}$$

$$
\begin{aligned}
{}_S\beta^{bulk}_{S_iP_r} = \frac{jk_Pk_S}{8\rho}\Big[\big\{ &-2k_P(\lambda+\mu)\cos(\theta_P) + k_S(4\lambda+8\mu+2\mathcal{A}+4\mathcal{B})\cos(\theta_S) \\
&+ (\lambda+3\mu+\mathcal{A}+2\mathcal{B})(-k_S\cos(2\theta_P+\theta_S) - 3k_P\cos(\theta_P+2\theta_S) \\
&+ k_P\cos(3\theta_P+2\theta_S) + k_S\cos(2\theta_P+3\theta_S))\big\}\cos(\Psi) \\
&+ \big\{2k_P(\lambda+\mu)\sin(\theta_P) + k_S(4\lambda+8\mu+2\mathcal{A}+4\mathcal{B})\sin(\theta_S) \\
&+ (\lambda+3\mu+\mathcal{A}+2\mathcal{B})(k_S\sin(2\theta_P+\theta_S) - 3k_P\sin(\theta_P+2\theta_S) \\
&- k_P\sin(3\theta_P+2\theta_S) + k_S\sin(2\theta_P+3\theta_S))\big\}\sin(\Psi)\Big]
\end{aligned} \tag{A.17}
$$

$$
{}_P\beta^{bulk}_{S_iS_r} = -j\frac{k_S^3}{2\rho}\left(\lambda+\mu+(\lambda+3\mu+\mathcal{A}+2\mathcal{B})\cos(4\theta_S)\right)\sin(\theta_S) \tag{A.18}
$$

$$
{}_S\beta^{bulk}_{S_iS_r} = 0 \tag{A.19}
$$

$$
\begin{aligned}
{}_P\beta^{bulk}_{P_rS_r} = \frac{jk_Pk_S}{8\rho}\Big[&2k_P(\lambda+\mu)\sin(\Phi-\theta_P) \\
&+ k_S(\lambda+3\mu+\mathcal{A}+2\mathcal{B})\sin(\Phi+2\theta_P-3\theta_S) \\
&+ k_P(3\lambda+9\mu+3\mathcal{A}+6\mathcal{B})\sin(\Phi+\theta_P-2\theta_S) \\
&+ k_S(4\lambda+8\mu+2\mathcal{A}+4\mathcal{B})\sin(\Phi-\theta_S) \\
&- k_S(\lambda+3\mu+\mathcal{A}+2\mathcal{B})\sin(\Phi-2\theta_P+\theta_S) \\
&- k_P(\lambda+3\mu+\mathcal{A}+2\mathcal{B})\sin(\Phi-3\theta_P+2\theta_S)\Big]
\end{aligned} \tag{A.20}
$$

$$
\begin{aligned}
{}_S\beta^{bulk}_{P_rS_r} = \frac{jk_Pk_S}{8\rho}\Big[&2k_P(\lambda+\mu)\cos(\Phi-\theta_P) \\
&+ k_S(\lambda+3\mu+\mathcal{A}+2\mathcal{B})\cos(\Phi+2\theta_P-3\theta_S) \\
&+ k_P(3\lambda+9\mu+3\mathcal{A}+6\mathcal{B})\cos(\Phi+\theta_P-2\theta_S) \\
&+ k_S(4\lambda+8\mu+2\mathcal{A}+4\mathcal{B})\cos(\Phi-\theta_S) \\
&- k_S(\lambda+3\mu+\mathcal{A}+2\mathcal{B})\cos(\Phi-2\theta_P+\theta_S) \\
&- k_P(\lambda+3\mu+\mathcal{A}+2\mathcal{B})\cos(\Phi-3\theta_P+2\theta_S)\Big]
\end{aligned} \tag{A.21}
$$

APPENDIX B

SECONDARY WAVES

B.1 P-Wave Incidence

$$
{}_P\boldsymbol{u}^{(2)}_{P_iP_i} = \frac{U^2_{P_i}}{4jk_Pc^2_P}\left[{}_P\beta^{surf}_{P_iP_i}\sin\theta_P(x+L\tan\theta_P) + \frac{{}_P\beta^{bulk}_{P_iP_i} - {}_P\beta^{surf}_{P_iP_i}\sin^2\theta_P}{\cos\theta_P}(L-z)\right]
$$
$$
\cdot\ e^{j(2\omega t - 2k_Px\sin\theta_P + 2k_Pz\cos\theta_P)}\begin{bmatrix}\sin\theta_P\\0\\-\cos\theta_P\end{bmatrix} \tag{B.1}
$$

$$
{}_P\boldsymbol{u}^{(2)}_{P_iP_r} = \frac{U_{P_i}U_{P_r}}{c^2_P(k^2_{P_iP_r}-4k^2_P)}{}_P\beta^{bulk}_{P_iP_r}e^{j(2\omega t - k_{P_iP_r}x)}\begin{bmatrix}1\\0\\0\end{bmatrix} \tag{B.2}
$$

$$
{}_P\boldsymbol{u}^{(2)}_{P_iS_r} = \frac{U_{P_i}U_{S_r}}{c^2_P(k^2_{P_iS_r}-4k^2_P)}{}_P\beta^{bulk}_{P_iS_r}e^{j(2\omega t - k_{P_iS_r}x\sin\Psi - k_{P_iS_r}z\cos\Psi)}\begin{bmatrix}\sin\Psi\\0\\\cos\Psi\end{bmatrix} \tag{B.3}
$$

$$
{}_S\boldsymbol{u}^{(2)}_{P_iS_r} = \frac{U_{P_i}U_{S_r}}{c^2_S(k^2_{P_iS_r}-4k^2_S)}{}_S\beta^{bulk}_{P_iS_r}e^{j(2\omega t - k_{P_iS_r}x\sin\Psi - k_{P_iS_r}z\cos\Psi)}\begin{bmatrix}\cos\Psi\\0\\-\sin\Psi\end{bmatrix} \tag{B.4}
$$

$$
{}_P\boldsymbol{u}^{(2)}_{P_rP_r} = \frac{U^2_{P_r}}{4jk_Pc^2_P}\left[{}_P\beta^{surf}_{P_rP_r}\sin\theta_Px + \frac{{}_P\beta^{bulk}_{P_rP_r} - {}_P\beta^{surf}_{P_rP_r}\sin^2\theta_P}{\cos\theta_P}z\right]
$$
$$
\cdot\ e^{j(2\omega t - 2k_Px\sin\theta_P - 2k_Pz\cos\theta_P)}\begin{bmatrix}\sin\theta_P\\0\\\cos\theta_P\end{bmatrix}
$$
$$
+\ {}_P\gamma^{surf}_{P_rP_r}\,e^{j(2\omega t - 2k_Px\sin\theta_P - 2k_Pz\cos\theta_P)}\begin{bmatrix}\sin\theta_P\\0\\\cos\theta_P\end{bmatrix} \tag{B.5}
$$

$$
{}_P\boldsymbol{u}^{(2)}_{P_rS_r} = \frac{U_{P_r}U_{S_r}}{c^2_P(k^2_{P_rS_r}-4k^2_P)}{}_P\beta^{bulk}_{P_rS_r}e^{j(2\omega t - k_{P_rS_r}x\sin\Phi - k_{P_rS_r}z\cos\Phi)}\begin{bmatrix}\sin\Phi\\0\\\cos\Phi\end{bmatrix} \tag{B.6}
$$

$$
{}_S\boldsymbol{u}^{(2)}_{P_rS_r} = \frac{U_{P_r}U_{S_r}}{c^2_S(k^2_{P_rS_r}-4k^2_S)}{}_S\beta^{bulk}_{P_rS_r}e^{j(2\omega t - k_{P_rS_r}x\sin\Phi - k_{P_rS_r}z\cos\Phi)}\begin{bmatrix}\cos\Phi\\0\\-\sin\Phi\end{bmatrix} \tag{B.7}
$$

$$
\begin{aligned}
{}_S\boldsymbol{u}^{(2)}_{S_rS_r} = \frac{U_{S_r}^2}{4jk_Sc_S^2}\left[{}_S\beta^{surf}_{S_rS_r}\sin\theta_S x - \frac{{}_S\beta^{surf}_{S_rS_r}\sin^2\theta_S}{\cos\theta_S}z\right] \\
\cdot\ e^{j(2\omega t-2k_Sx\sin\theta_S-2k_Sz\cos\theta_S)}\begin{bmatrix}\cos\theta_S\\0\\-\sin\theta_S\end{bmatrix} \\
+\ {}_S\gamma^{surf}_{S_rS_r}\,e^{j(2\omega t-2k_Sx\sin\theta_S-2k_Sz\cos\theta_S)}\begin{bmatrix}\cos\theta_S\\0\\-\sin\theta_S\end{bmatrix}
\end{aligned}
\tag{B.8}
$$

$$
{}_P\boldsymbol{u}^{(2)}_{S_rS_r} = \frac{U_{S_r}^2}{c_P^2(4k_S^2-4k_P^2)}{}_P\beta^{bulk}_{S_rS_r}e^{j(2\omega t-2k_Sx\sin\theta_S-2k_Sz\cos\theta_S)}\begin{bmatrix}\sin\theta_S\\0\\\cos\theta_S\end{bmatrix}
\tag{B.9}
$$

B.2 SV-Wave Incidence

$$ {}_P\boldsymbol{u}^{(2)}_{S_iS_i} = \frac{U^2_{S_i}}{c^2_P(4k^2_S - 4k^2_P)} {}_P\beta^{bulk}_{S_iS_i} e^{j(2\omega t - 2k_S x \sin\theta_S + 2k_S z\cos\theta_S)} \begin{bmatrix} \sin\theta_S \\ 0 \\ -\cos\theta_S \end{bmatrix} \tag{B.10} $$

$$ {}_P\boldsymbol{u}^{(2)}_{S_iS_r} = \frac{U_{S_i}U_{S_r}}{c^2_P(k^2_{S_iS_r} - 4k^2_P)} {}_P\beta^{bulk}_{S_iS_r} e^{j(2\omega t - k_{S_iS_r}x)} \begin{bmatrix} 1 \\ 0 \\ 0 \end{bmatrix} \tag{B.11} $$

$$ \begin{aligned} {}_P\boldsymbol{u}^{(2)}_{P_rP_r} = {} & \frac{U^2_{P_r}}{4jk_Pc^2_P} \left[{}_P\beta^{surf}_{P_rP_r} \sin\theta_P x + \frac{{}_P\beta^{bulk}_{P_rP_r} - {}_P\beta^{surf}_{P_rP_r}\sin^2\theta_P}{\cos\theta_P} z \right] \\ & \cdot\ e^{j(2\omega t - 2k_P x\sin\theta_P - 2k_P z\cos\theta_P)} \begin{bmatrix} \sin\theta_P \\ 0 \\ \cos\theta_P \end{bmatrix} \\ & +\ {}_P\gamma^{surf}_{P_rP_r}\, e^{j(2\omega t - 2k_P x\sin\theta_P - 2k_P z\cos\theta_P)} \begin{bmatrix} \sin\theta_P \\ 0 \\ \cos\theta_P \end{bmatrix} \end{aligned} \tag{B.12} $$

$$ {}_P\boldsymbol{u}^{(2)}_{P_rS_r} = \frac{U_{P_r}U_{S_r}}{c^2_P(k^2_{P_rS_r} - 4k^2_P)} {}_P\beta^{bulk}_{P_rS_r} e^{j(2\omega t - k_{P_rS_r}x\sin\Phi - k_{P_rS_r}z\cos\Phi)} \begin{bmatrix} \sin\Phi \\ 0 \\ \cos\Phi \end{bmatrix} \tag{B.13} $$

$$ {}_S\boldsymbol{u}^{(2)}_{P_rS_r} = \frac{U_{P_r}U_{S_r}}{c^2_S(k^2_{P_rS_r} - 4k^2_S)} {}_S\beta^{bulk}_{P_rS_r} e^{j(2\omega t - k_{P_rS_r}x\sin\Phi - k_{P_rS_r}z\cos\Phi)} \begin{bmatrix} \cos\Phi \\ 0 \\ -\sin\Phi \end{bmatrix} \tag{B.14} $$

$$ \begin{aligned} {}_S\boldsymbol{u}^{(2)}_{S_rS_r} = {} & \frac{U^2_{S_r}}{4jk_Sc^2_S} \left[{}_S\beta^{surf}_{S_rS_r} \sin\theta_S x - \frac{{}_S\beta^{surf}_{S_rS_r}\sin^2\theta_S}{\cos\theta_S} z \right] \\ & \cdot\ e^{j(2\omega t - 2k_S x\sin\theta_S - 2k_S z\cos\theta_S)} \begin{bmatrix} \cos\theta_S \\ 0 \\ -\sin\theta_S \end{bmatrix} \\ & +\ {}_S\gamma^{surf}_{S_rS_r}\, e^{j(2\omega t - 2k_S x\sin\theta_S - 2k_S z\cos\theta_S)} \begin{bmatrix} \cos\theta_S \\ 0 \\ -\sin\theta_S \end{bmatrix} \end{aligned} \tag{B.15} $$

$$ {}_P\boldsymbol{u}^{(2)}_{S_rS_r} = \frac{U^2_{S_r}}{c^2_P(4k^2_S - 4k^2_P)} {}_P\beta^{bulk}_{S_rS_r} e^{j(2\omega t - 2k_S x\sin\theta_S - 2k_S z\cos\theta_S)} \begin{bmatrix} \sin\theta_S \\ 0 \\ \cos\theta_S \end{bmatrix} \tag{B.16} $$

APPENDIX C

GENERATION OF SECOND HARMONIC LAMB WAVES

In this appendix, we will quickly show how the framework of reflection at a free boundary can be used to analyze the generation of second harmonic Lamb waves in a thin isotropic plate. Since the propagation of Lamb waves is not the primary focus of this thesis, we will only give a brief overview with the goal of showing that the techniques introduced above can also be applied to this problem.

C.1 Lamb Waves

Lamb waves are guided waves, i.e. they travel through a waveguide. In the case of Lamb waves, this waveguide is a thin plate with two free boundaries, as illustrated in Fig. C.1. Lamb waves consist of P- and SV-waves that are reflected from the free boundaries. Due to mode conversion, this leads to an interference pattern of a standing wave, which is also shown in Fig. C.1.

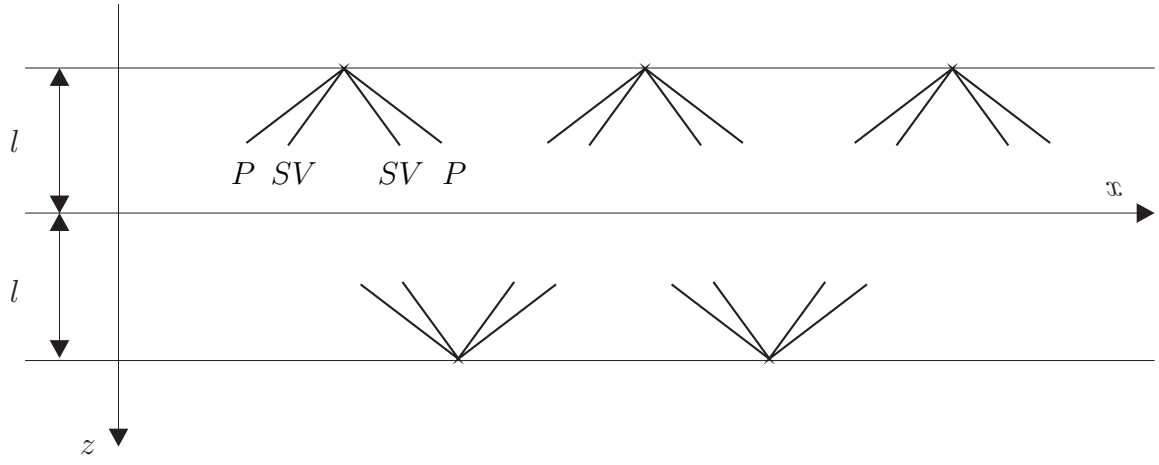

Figure C.1: Mode Conversion in a Waveguide.

Using potentials F and $\boldsymbol{H}$, the wave equation can be stated as

$$\frac{\partial^2 F}{\partial x^2} + \frac{\partial^2 F}{\partial z^2} = \frac{1}{c_P^2}\frac{\partial^2 F}{\partial t^2} \tag{C.1}$$

$$\frac{\partial^2 \boldsymbol{H}}{\partial x^2} + \frac{\partial^2 \boldsymbol{H}}{\partial z^2} = \frac{1}{c_S^2}\frac{\partial^2 \boldsymbol{H}}{\partial t^2} \tag{C.2}$$

with

$$\nabla \cdot \boldsymbol{H} = 0. \tag{C.3}$$

Assuming solutions

$$F = f(z)e^{j(\omega t - kx)} \tag{C.4}$$

$$\boldsymbol{H} = \boldsymbol{h}(z)e^{j(\omega t - kx)}, \tag{C.5}$$

we obtain solutions

$$f(z) = A_1 \sin(pz) + A_2 \cos(pz) \tag{C.6}$$

$$h_y(z) = B_1 \sin(qz) + B_2 \cos(qz) \tag{C.7}$$

with h_y being the component of $\boldsymbol{h}$ in y-direction and

$$p^2 = \frac{\omega^2}{c_P^2} - k^2 \tag{C.8}$$

$$q^2 = \frac{\omega^2}{c_S^2} - k^2. \tag{C.9}$$

Applying the boundary conditions

$$\sigma_{33}|_{z=\pm l} = 0 \tag{C.10}$$

$$\sigma_{31}|_{z=\pm l} = 0, \tag{C.11}$$

we obtain four equations. These four equations finally result in the *Rayleigh-Lamb frequency equations*,

$$\frac{\tan(qh)}{\tan(ph)} = -\frac{4k^2pq}{(k^2-q^2)^2} \tag{C.12}$$

for the propagation of *symmetric modes*, and

$$\frac{\tan(qh)}{\tan(ph)} = -\frac{(k^2-q^2)^2}{4k^2pq} \tag{C.13}$$

for the propagation of *antisymmetric modes*. The terms symmetric and antisymmetric refer to the symmetry of the displacements u_x (for a symmetric mode) and u_z (for an antisymmetric mode) with respect to the x-axis. For more details on the propagation of Lamb waves, the books by Achenbach [1] and Graff [12] are recommended.

C.2 Second Harmonic Lamb Waves

As in the case for bulk waves, nonlinearities in the material lead to the generation of higher harmonics. Possible frameworks to model the generation of higher harmonics of Lamb wave modes include a modal analysis approach [19, 9] and an investigation of the reflection at the free boundary [10]. The latter approach was used by Deng, and since it is based on the framework used above, we will outline the major results in this thesis.

C.2.1 Primary Field

The primary wave field in a thin plate of thickness $2l$ consists of four partial bulk waves: two P-waves and two SV-waves. We assume that the guided wave is composed of these partial bulk waves. The primary field is illustrated in Fig. C.2 and it is mathematically represented by

$$\boldsymbol{u}^{(1)} = \boldsymbol{u}^{(1)}_{P_1} + \boldsymbol{u}^{(1)}_{S_1} + \boldsymbol{u}^{(1)}_{P_2} + \boldsymbol{u}^{(1)}_{S_2} \tag{C.14}$$

with

$$\boldsymbol{u}^{(1)}_{P_1} = U_{P_1} \begin{bmatrix} \sin\theta_P \\ 0 \\ -\cos\theta_P \end{bmatrix} e^{j(\omega t - k_P x \sin\theta_P + k_P z \cos\theta_P)}, \tag{C.15}$$

$$\boldsymbol{u}^{(1)}_{S_1} = U_{S_1} \begin{bmatrix} \cos\theta_S \\ 0 \\ \sin\theta_S \end{bmatrix} e^{j(\omega t - k_S x \sin\theta_S + k_S z \cos\theta_S)}, \tag{C.16}$$

$$\boldsymbol{u}^{(1)}_{P_2} = U_{P_2} \begin{bmatrix} \sin\theta_P \\ 0 \\ \cos\theta_P \end{bmatrix} e^{j(\omega t - k_P x \sin\theta_P - k_P z \cos\theta_P)}, \tag{C.17}$$

$$\boldsymbol{u}^{(1)}_{S_2} = U_{S_2} \begin{bmatrix} \cos\theta_S \\ 0 \\ -\sin\theta_S \end{bmatrix} e^{j(\omega t - k_S x \sin\theta_S - k_S z \cos\theta_S)}. \tag{C.18}$$

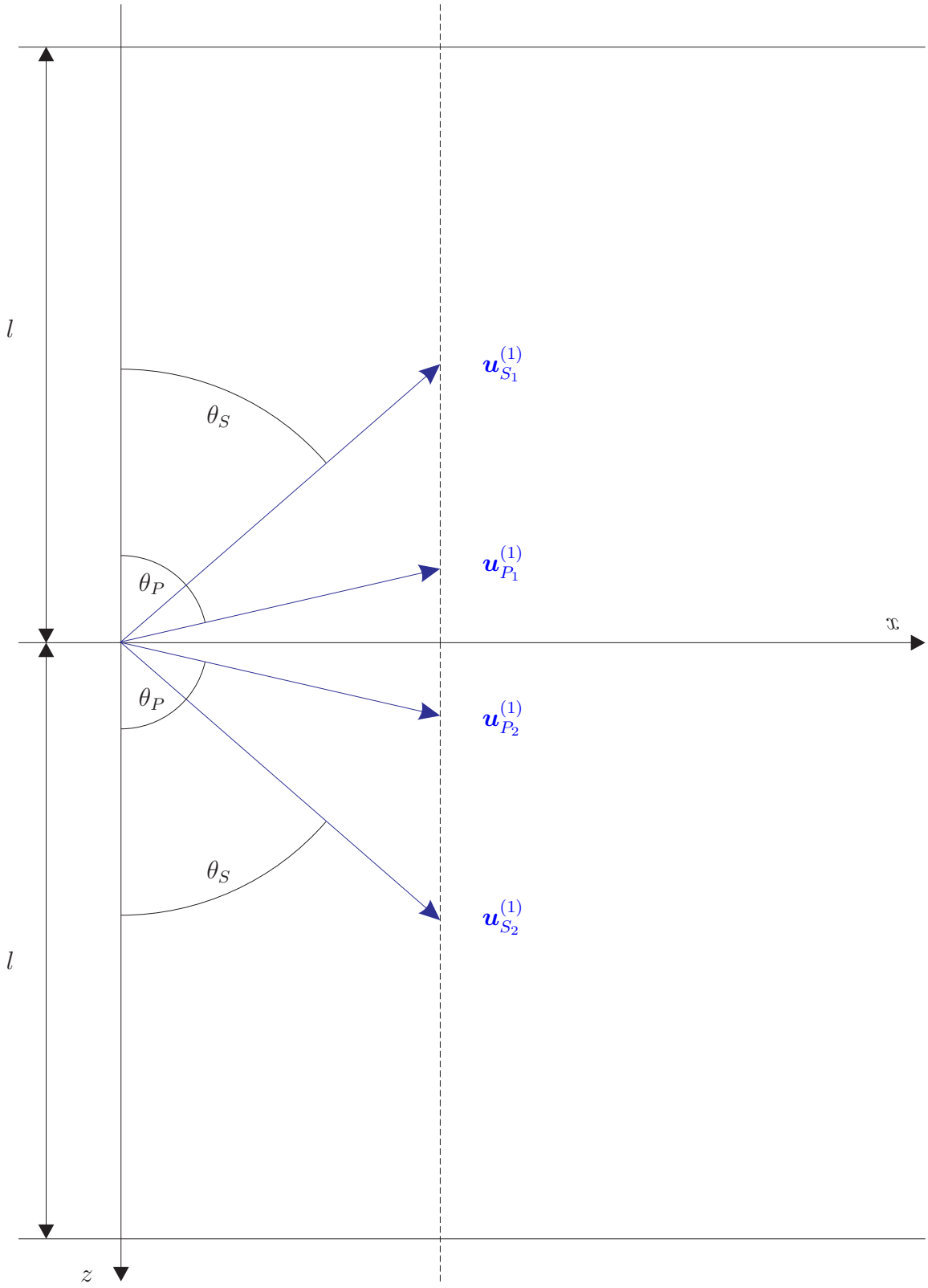

Figure C.2: Primary Wave Field for Lamb Wave Propagation.

A relationship between the amplitudes U_{P_1}, U_{S_1}, U_{P_2} and U_{S_2} can be determined using the boundary conditions (C.10) and (C.11). This will also result in the two dispersion equations (C.12) and (C.13). Substituting (C.12) into the boundary conditions leads to

$$U_{P_1} = U_{P_2}, \qquad U_{S_1} = U_{S_2}, \tag{C.19}$$

which represents a symmetric mode. Similarly, if we substitute (C.13) into the boundary conditions, we obtain the amplitude relationship for an antisymmetric mode,

$$U_{P_1} = -U_{P_2}, \qquad U_{S_1} = -U_{S_2}. \tag{C.20}$$

C.2.2 Secondary Field

Interactions of the primary waves lead to the generation of second harmonic lamb waves. The resulting secondary field is given in Fig.C.3. Expressions for the generated waves can be obtained applying the perturbation method. We will not state the complete expressions here but instead refer to the work by Deng [10]. Note that there also appear accumulating second harmonics, i.e. modes satisfying the resonance condition will have amplitudes that increase with propagation distance. As a conclusion, we can say that the framework used in this thesis does not only prove useful for single reflection problems, but it can also be applied for multiple reflections, as in the outlined case of Lamb wave generation.

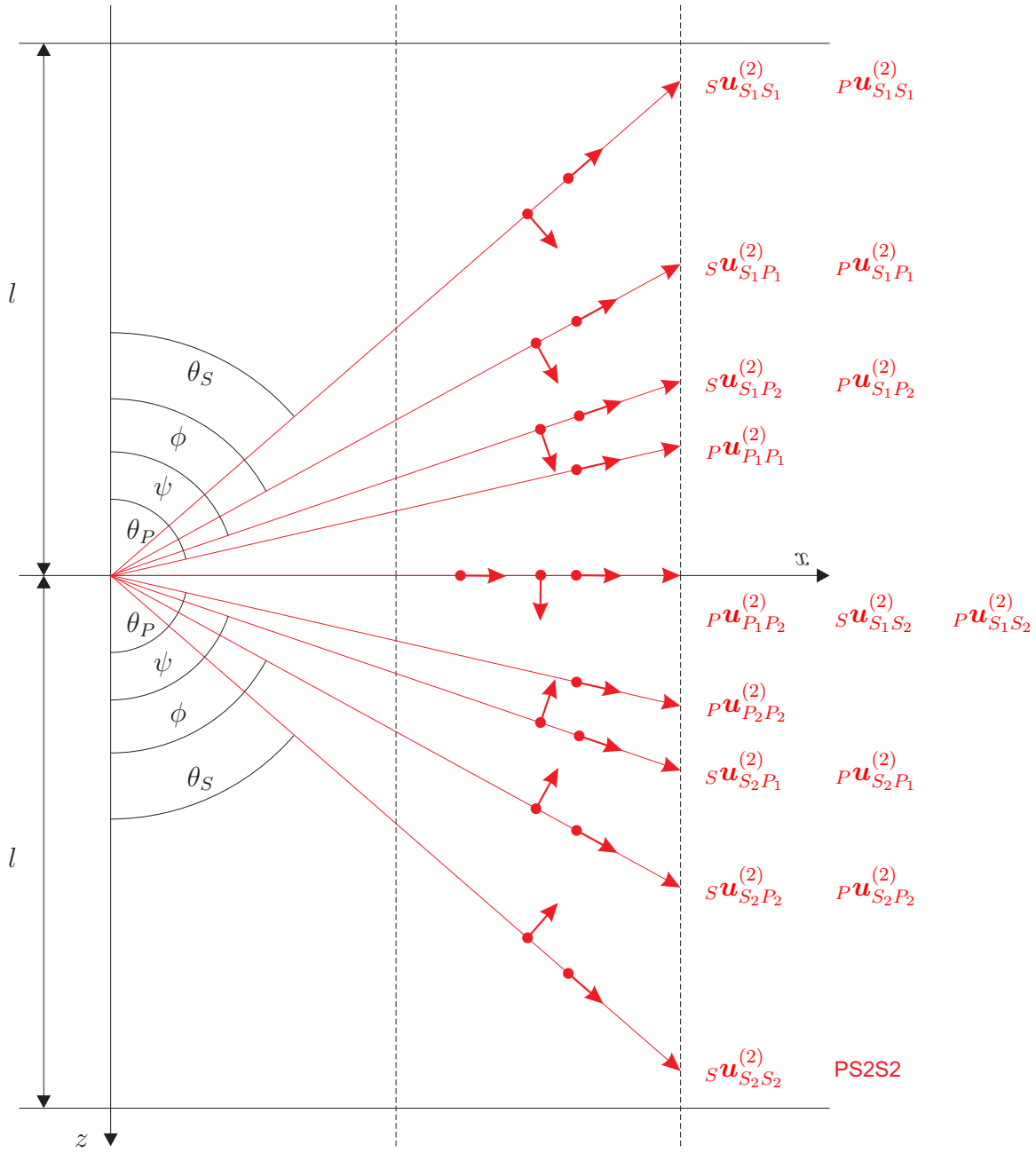

Figure C.3: Secondary Wave Field for Lamb Wave Propagation.

REFERENCES

[1] Achenbach, J. D., *Wave Propagation in Elastic Solids*. Elsevier Science Publishers B. V., Amsterdam, 1975.

[2] Auld, B. A., *Acoustic Fields and Waves in Solids*, vol. II. Robert E. Krieger, 1990.

[3] Bender, C. M. and Orszag, S. A., *Advanced Mathematical Methods for Scientists and Engineers*. McGraw-Hill, New York, 1978.

[4] Braun, M. R., "Characterization of nonlinearity parameters in an elastic material with quadratic nonlinearity with a complex wave field," Master's thesis, School of Civil and Environmental Engineering, Georgia Institute of Technology, December 2008.

[5] Braun, M. R., Jacobs, L. J., Qu, J., and Kuechler, S., "Determination of third-order elastic constants using second-harmonic generation in an elastic material with quadratic nonlinearity," in *Review of Progress in Quantitative Nondestructive Evaluation*, vol. 1096 of *AIP Conference Proceedings*, pp. 246–253, AIP, March 2009.

[6] Buck, O. and Thompson, D. O., "Relation of finite amplitude waves to third-order elastic constants," *Materials Science and Engineering*, vol. 1, pp. 118–140, 1966.

[7] Cantrell, J. H. and Yost, W. T., "Nonlinear ultrasonic characterization of fatigue microstructures," *International Journal of Fatigue*, vol. 23, pp. 487–490, 2001.

[8] Chen, J., Jiang, W., and Shui, Y., "Observation of nonlinear acoustic effects at isotropic solid-solid interfaces," *Journal of the Acoustical Society of America*, vol. 109, pp. 501–507, February 2001.

[9] DeLima, W., *Harmonic Generation in Isotropic Elastic Waveguides*. PhD thesis, The University of Texas at Austin, December 2000.

[10] Deng, M., "Cumulative second-harmonic generation of lamb-mode propagation in a solid plate," *Journal of Applied Physics*, vol. 85, pp. 3051–3058, March 1999.

[11] Gol'dberg, Z. A., "Interaction of plane longitudinal and transverse elastic waves," *Journal of Soviet Physics - Acoustics*, vol. 6, pp. 306–310, 1961.

[12] Graff, K. F., *Wave Motion in Elastic Solids*. Dover, 1975.

[13] Green, R. E., *Ultrasonic Investigation of Mechanical Properties*, vol. 3 of *Treatise on Materials Science and Technology*. Academic Press, 1973.

[14] Herrmann, J., Kim, J.-Y., Jacobs, L. J., Qu, J., Littles, J. W., and Savage, M. F., "Assessment of material damage in a nickel-base superalloy using nonlinear rayleigh surface waves," *Journal of Applied Physics*, vol. 99, 2006.

[15] Jones, G. L. and Kobett, D. R., "Interaction of elastic waves in an isotropic solid," *Journal of the Acoustical Society of America*, vol. 35, pp. 5–10, January 1963.

[16] Kim, J.-Y., Jacobs, L. J., Qu, J., and Littles, J. W., "Experimental characterization of fatigue damage in a nickel-base superalloy using nonlinear ultrasonic waves," *Journal of the Acoustical Society of America*, vol. 120, pp. 1266–1273, September 2006.

[17] Landau, L. D. and Lifshitz, E. M., *Theory of Elasticity*, vol. 7 of *Course of Theoretical Physics*. Pergamon Press, 2nd ed., 1970.

[18] Malvern, L. E., *Introduction to the Mechanics of a Continuous Medium*. Series in Engineering of the Physical Sciences, Prentice-Hall, 1969.

[19] Mueller, M., "Analytical investigation of internally resonant second harmonic lamb waves in nonlinear elastic isotropic plates," Master's thesis, School of Civil and Environmental Engineering, Georgia Institute of Technology, December 2009.

[20] Pruell, C., Kim, J.-Y., Qu, J., and Jacobs, L. J., "Evaluation of fatigue damage using nonlinear guided waves," *Smart Materials and Structures*, vol. 18, pp. 1–7, January 2009.

[21] Renton, J. D., *Applied Elasticity: Matrix and Tensor Analysis of Elastic Continua*. Ellis Horwood Limited, Chichester, 1987.

[22] Shu, K. T. and Ginsberg, J. H., "Oblique reflection of a nonlinear p wave from the boundary of an elastic half space," *Journal of the Acoustical Society of America*, vol. 89, pp. 2652–2662, June 1991.

[23] Thompson, R. B. and Tiersten, H. F., "Harmonic generation of longitudinal elastic waves," *Journal of the Acoustical Society of America*, vol. 62, pp. 33–37, July 1977.

[24] Wolfram, S. and Beck, G., *Mathematica - The Student Book*. Addison-Wesley, 1994.

[25] Xi, D. M., "Second-harmonic generation accompanying nonlinear reflection of shear waves in an isotropic layered structure," *Journal of Applied Physics*, vol. 82, pp. 1026–1030, August 1997.

[26] Zhou, S. and Shui, Y., "Nonlinear reflection of bulk acoustic waves at an interface," *Journal of Applied Physics*, vol. 72, pp. 5070–5080, December 1992.

[27] Zhou, S., Jiang, W., and Shui, Y., "Nonlinear bulk acoustic waves in anisotropic solids: Propagation, generation, and reflection," *Journal of Applied Physics*, vol. 78, pp. 39–46, July 1995.